Development of a Finite Element Model to Examine the Response of the Advanced System for Implant Stability Testing (ASIST) in Dental Implants

by

Tod Michael Vandenberg

A thesis submitted in partial fulfillment of the requirements for the degree of

Master of Science

Department of Mechanical Engineering

University of Alberta

Abstract

The health of the bone-implant interface (BII) of a dental implant is integral to the success of the implant. The evaluation of the development process of these tissues during the healing stages is important in analyzing the risks of failure and to determining when loading can be prescribed. The Advanced System for Implant Stability Testing (ASIST) is a device and process created to analyze the dynamic response of an implant undergoing a low-force impact load and determine the stability of the structure provided by the BII. The primary purpose of this study is to develop a modelling process that will lead to a finite element model of any dental implant and abutment system undergoing the same loading as the ASIST such that the acceleration response extracted from the model will match the measurement of the ASIST. This model will be validated by experimental result and predict the responses of new systems.

The finite element model showed that changes in impact angle, clamping conditions, and implant protrusion all have significant effects on the ASIST Stability Coefficient (ASC) of an implant system which can lead to variance between similar experimental samples. The model showed that the ASIST is sensitive to the properties of the material surrounding an implant and can measure the stability independently of the implant or abutment geometry. The finite element model was able to represent the available data with an R^2 value of 0.94 and provided a good representation of the experimental samples.

The model was adapted to incorporate a dental crown, composite bone, or bone resorption. The model of the dental crown highlighted a sensitivity in the ASIST to the striking height on the crown surface. Changes in the striking height of the impact rod on the surface of the crown resulted in ASC values ranging from 13.8 to 22.2 depending on the striking height. For the composite bone, the definition of the ASC was adjusted to incorporate the two different stiffnesses of the

surrounding material. The results of this simulation reinforced the necessity in accounting for a non-uniform material by showing that assuming a uniform material can make a measurement appear higher than the actual stability.

The model was used to predict the response of an implant undergoing bone resorption. The results showed a decrease in ASC of about 2 per mm of bone loss showing evidence that the ASIST could be useful in long term monitoring of implant health.

Using a finite element model of a dental implant has shown that the ASIST can isolate a measure of dental implant stability regardless of implant and abutment geometry. There is strong evidence to support that the measurements are based on the properties of the BII. The ASIST can be used as a tool to evaluate the short-term healing process of this region, as well as monitor the long-term health by being sensitive to bone resorption.

Preface

This Thesis is an original work by Tod Vandenberg. Elements of Chapter 3 of this work were presented at the Annual Alberta Biomedical Engineering Conference in 2022.

T. Vandenberg, C. Jar, L. Westover."Development of a Finite Element Model to Examine the Response of the Advanced System for Implant Stability Testing," in *23rd Annual Alberta Biomedical Engineering Conference*, Banff Alberta Canada, October 21 – 22, 2022 (Poster).

Acknowledgements

I would like to Acknowledge and thank:

My supervisor Lindsey Westover for your support and advice. I am thankful to have had the opportunity to work with you on this project.

Dr. Dan Romanyk, Dr. Xinming Li, and Dr. Kajsa Duke. Thank you for taking the time to serve on my examination committee.

My office-mate Chester. Thank you for working together with me on this project.

My family, friends, and church community who have supported and encouraged me throughout my many exams.

And especially my wife Renae. You have loved me through everything, and I am so lucky to have you.

Table of Contents

List of Tables

List of Figures

Chapter 1: Introduction

1.2 Background

Tooth loss is an extremely prevalent issue, affecting more than 276 million people around the world [1]. Caries, periodontal disease, and traumatic injury are all causes for tooth loss or removal. The loss of a tooth is detrimental to the ability of a person to eat or talk and can be harmful to a person's self-image due to the change in their smile. Tooth loss can affect a person emotionally and socially as well as physically [2, 3, 4].

One treatment option for lost teeth is osseointegrated dental implants. These implants are inserted into the bone and are used to hold a functional prosthetic to give a patient an aesthetically "normal" smile and return the patient to their natural speaking and eating processes [5]. The success of these implants is defined by several factors including the survival of the implant over the lifetime of the patient. Successful bone growth around the implant is vital to the long-term survival of the implant [6]. The creation of a bond between an implant and the bone is called osseointegration. This process relies on a number of factors including implant design, surgical procedure, and bone properties [7, 8]. In the initial healing phase, it is important that the implant be immobile to allow bone growth [9]. This resistance to displacement is called stability and, in this initial stage, is more specifically called primary stability. During the osseointegration process, as solid bone forms around the implant, the implant develops secondary stability: a resistance to displacement due to the strength and stiffness of the surrounding bone tissue and bone-implant interface (BII) [6].

The measurement of both primary and secondary stability is important in evaluating the success of the implantation surgery, monitoring the healing process of the implant, monitoring long-term health, and identifying conditions such as periodontitis or bone-resorption. Methods such as radiological examinations can be used to observe bone resorption around the implant but expose the patient to ionizing radiation [10]. Several devices have been created to measure implant stability including the Periotest, the DMC (Dental Mobility Checker), the Osstell, and the Penguin [11, 12]. The currently available devices have several limitations that make it difficult to accurately assess the health of the BII. Several of the devices require a component to be attached to the implant, which cannot be done in later stages of healing due to the presence of the prosthetic tooth. Additionally, some devices use a heavily filtered response signal that causes important information

to be lost in the analysis. These devices rely primarily on resonance frequency analysis, or analysis of the natural frequency of the system, with the idea that a stiffer implant will have a higher natural frequency. However, the natural frequency of the system will vary with the implant/abutment size, geometry, and inertia properties. No currently available devices have considered these geometric and inertia parameters and thus they do not allow different designs of implants and abutments to be quantitatively compared using absolute values that reflect implant stability.

The Advanced System for Implant Stability Testing (ASIST) has been developed as a new way to monitor implant stability [13]. The ASIST uses low-force impact loading to generate an acceleration response of an impacted system (an implant and abutment and/or prosthetic tooth) and uses an analytical model to extract a stiffness value for the BII from the unfiltered acceleration signal [14]. Including the analytical model allows the stability measure to isolate the BII and be independent from attached components [15]. The ASIST has been developed for different implant-abutment systems including bone conduction hearing aids [14], and has been recently adapted for dental implants [16]. A finite element (FE) model was developed to investigate the ASIST method in isolating the behavior of the BII from the system's geometry [17, 18]. This model provided evidence that the ASIST measurement is primarily a function of the BII properties and that the analytical model is representative of the more complex system. Adapting the ASIST for use with dental implants requires changes to the analytical model. The ASIST system for dental implants has not yet been investigated using finite element modelling.

The dental implant system can be modelled under impact loading using finite element analysis (FEA) to extract a signal similar to the experimental response. By modelling the system, the effects of certain variables such as impact angle and implant model can be analyzed to examine their effects on a measurement. An in-silico model could also be used to predict the changes in a stability measurement that could occur due to bone resorption in a clinical setting. This research is focused on creating a finite element model that can be used to explain the measured responses of a tested system or predict the response of a new system. A finite element model can be used to examine the effectiveness of the ASIST in isolating the interface stiffness regardless of implant and abutment design, examine the effects of variables involved with experimental sample preparation on stability measurements, and predict the trend in stability measurements with respect to bone

resorption. If the ASIST measurements could reflect bone resorption, radiation due to scans could be avoided.

1.3 Objectives

The objective of this study is to build on the work of previous researchers in testing and validating a measurement system for evaluating the osseointegration and stability of dental implants through the development of a dynamic FE model.

The systems consisting of the ASIST, a dental implant and abutment, and the surrounding substrate (bone simulant; Sawbones Pacific Research Company) will be simulated in a dynamic FE model. The impact event will be simulated, and the acceleration of the impact rod will be extracted as a model output. Experimental data with dental implants representing both primary and secondary stability has been collected in a laboratory setting as part of a parallel project and will be used to validate the developed FE model.

The developed FE model will be used to understand variation found in experimental data by creating models to represent implant samples with an under drilled hole (implant protrusion), different clamping configurations, and different striking angles. The impact of each of these variables on the measured ASC will be examined. The model will be compared to experimental data to examine the ability of the measurement approach to isolate the BII stability from the design of the implant and abutment. The ability of the model to represent the data collected from experiments will be examined. Models will be made to predict the ASIST responses of an implant with an attached dental crown, undergoing bone resorption, or embedded in composite bone to predict the expected responses of an implant being used in various clinical settings. The impact of bone resorption and the incorporation of a composite bone layer on the measured ASC will be examined. It is expected that the addition of a stiffer layer of bone increases the stability measurement of the implant, and the loss of bone around the implant would reduce the stiffness. Taken together, these analyses will provide an understanding of the sensitivity of the ASIST approach to variations in experimental and clinical parameters that can be used to inform future development of the technique for clinical applications

1.3 Thesis Outline

This thesis presents the development of an FE model to evaluate the application of dynamic impact loading with the ASIST to a dental implant system.

Chapter 1 provides an introduction to the research topic and outlines the thesis objectives.

Chapter 2 provides a review of the literature pertaining to the research topic. It provides a brief overview of tooth loss, the need for successful dental implants, and the factors leading an implant to being successful. It contains an explanation for the function of the ASIST, and the previous work done to develop and validate the system as a viable tool for measuring implant stability in both bone conduction hearing and dental implants. The process of extracting an ASIST Stability Coefficient (ASC) from the acceleration data recorded by the ASIST handpiece using an analytical model is explained in this Chapter. The collection and analysis of empirical tests will be briefly presented.

Chapter 3 focuses on the development of an FE model that will output data similar to that measured by the accelerometer present in the ASIST. The simplification of implant geometry, the chosen material properties, and the model parameters are presented and explained.

Chapter 4 examines possible variables that may cause inconsistencies in presumably similar experiments using a series of simulations analyzed in the form of a 2k factorial experiment.

Chapter 5 presents an analysis of the simulation approach for the BII.

Chapter 6 focuses on further additions to the model to incorporate features that more closely represent a clinical system. Features such as composite bone, dental crowns, and bone resorption are examined.

In Chapter 7 the modelling process will be used to model each of the experimentally tested implants, abutments, and bone simulant blocks to demonstrate the applicability of the model to the entire range of experiments.

Chapter 8 summarizes and discusses the main results of this study, the research contributions, and suggested areas of improvement or future study opportunities.

Chapter 2 : Literature Review

2.1 The Structure and Composition of Teeth

The structure of a tooth is made up of four layers: enamel, dentin, cementum, and pulp as shown in Figure 2.1. The enamel is a highly mineralized structure made up of hydroxyapatite crystals [19]. This is the outer layer of the tooth exposed to the environment of the mouth.

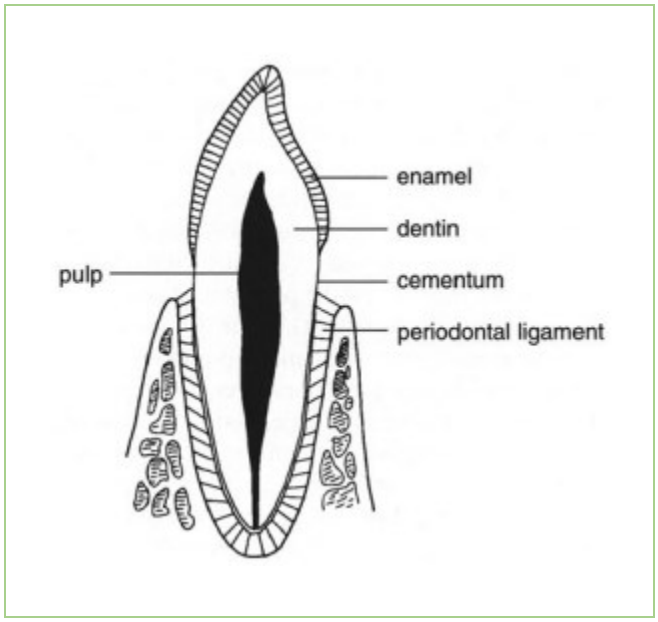

Figure 2.1: Structure of a Tooth [19]

Dentin is the second layer of the tooth. It is also highly mineralized, comprised of hollow tubules surrounded by collagen bundles [20]. The collagen fibers give this material more flexibility compared to enamel, and the structure of the tubules prevent fractures from spreading to the pulp of the tooth [21]. The dental pulp is in the center of the tooth and contains nerve fibers, blood vessels, and cells that maintain the tooth. The cementum is a layer on the outside of the root of the tooth that is not exposed to the environment. It serves as an anchoring surface for the periodontal ligament to hold the tooth in place [19].

The periodontal ligament is primarily composed of collagen fibers which bridge the gap between the root of the tooth and the surrounding bone. These tissues create an elastic connection that absorbs impacts during the normal functions of the mouth [19]. Understanding the structure and anatomy of a tooth provides insight into the possible ways it might be damaged.

2.2 Cause and Effect of Tooth Loss

Tooth loss or extraction can be a result of many different factors and/or events including caries, periodontal disease, traumatic oral injury, and age-related factors [22, 23]. A damaged tooth can cause infection to the surrounding tissues or pain to the patient and therefor can require removal [22]. According to the World Health Organization, oral diseases affect close to 3.5 billion people worldwide. Further, 7% of people 20 and older, and 23% of people over 60 are edentulous [24]. According to one review, in 2010, the incidence rate of tooth loss was 205 cases per 100,000 people per year [25]. Tooth loss can have complex effects on patients physically, emotionally, and mentally.

2.2.1 Caries

Dental caries are caused by sugar-fermenting acidogenic microorganisms in the mouth [26] and are one of the primary causes of tooth loss. Caries in the permanent teeth are present in the majority of the global population [24, 26] and can be treated in a number of ways depending on severity. Controlling sugar intake is a large factor in arresting the production and development of caries [27]. High sugar diets and diets involving the consumption of sugar between meals is associated with increased number and severity of caries. Certain nutrient such as vitamin D and calcium can strengthen the enamel of teeth to protect against the malignant organisms. Proper oral hygiene and fluoride exposure are also beneficial to caries prevention. As caries become severe, they can cause severe pain, and possible infection requiring treatment in the form of a dental filling, antibiotics, or a tooth extraction [28]. Several studies have found that severe caries are a significant cause leading to tooth extraction [29, 30] if they are not treated, or if the treatment fails.

2.2.2 Periodontal Disease

Severe periodontal disease has a prevalence of 19% in people over 15 [24]. Similar to caries, it is caused by microorganisms, however periodontal diseases occur in the soft tissues around the teeth [27, 3]. Gingivitis occurs when plaque is allowed to build up around the gum line. This plaque creates pockets alongside the tooth that will initially cause an inflammatory response as shown in Figure 2.2.

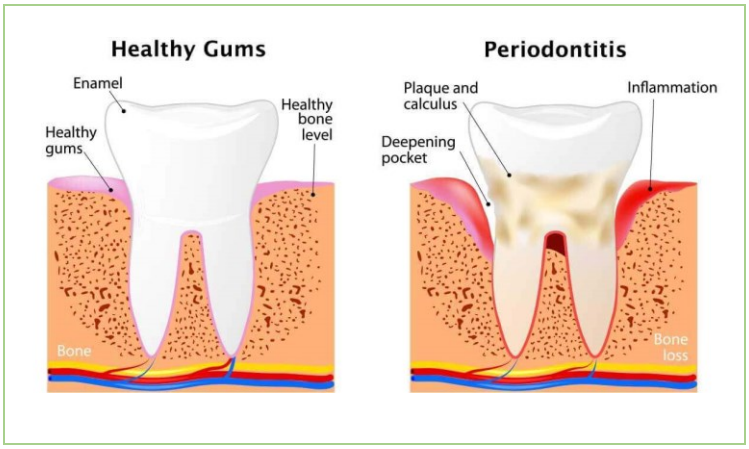

Figure 2.2: Characteristics of Periodontitis (from https://www.dentalsolutions.ca/patient-info/stages-periodontal-disease/)

If the plaque is not removed through brushing or dental cleaning, periodontitis disease will develop. The primary symptom of periodontitis is the destruction of the periodontal ligament and bone tissue surrounding the teeth [27]. A loss of attachment greater than 4 mm will increase the risk of tooth loss and compromise the function of the tooth [3].

2.2.3 Traumatic Tooth Loss

Traumatic dental injuries (TDIs) occur when a wound to the teeth and/or surrounding support structures triggers a healing response [31]. This occurs most often to children, with males being more prone than females [32]. The World Health Organization found that 20% of children under 12 have experienced a traumatic dental injury, with an estimated total of 1 billion people worldwide being affected [24]. A Swedish study found that 5% of patients seeking treatment for accidental injuries are affected in the oral region [33]. TDIs that result in avulsion (dislodging of a tooth from its socket), intrusion (vertical displacement of a tooth into the bone), or root fractures are at a high risk of permanent tooth loss. After the avulsion of a tooth, immediate replantation creates an opportunity for healing, however this only occurs with a 73% chance of success if replanted within 5 minutes of avulsion, and an 18% chance of success after storage of the tooth [34]. Intrusion of a tooth causes damage to the underlying bone and/or root of the tooth. Over time, pulp necrosis, root resorption, and marginal bone loss, which can all be triggered by the intrusion, can cause a complete failure of the tooth. After intrusion, there is a 30% tooth survival rate after a period of 15 years [35]. In the case of root fractures, there are several surgical treatments that can

be used to preserve some or all of the damaged tooth. Where surgical techniques cannot be performed, or if necrosis and root resorption occur, extraction must be done. In the case of tooth failure, the tooth will be lost, and other treatment options can be investigated.

2.2.4 Age Related Factors

Loss of teeth is positively correlated with age [36]. Although there are few age-related changes that directly affect oral health, changes such as increased use of medicines, reduced muscle bulk, and forgetfulness can lead to lifestyle and diet changes that do have an impact [27]. A lack of oral hygiene due to fatigue, or forgetfulness can increase the effects of caries in addition to the cumulative damage that may have been caused over time. Elderly patients can also suffer from tooth wear. After a lifetime of normal function, teeth become irreversibly eroded, damaging the tooth. Once a tooth becomes sufficiently damaged, and other treatments have been attempted, extraction becomes the last treatment option.

2.2.5 Effects of Tooth Loss

Loss of a tooth can affect an individual physically, emotionally, and socially. Surgical procedures (including tooth extraction) are never without risk. Extraction of a tooth can cause traumatic experience during the surgery such as tooth fracture, failure of anesthesia, or collateral damage to surrounding tissues [1, 22]. There is also a risk of infection or nerve damage that could cause significant stress to the patient [22].

Once teeth are extracted, there are several functional disorders that may occur. A space where a tooth is lost will not provide the antagonistic support on the matching tooth in the opposite jaw causing the remaining teeth to migrate downward [37]. This is called elongation and it exposes the neck of the moving tooth, increasing the risk of cervical carries [37]. The absence of a tooth could also cause the teeth on either side of a space to migrate causing tipping, the breaking down of the supporting bone, and reducing the support of all surrounding teeth. Missing teeth can be detrimental to the way a patient talks, eats, and the way their resting bite feels [2]. Negatively impacting the way a person eats can impact the dietary choices they make, which can, in turn, harm their health in indirect ways [3].

There are many ways that missing teeth can physically harm a patient, and many of these also cause aesthetic changes that can be emotionally damaging [2]. A person's face plays an important role in their sense of identity, and changes to their face that they may perceive as unattractive could negatively impact their self-esteem. There is also evidence that tooth loss causes an emotional sense of loss or shame, as if tooth extraction is done as a punishment [4]. Tooth loss can also affect a person socially. Children with dental deformities show patterns of limited social interaction due to a history of teasing and harassment [2]. Missing teeth may cause speech impediments or changes in eating that can alienate a patient from their peers.

Tooth loss can affect a patient in many complex ways, but it can be treated using partial or full removable dentures, fixed dentures, or osseointegrated dental implants.

2.3 Application and Healing Process of Dental Implants

2.3.1 Dental Implantation Procedure

One treatment option for a lost tooth is a dental implant. In 2009, there were close to 600 different dental implant systems produced by over 146 manufacturers [38]. In 2016, the prevalence of dental implants in the US was 5.7% [39]. Dental implants are made with differing designs, materials, and surface finishes, all with the purpose of transmitting force from the dentition to the bone, creating a stable anchor for a crown, and promoting healing for the implant site [5]. They are typically made up of three pieces as shown in Figure 2.3: the implant or screw, the abutment, and the crown.

Figure 2.3: Structure of The Dental Implant (from https://agapedental.ca/dental-implants-replacing-missing-teeth/)

The insertion process for an implant typically starts with an assessment of the patient and the implant site [40]. Bone quality needs to be assessed to choose the correct drilling procedure [41], and jaw atrophy or bone defects may be cause for bone grafting prior to a dental implant procedure [42]. Once the bone is assessed, a hole must be drilled for the appropriate implant. The specific drilling procedure may be different for each implant, but they all employ a low-speed technique for minimal tissue damage [5]. The implant is then placed, and either held in place by threads that are screwed into the bone, or a wedge force due to compression by the drilled socket and friction between the implant and bone [37]. The stability of the implant due to these initial forces is called the primary stability.

After the initial placement, there are two possible options. The implant either undergoes a two-step method where the implant is covered again by soft tissue, is allowed to heal for 3-6 months, and then exposed again for the placement of a healing abutment, or a one-step method where a healing abutment is placed immediately [43]. In both cases the implant is typically allowed to heal without loading for 3-6 months. In a two-stage procedure, a healing abutment would be placed after the initial healing period in a second-stage surgery, and then be unloaded for another month. The healing abutment allows the soft tissues to heal into the proper shape around the abutment, but without loading to the implant that may damage the healing bone. The stability caused by the formation of bone around the implant after the healing period is called secondary stability.

After the period of healing with no loading, the healing abutment is removed, and a final abutment is placed onto the implant [44]. A crown is cemented onto the final abutment and can act functionally as a tooth in the processes of chewing, smiling, et cetera.

2.3.2 Bone Properties of the Jaws

One of the critical factors in the primary stability of an implant is the quality of the bone at the implantation site [45, 46, 47, 48]. Bone can be separated into two components: the outer cortical layer, and the inner trabecular bone. The cortical bone is denser than trabecular bone, due to the 80% of the space within the trabecular region being filled with marrow and fat. The soft tissue in the trabecular regions absorb shock and holds the cells for generating blood cells [49]. The quality of bone with regard to implantation is classified by a combination of the properties and thickness of the cortical bone, and the properties of the trabecular bone underneath. The standard classification method sorts the bone into 4 groups [50]:

Type 1: Entirely homogenous compact bone
Type 2: Thick layer of compact bone surrounding a core of dense trabecular bone
Type 3: Thin layer of compact bone surrounding a core of dense trabecular bone
Type 4: Thin layer of compact bone surrounding a core of low-density trabecular bone

This method required scans of the bone to examine the thickness and density of each layer. Another method of categorization was developed based off the drilling resistance of the bone specifically during dental implant preparation [51]. This method categorized the bone into 5 levels, each with a tactile analog of the drilling resistance (e.g., A type of Wood or Styrofoam). Typically, at potential implantation sites, both the bone quality and cortical bone thickness in the lower jaw (mandible) are higher than in the upper jaw (maxilla) [51]. One study found that one average, the thickness in the posterior of the mandible is the highest (1.07 ± 0.44 mm) followed by its anterior (0.99 ± 0.30 mm) [45]. The anterior maxilla region has the next highest cortical thickness (0.82 ± 0.32 mm) with the posterior being the lowest (0.71 ± 0.27). Figure 2.4 shows cross sectional scans of potential implant sites in each of these regions and highlights the cortical thickness of each in this particular set of scans. Studies show that despite the cortical thickness being close in scale to a single thread of a screw implant, this value is a significant factor in the primary stability of the implant [47]. When a dental implant is inserted, the top threads are in contact with the cortical

layer of bone, and most of the implant sits below the bone surface level [41]. The contact with the cortical layer is critical for the initial stability of the implant but the majority of the implant-to-bone contact is in the trabecular bone. The trabecular bone contains the types of cells necessary to facilitate healing around the implant.

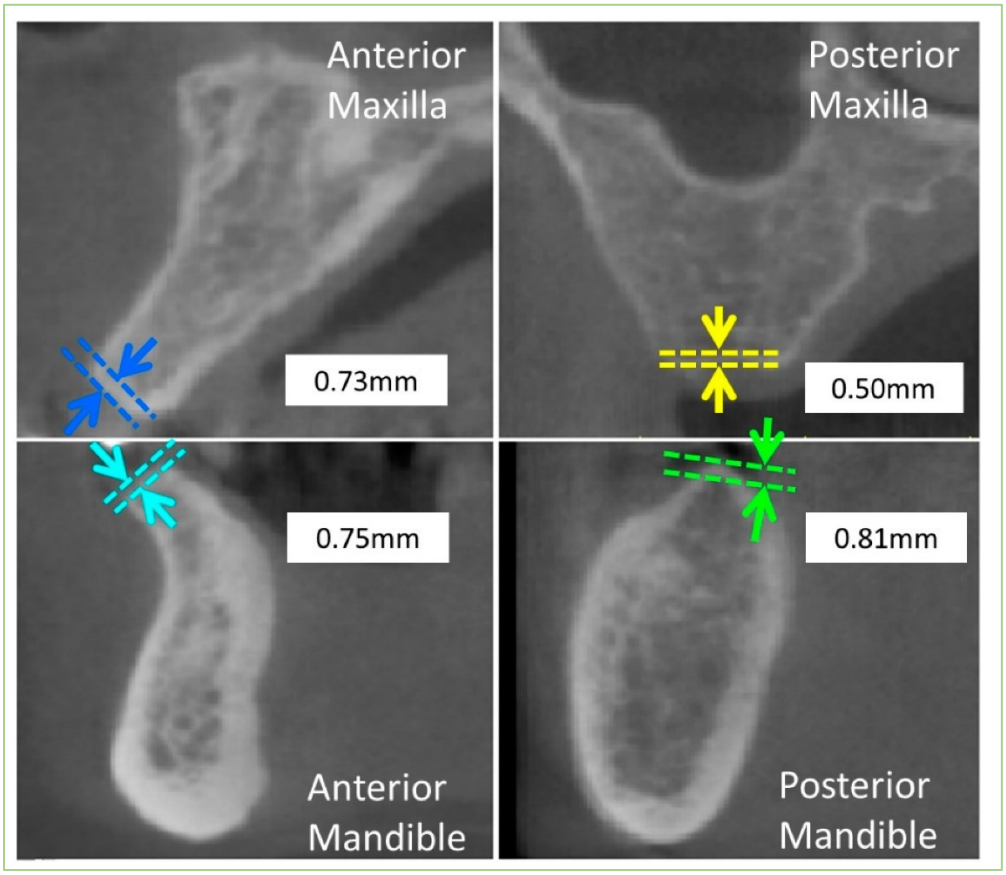

Figure 2.4: Cone Beam Computed Tomography Cross Sectional Images Displaying Cortical Bone Thickness at Implant Sites in the Four Jaw regions [48]

2.3.3 Osseointegration

Osseointegration is the process of bone forming around an implant to create a bond between tissue and synthetic material [6, 52, 53]. For successful osseointegration, this bond should be permanent over the life of a patient, and able to resist functional loading with no relative motion between bone and implant [5]. When an implant site is prepared and a hole is drilled into the bone, a healing

response is triggered in the body to repair this hole. When an implant is placed inside the socket, either new bone will heal up to the surface of the implant, or the space between implant and bone will be filled with fibrous tissue resulting in a loose or failed implant [54]. The successful osseointegration of an implant is determined by many factors where implant design, surgical technique, bone properties, and loading conditions all play an important role in implant success [55] [5].

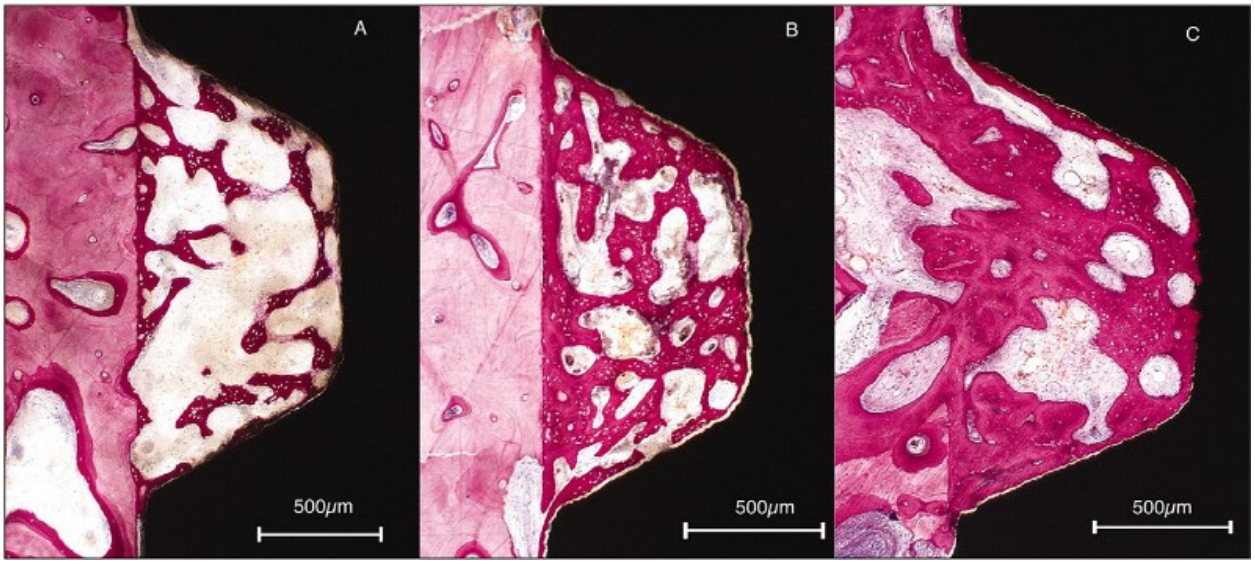

Figure 2.5: Histological Section of a Dental Implant Showing the Development of Bone Tissue. (a)Woven Bone Formation at 2 Weeks After Placement. (b) Bone Deposition at 4 Weeks After Placement. (c) Bone Remodelling at 8 Weeks After Placement [56]

The healing process of an implant can be divided into three stages: woven bone formation, bone deposition, and bone remodeling [6]. Each phase is shown in Figure 2.4. Much of the healing done in bone is the work of osteoblasts, which are cells that help regulate the structure of bone by producing the extracellular matrix, and then forming osteocytes, which are the bone cells [57]. Osteoblasts are complex cells that have receptors for many hormones and growth factors used to regulate the body. An initial blood clot allows cells to navigate around the void between the implant and the bone surface [6]. In the first 4 to 6 weeks after an implant surgery, osteoblasts are forming a scaffold of woven bone material (shown in Figure 2.5[a]) within the clot made up of mostly collagen fibrils and a vascular net. This tissue is able to grow rapidly and can span across a 1 mm void within a couple of days [6]. After 4-6 weeks, bone deposition starts within the

scaffolding. This new bone tissue (shown in Figure 2.5[b]) forms slower than the scaffolding and is more mineralized but can only form on an existing surface. The third stage of the healing process involves cells called osteoclasts [6]. Osteoclasts work together with osteoblasts by reabsorbing the extracellular bone matrix, which keeps the bone surface in equilibrium while slowly substituting the bone surface for new bone material (Shown in Figure 2.5[c]). This process is called bone remodeling and allows bone tissue to be optimized for external loading conditions [8, 6]. Bone remodeling improves bone quality by replacing the initial bone tissue with more mature bone and changing the dimension and orientation of the bone tissue.

2.3.4 Dental Implant Design

The design of a dental implant is focused on promoting osseointegration with the surrounding bone while transmitting the functional load from a crown or other dental prosthetic to the bone. The implant must have a mechanism of primary stability, a material that can transmit load and will not be rejected by the body's immune response, and a surface finish that encourages bone growth and osseointegration.

Figure 2.6: A Selection of the Different Designs of Dental Implants Available [58]

There are many designs that achieve these goals, as evident in the many types of dental implants available, some of which are shown in Figure 2.6. In a cylindrical or tapered implant, the two common methods of primary stability are threads, or wedge force around non-threaded implants. In either case, an implant must be securely embedded while also avoiding regions of high stress in the surrounding bone. Both high stresses and large implant displacements can be detrimental to the surrounding interface. High stresses can cause bone micro-fractures and inhibit the formation of the woven scaffolding [59]. This will cause the bone to be resorbed but stop any new bone from forming, which will lower the stability of the implant and could lead to failure. Greater strains in the tissue lead to the formation of fibrous tissue rather than bone tissue, which will prevent osseointegration and limit the secondary stability of the implant likely resulting in failure. Large displacements are the result of a lack of stability, which will also prevent woven bone scaffolding from forming between the bone and the implant resulting in similar fibrous encapsulation [9].

The material of the implant must be strong enough to withstand the functional loads of the mouth, but not so stiff as to cause stress shielding [59, 60]. Overloading an implant can cause fracture of the implant in rare cases but will more likely case high stresses in the bone as mentioned above [60]. Stress shielding occurs when a stiff material shares a load with a less stiff material. The stiffer material bears most of the stress and prevents the softer material from taking the load. Over time, without loading, bone tissue will remodel itself to be distributed efficiently according to its loading. If the bone is not loaded, it could cause atrophy, as the bone is resorbed and redistributed to locations of higher stress.

Implants with a rough surface finish have been shown to heal faster than those that are smooth [59, 61, 7]. Figure 2.7 Shows that the contact between the bone and implant is stronger on the surface blasted (rougher) implant (c), as opposed to the polished implants (a, b, d). This is likely due to the interaction between the initial blood clot, and the surface of the implant. The blood clot's retention to the implant surface is critical for the formation of tissue on the surface [62]. A rough surface will also increase the friction between the implant and the bone, increasing the primary stability. An implant could also be given a surface coating to facilitate healing. Titanium is a bio-inert material that does not interact chemically with living tissues. Bio-active materials such as a hydroxyapatite coating have been used to improve the bone deposition rate of the implant surface and form a strong chemical bond between the implant and the bone [63]. This form of coating also

has disadvantages, including the risk of delamination with the titanium implant, and the possibility of increased osteoclast bone resorption activity [63]. The surface material, and roughness can affect both the primary stability and the osseointegration of the implant.

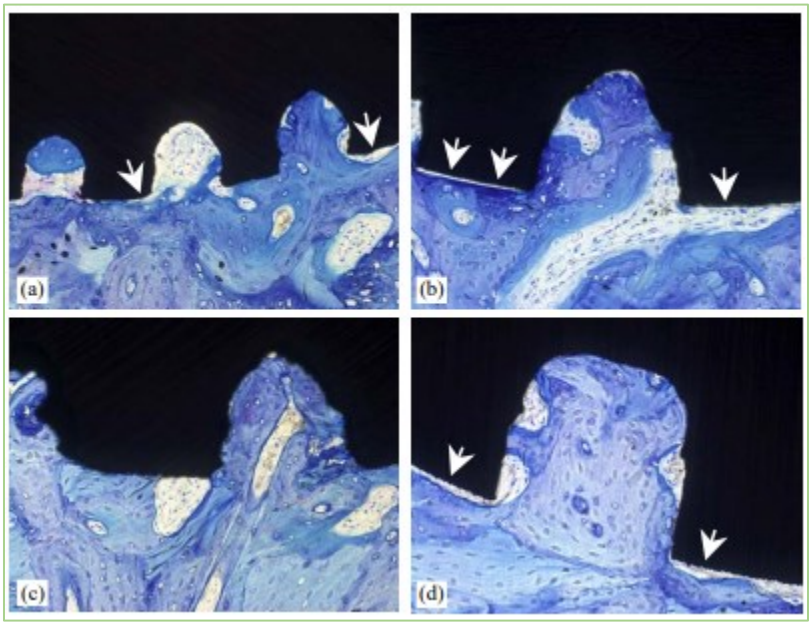

Figure 2.7: Bone Growth at 12 Weeks After Implantation of implants with (a) 100, (b) 200, (c) surface blasted 200, and (d) 300 nanometer pores. Arrows Highlight Visible Gaps Between Bone and Polished Implant Surface [7]

2.4 Evaluation of Implant Stability

There are over 147 dental implant manufacturers around the world [64]. With the number of implants and implant manufacturers constantly increasing, methods of evaluating and comparing the success of implants must be determined. The earliest criteria for implant success were proposed in the 1980's: [55]

- An implant should be physically able to connect to a functional prosthesis that was planned and accepted by the dentist and the patient.

- No pain, infection, or discomfort should be the result of the implant.
- Implants should be immobile when tested clinically.
- Mean bone resorption is less than 0.2mm annually after the first year of loading.

Some of these criteria lack specificity, quantifiability, and a continuous scale to compare the level of success of different systems [55]. A slightly more current paper from 2013 suggests that other important criteria are adequate width of attached gingiva showing soft tissue growth as well as osseointegration, and an absence of implant radiolucency (evidence of inflammation under the implant) along with the factors listed above [65]. Of these factors, the immobility of the implant and the bone resorption reflect the status of the osseointegration of the implant and the quality of the BII over time.

Bone resorption is typically measured using radiological examinations; however, these methods typically cannot show the bone in the buccal-lingual direction and expose a patient to radiation [10]. Computed tomography has been suggested as a method to evaluate bone loss in all directions, however this does not eliminate the use of radiation that the patient is exposed to [10].

One way to measure the osseointegration of the implant is to test the level of immobility, or the stability of the implant. The primary methods of implant stability testing can be separated into two categories: destructive, or non-destructive. Destructive methods include reverse torque tests and pull-out tests and are not recommended for clinical use because they damage the bone surrounding the implant [11]. For implant stability testing in patients, non-destructive tests must be used that rely on vibration analysis, or otherwise benign testing. The DMC (Dental Mobility Checker), Periotest, Osstell, and Penguin systems are three commercially available measurement devices that can evaluate implant stiffness [12, 11].

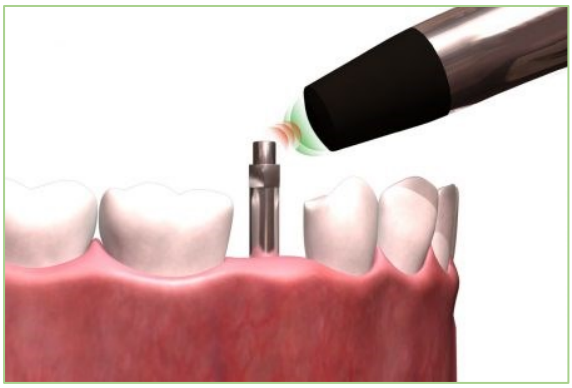

Figure 2.8: Osstell Mechanism Using an Electromagnetic Pulse to Excite a Transductor Attached to an Implant (from https://www.osstell.com/clinical-guidelines/the-technique-behind-osstell/#:~:text=Osstell's%20patented%20technology%20uses%20Resonance,frequency%20ch)

The Osstell and Penguin systems use electromagnetic impulses to stimulate transductors that can be mounted to the implant (Shown in Figure 2.8). The transductor and implant vibrate causing a lateral displacement that is then converted into an implant stability quotient (ISQ) between 0 and 100 with 100 corresponding to maximum stability [12]. These systems use resonant frequency analysis (RFA) to give a value for the stability of a system, with the idea that a stiffer system will have a higher resonant frequency. However, the natural frequency at which the implant vibrates is a function of the implant and transductor geometry and inertia parameters, which are not accounted for in these systems resulting in a measure that does not allow for comparison between two different implants.

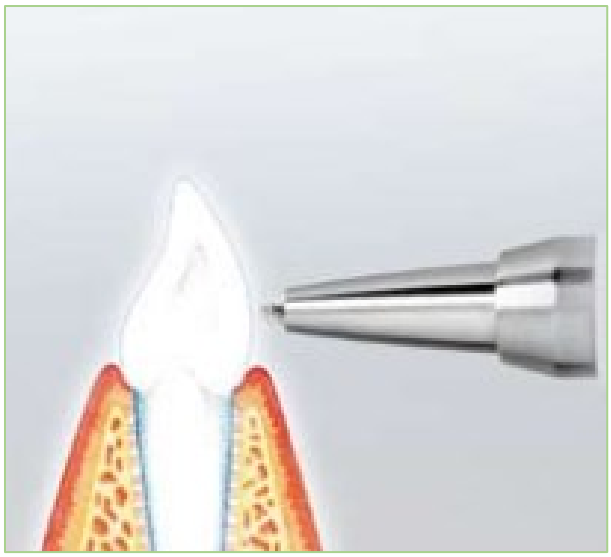

Figure 2.9: Periotest Mechanism Applying an Impact Load to Excite Vibration in a Tooth (from http://www.med-gulden.com/downloads/02_english/01_Productinformation/Periotest_procedure.pdf)

The Periotest system and DMC both use impact loading to excite a tooth or implant [11]. The DMC uses a small impact hammer to lightly strike a dental crown or tooth and measures the acoustic response using a microphone. The frequencies found in the signal give information about the rigidity of the BII. The Periotest strikes the abutment or dental crown with an electromagnetically driven rod contained in a handpiece (Figure 2.9). The acceleration over time of the rod is measured, and the contact time is used to calculate a Periotest Value (PTV) which is related to the stability of the implant. The PTV is based on the idea that a stiffer interface will result in a smaller contact time for the strike.

None of the currently available measurement systems sufficiently account for the geometry or inertia of different implants, even though the resonance frequency, contact time, and acoustic response are all influenced by the geometry and inertia parameters [11]. The limitations of currently available techniques led to the development of the Advanced System for Implant Stability Testing [13, 14, 66, 18, 17, 67] that is intended to account for implant geometry in its measurements, allowing the system to isolate the interface properties from the rest of the system.

2.5 The Advanced System for Implant Stability (ASIST)

The ASIST was developed at the University of Alberta to measure the stability of osseointegrated implants [13, 14]. The ASIST uses impact loading to excite an implant-abutment system, then measures the acceleration response of an impact rod in contact with the abutment. This response is compared to an analytical model accounting for the geometry and specific properties of the implant-abutment system to determine the interface stiffness that would create the measured response [14].

2.5.1 System Components

The ASIST hardware consists of a handpiece and an ASIST unit that connects by Bluetooth to a computer [14] shown in Figure 2.11. The handpiece contains an impact rod with an accelerometer, and an electronic mechanism for driving the impact rod to strike an implant-abutment system, and then reset the rod's position after each strike. The ASIST unit contains the hardware to control these mechanisms, record the acceleration data from the accelerometer, and transmit the data to a computer. When the button is pushed on the handpiece, the impact rod strikes 16 times in four seconds. The acceleration strike data is then transferred to a computer for analysis. The data collection software will filter and display all the 'valid' strikes of the implant. Strikes may be determined as invalid if there is movement in the patient or clinician, or a small error in the device's data collection systems. Since the ASIST takes 16 measurements in quick succession, all 16 measurements are expected to be very similar. A strike that is visually highly divergent (Figure 2.10) from the majority is typically treated as invalid.

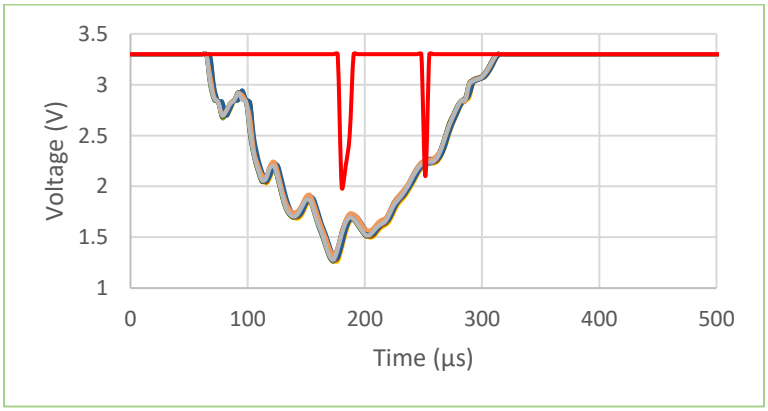

Figure 2.10: ASIST Measurement Containing 15 Valid Strikes and a Single Invalid Strike

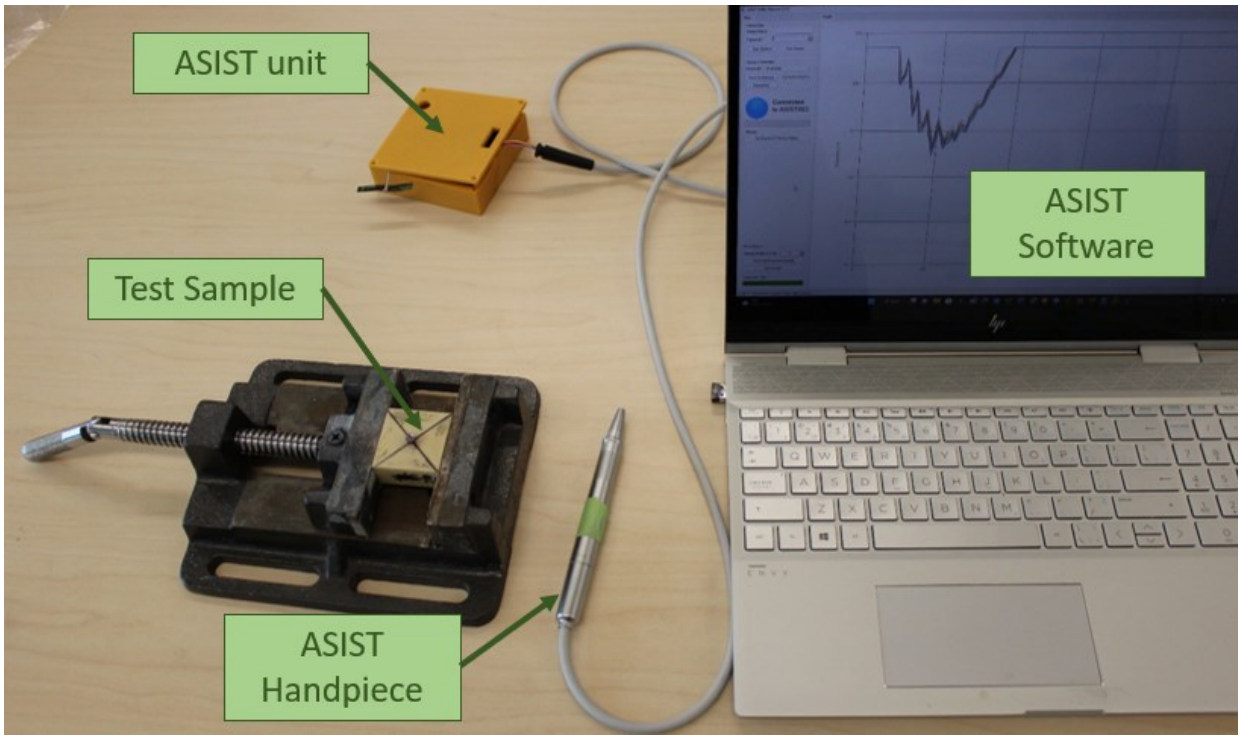

Figure 2.11: ASIST Components

2.5.2 ASIST Analytical Model

Once the strike data is collected using the ASIST unit, it is matched to an analytical model through numerical optimization [14]. The analytical model was first developed for bone conduction hearing aid implants [13] and has been adapted for dental implants as part of a parallel project [13]. The dental implant model will be briefly described here. The impact rod, implant, abutment, and BII are modelled as a four-degree of freedom (4-DOF) system. Figure 2.12 displays these components for a generic dental implant geometry. The implant and abutment are modelled as rigid bodies with masses (m_i and m_A) and moments of inertia (J_i and J_A) with a torsional spring with stiffness K_T connecting them. These bodies each have a center of mass (G_i and G_A), length (l_i and l_A), and diameter (D_i and D_A). The heights of the center of mass are labelled as y_i and y_A for the implant and abutment respectfully. To allow the analysis of tapered implants, a taper length l_t and taper angle β are incorporated into the model. The BII is represented as a stiffness k_i per unit area

surrounding the implant, and the impact rod is modelled as a massive particle connecting to the top of the abutment (site of impact) by a linear spring with an impact stiffness value (K_{impact}). Viscous damping is included only at the BII and is assumed to be negligible elsewhere.

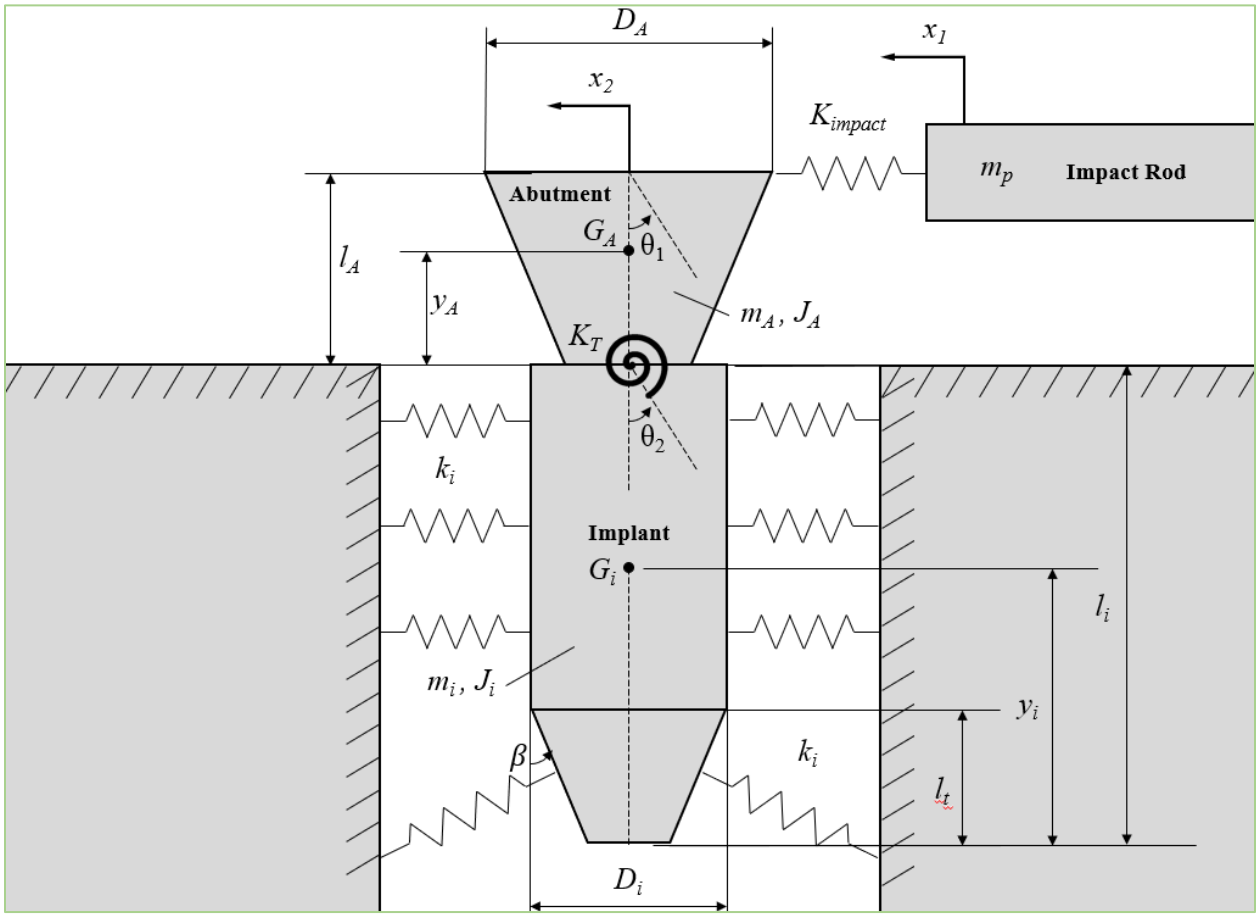

Figure 2.12:Schematic of the 4-DOF model of the Dental Implant and Abutment System

The four coordinates used to describe the motion of an impacted implant are: the displacement of the impact rod (x_1), the displacement of the center of the abutment at the height of the impact rod (x_2), the rotation of the abutment (θ_1), and the rotation of the implant (θ_2). The measured signal corresponds to the acceleration of the impact rod ($\ddot{x}_1$). The equations of motion of a 4-DOF system are:

$$[M]\{\ddot{x}\} + [C]\{\dot{x}\} + [K]\{x\} = 0$$

Where $[M]$, $[K]$, and $[C]$ are the mass, stiffness, and damping matrices that account for the geometry and mass properties of each implant and abutment, varying torsional, impact, and

interface stiffnesses for each system, and the damping due to energy loss into the BII and surrounding material. The complete matrices are given in Appendix A. When an acceleration response is recorded from an impact, it is processed using a custom Mathematica program (Wolfram Mathematica 10, Champaign, IL, USA). An example response is shown in Figure 2.13 in yellow. A two-term sinusoidal function is created, and curve fitted to the data using initial estimates for the first and second frequencies, amplitudes, and phases angles. This function (shown in red in Figure 2.13) is used to provide an estimate of the amplitude and damping in the response. Finally, the measured response is fit to the analytical 4-DOF model (shown in black). From the stiffness matrix in the analytical model, an appropriate BII stiffness value can be found and then converted to the form of an ASIST Stability Coefficient (ASC). This value takes in to account the individual parameters of each implant and should allow direct comparison of the stability for varying geometries. The interface stiffness per unit area is found with the units of N/m^3 . This value is dependent on the surface area of the implant and is converted to the ASC by the formula:

$$ASC = \frac{K_{eff}}{K_{nom}} = \frac{2l_i d_i k_i}{4 \text{ x } 10^6 \text{N/m}}$$

Where the numerator is the effective interface stiffness accounting for the surface area through the length and diameter of the implant, and the denominator is a nominal impact stiffness used to normalize the value and bring it to a range than can be easily interpreted in a clinical setting [14].

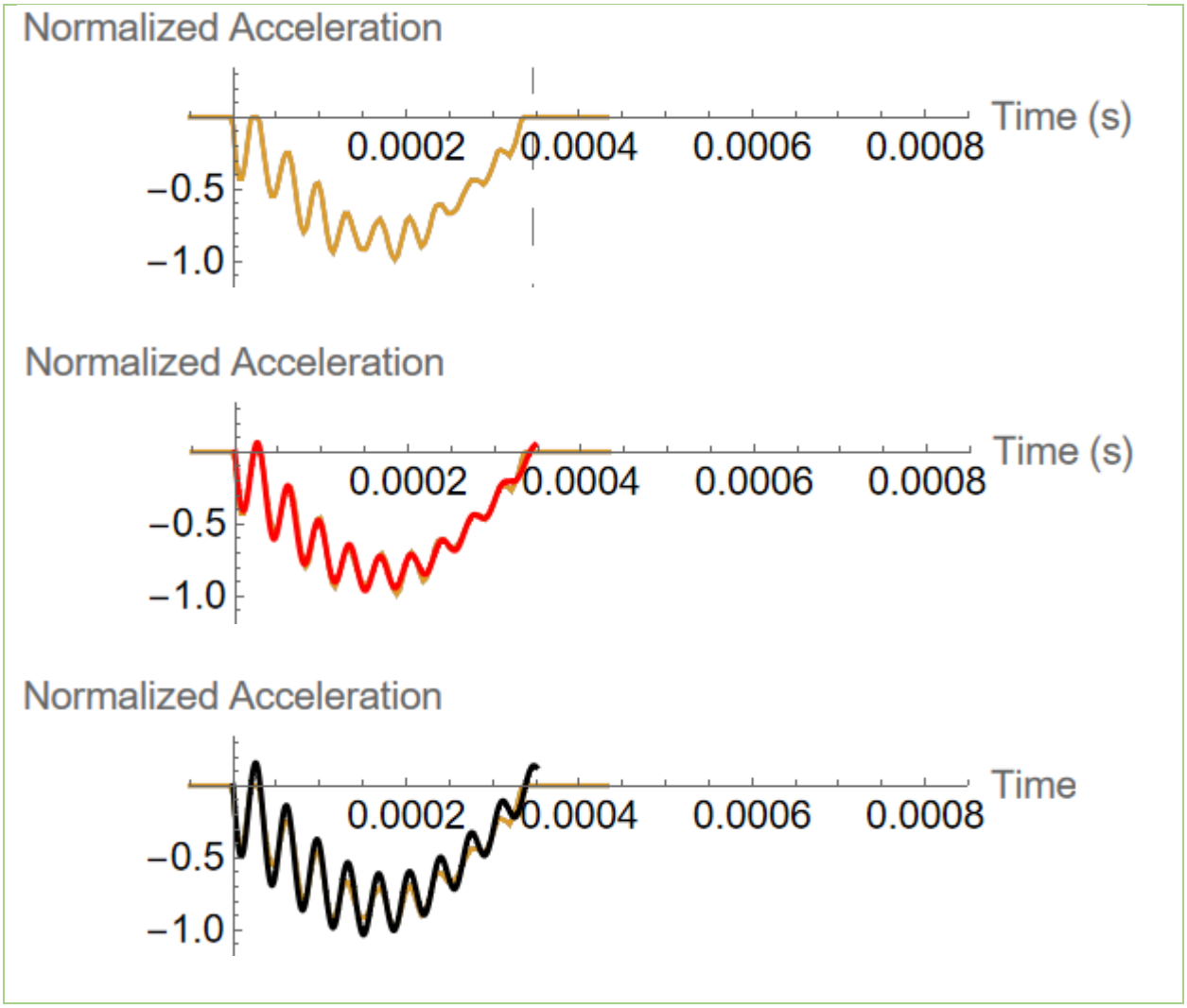

Figure 2.13: Two Step Curve Fitting Process of the ASIST. Acceleration Response is Shown in Yellow, Curve Fitted Function in Red, and Analytical Model in Black.

2.5.3 Validation of the ASIST

The ASIST was originally designed and tested using bone anchored hearing aid (BAHA) implants [13], but has since been tested on teeth [66], transfemoral implants [17], and currently dental implants. When tested on single rooted teeth, the analytical model was adjusted to use a single rigid body with simplified tooth geometry, and CBCT scanned geometry. There was a good match between the two data sets indicating that a simplified model could accurately represent the clinical system. The analytical model was able to accurately fit the experimental data indicating an accurate

representation of the interface between tooth and bone. The ASC found for natural tooth can be used to compare the stability of different teeth or monitor changes in tooth stability.

With respect to the BAHA implants, the ASIST has been used for a one-year longitudinal study [67], compared with stability measurements from the Osstell method [15], and verified with an FE Model [18, 68]. In the longitudinal study, the ASIST was able to make a good match between the analytical model and the measured acceleration data [67]. There was evidence that differences in the stability could be detected between surgical techniques, and implant designs. The study also gave evidence to show that the ASC could be used to show the healing patterns of implants over time. By comparing the ASIST to the already developed Osstell system, the device was further validated [15]. The ASIST was more sensitive to changes in the BII than the Osstell and less sensitive to the BAHA implant and abutment geometry. The ASC gave a measure of stability that was unbiased by abutment geometry allowing measurements from different designs to be more accurately compared. An FE model was developed of a BAHA implant system that showed the possibility of modelling the ASIST, the sensitivity of the measurement to the interface conditions, and the insensitivity of the measurement to the length of the abutment. The model also indicated that the implant stability relied on the bone properties as well as the BII properties [68].

2.5.4 The ASIST and Dental Implants

Recently, the ASIST has been tested for use with dental implants [16, 69]. The advantage of the ASIST for dental implants compared to commercially available techniques is that a clinician could use the ASIST to measure implant stability without removing the permanent dental crown and the ASC would still be a meaningful measurement of the degree of healing that accounts for the crown and system geometry. By including information about the system, the BII can be effectively isolated, and the ASC is directly related to the interface.

Benchtop experimental data has been collected with Straumann dental implants installed in Sawbones polyurethane blocks [70]. To create a test sample, the block is prepared as if it were real bone according to the Straumann surgical manual [41]. A Straumann implant is then inserted into the block with an appropriate insertion torque (5-35 Ncm). An abutment is attached to the implant, and the block is held in place by a table clamp for experimental stability measurements, as shown in Figure 2.14.

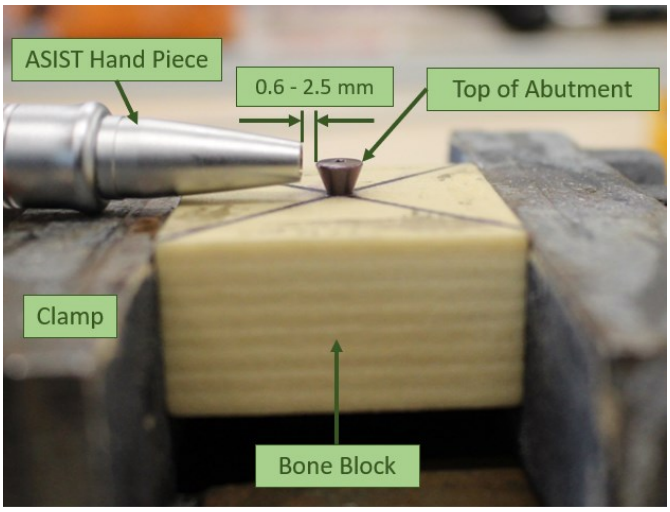

Figure 2.14: Test Sample of an RC Implant With 6mm Abutment in Sawbones 40pcf Polyurethane Foam

The ASIST handpiece is then held 0.6-2.5 mm away [71] from the top edge of the abutment and then used to strike the implant/abutment system perpendicular to the clamped surface. This process has been repeated for two different Straumann bone-level implants (RC [Regular CrossFit®] 4.1 mm diameter and NC [Narrow CrossFit®] 3.3 mm diameter) that are 10 mm in length. Two abutment types have been used for each implant (healing abutment [HA] 6 mm and HA 4.5 mm for the RC implant and HA 3.6mm and HA 3.3 mm for the NC implant). Each abutment is classified by its diameter at the top of the abutment. These implant/abutment combinations were implanted into five different densities of Sawbones artificial bone block (40, 30, 20 and 10 pcf and a composite block of 20 pcf with a 3 mm layer of 50 pcf on top) which were all tested with the ASIST. Three dental crowns were also acquired and measured in each of the block densities. The experimental benchtop data from the ASIST measurements with these Straumann dental implant models are compared to the FE model results presented in this work.

2.6 Finite Element Modelling of Dental Implants

Finite element modelling has previously been used to explore the behavior of dental implants in the areas of resonant frequency analysis [72, 73, 74], static stresses and strains in the surrounding bone [75, 74], and dynamic response of an implant/abutment system [76, 73]. Studies done to examine the resonant frequencies of implants found notable changes in the vibration of the

implants sensitive to the interface conditions between the implant and the bone [74, 72, 73]. Devices such as the Osstell use the resonant frequency as a measurement of stability, however, this method was shown to have disadvantages such as the effects of the jawbone geometry and implant location on the frequency [73]. This model was also used to show how adding an Osstell SmartPeg changes the natural frequency of the system. In another model, the resonant frequency analysis method of the Osstell System was compared to Periotest measurements based on contact time of an impacting mass to show good correlation between the two measurements at varying levels of osseointegration [72]. Each of these studies used a bonding layer between the implant and the bone with properties that were varied to simulate the osseointegration process.

In the studies examining the stresses and strains in the surrounding bone, the threads of the modelled implants were key features of the model since they transferred the applied force from the implant to the bone. These studies did not use a bonding layer, but used either a friction contact to simulate changes in BII development [74], or only examined the strains caused by the threads in a direct with the bone [75]. Using FEA, these studies found that the highest stress concentrations were typically near the first thread at the top of the implant, the maximum stresses are decreased as osseointegration develops, and surgical methods can affect the installation and removal torque of an implant.

Some studies have been done to examine the dynamic response of dental implants [76, 72]. These studies both used heavily simplified implant and abutment geometries embedded in simplified sections of bone material. The response of the implant to either an impact [72] or initial displacement [76] was examined for different levels of osseointegration modelled by the material properties of the surrounding material. These studies showed that the dynamic response of the model changed significantly with respect to changes in the BII and that there was useful information present in those responses to investigate the healing process of the BII.

2.7 Summary

The evaluation of dental implant stability is an important process to monitor the osseointegration process, and the long-term health of an implant. Measuring this stability can be done using many methods but no currently available methods sufficiently account for the geometry or inertia of different implants and abutments. The ASIST has been designed to measure the response of an

implant/abutment system undergoing an impact load and isolate the stiffness of the BII using an analytical model that accounts for the physical properties of the system. This system consisting of the ASIST handpiece, dental implant and abutment, and surrounding substrate (bone simulant; Sawbones Pacific Research Company) has been simulated in a dynamic FE model to investigate the ASIST's sensitivity to the material properties of the BII, implant and abutment geometry, and sample preparation techniques.

The FE model used a simplified implant/abutment geometry connected to a rectangular bone block with a bonding layer to represent the BII. The acceleration of an impact rod striking the implant was extracted as an output similar to a response recorded by the ASIST. The dynamic response collected from the model was then compared to responses collected experimentally by the ASIST in a parallel study to validate the model. The model was used to examine variation in the response caused by factors related to sample preparation. Models were made to predict the response for clinically relevant cases of bone resorption, an attached dental crown, and a composite bone substrate. The FE model provides deeper understanding of the ASIST method and its sensitivity to experimental and clinical parameters.

Chapter 3 : Development of Finite Element Model

This thesis presents the development of an FE model for the Straumann bone-level dental implants under low-force impact loading to simulate the ASIST approach for monitoring dental implant stability. This chapter presents the initial model development for the RC 4.1 mm implant and 6 mm healing abutment and model validation with experimental benchtop data.

3.1 Geometry

The implant and abutment geometry were modeled as solid bodies using Solidworks CAD software (Dassault Systèmes) (Figure 3.1). Dimensions for the implant and healing abutment were measured from implant/abutment samples supplied by the manufacturer (Figure 3.2) using a digital caliper. To simplify the model geometry and reduce computational time, the implant and abutment were modelled as a single unthreaded part. The actual threaded connection between the abutment and the implant is modeled as a torsional stiffness in the ASIST analytical model. However, the effect of this feature has been shown to be small where the two bodies tend to behave as a single rigid body. As a result, this connection was neglected in the FE model discussed here and the two parts were modeled as a single body [18]. The outer threads of the implant serve to anchor the implant to the bone and create space and surface area for bone growth. However, the detail of the threads was neglected in the model here to reduce the computational time in the dynamic simulation. A similar approach has been followed in previous work for BAHA implants and has been shown to provide a good representation of the dynamic response of the physical implant/abutment system [68, 18].

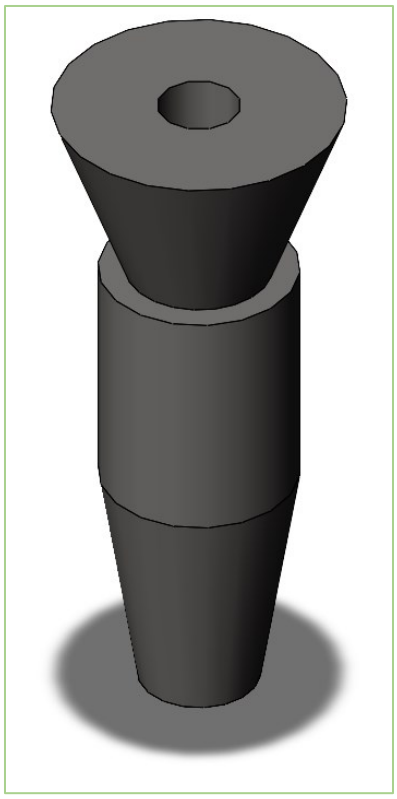

Figure 3.1: Simplified Implant and Abutment Model

Figure 3.2: Straumann Bone Level RC 4.1mm Implant (Right) and 6mm Healing Abutment (Left)

The hole at the top of the abutment was simplified to a circle rather than a torx screw-driver shape to retain mass properties but eliminate extraneous edges. Since the system was symmetrical, the entire system was "cut" in half (as shown in Figure 3.3) to further reduce computation time where a symmetry boundary condition was applied on the cut face in the FE software.

The bone block used in experiments was modelled as a 40 mm × 40 mm × 20 mm cuboid with constant density. Since the implant model was unthreaded, an interface layer was also created to represent the implant-substrate interface (or the BII in clinical applications). The interface layer was modelled to fit perfectly into a hole in the bone block and have a hole for the implant to fit perfectly into (Figure 3.3).

The final component of the model was a 15 mm long cylinder with 2 mm diameter representing the impact rod from the ASIST. The impact rod was modeled as a much shorter cylinder than the actual rod in order to reduce computational time. In order to maintain the correct mass for the part (and proper simulation of inertia parameters), the density of the modeled part was increased compared to the nominal value as described in the next section. In the hand piece of the ASIST, this is propelled by a solenoid, which is not directly connected to the rod. This rod also contains an accelerometer for collecting measurements. The geometry of any attached accelerometer was ignored for this model as it is physically contained within the impact rod. Each part was assembled in Solidworks with the implant and interface fitting into the bone block, and the impact rod lying horizontal and contacting the top edge of the abutment as shown in Figure 3.3. The assembly was imported into ABAQUS (Dassault Systèmes) for FE analysis.

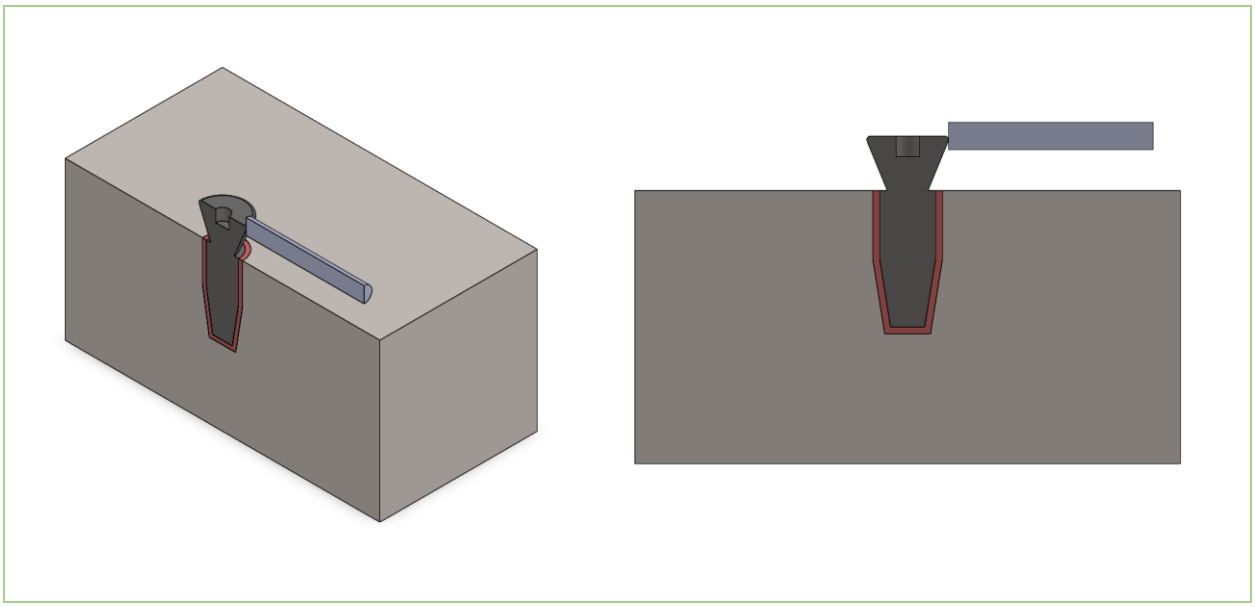

Figure 3.3: Implant Assembly

3.2 Material Properties

The material properties defined for the system were density, Young's modulus, and Poisson's ratio using a linear elastic and isotropic material model. The bone blocks used in the laboratory experiments were Sawbones Solid Rigid Polyurethane Foam (Sawbones, Pacific Research Company). Several different densities were available for testing but for initial modelling, the 40 pcf foam was used [70]. The density was reported by the manufacturer as 0.64 g/cm^3.The Poisson's ratio was assumed to be 0.3 since the value was not reported by the manufacturer and similar solid foam material has a reported Poisson's ratio between 0.30 and 0.32 [77].. Separate modulus values were reported by the manufacturer for tension (1000 MPa) and compression (759 MPa), so an average value of 879.5 MPa was used.

For the titanium implant/abutment, the mass of the part was more important than the actual density of the material in order to accurately model the inertia properties in the dynamic simulation. The physical components were weighed on a mass balance and the density was determined by dividing the target mass by the Solidworks calculated volume. The density was 4.506 g/cm^3, which was very close to an average of value reported for commercially pure titanium of 4.54 g/cm^3 [78]The

average Young's modulus and Poisson's ratio for titanium were determined from material datasheets as 116000 MPa and 0.34, respectively [79].

The impact rod of the ASIST was known to be made of stainless steel, so a Young's modulus of 193,000 MPa and Poisson's ratio of 0.27 were applied [80]. Similar to the implant/abutment, the mass of the rod was more important to model accurately than the density. The mass of the rod has been previously reported as 9.4 g [14, 13] or 4.7 g for the half rod model), so the density was calculated to be 200 g/cm^3. Note that this is much larger than the reported values for stainless steel (7.48 – 8.0 g/cm^3) [80] because the simulated impact rod was much shorter than the actual rod.

The material properties of the interface layer were initially set to the type of super glue used (Instant glue (Metal), CECCORP) and then adjusted to examine the change in response. The initial values for density, Young's modulus, and Poisson's ratio were 1.07 g/cm^3, 1.26GPa, and 0.17, respectively [81].

3.3 Contact Definition

The BII layer in the model is meant to simulate the interface material of the system as the growth of new bone into threads of an implant. The surfaces of the interface were tied to the surfaces of the bone block and the implant. The complex interaction between these components was modelled entirely by the material properties of the interface material. In both tie conditions, the stiffer material was selected as the master surface for the interaction. The implant was stiffer than the interface, and the interface was stiffer than the bone block (for the initial simulation, the system was being modelled as a fully integrated implant where the interface was very stiff). The interaction between the abutment and the impact rod was established as a hard contact, surface-to-surface, frictionless contact condition. The impact stiffness was naturally captured by the material properties of the impact rod and abutment.

3.4 Boundary Conditions

In the initial step, boundary conditions were created, and a predefined field was established. The outer faces of the polyurethane foam block were given an encastre condition (fully fixed) on two opposing sides simulating the hold of a clamp. A symmetry boundary condition was applied on

the “cut” face of the model. The impact rod was constrained in both non-axial directions simulating the constraints of the rod in the handpiece. An initial velocity of 200 mm/s was given to the rod along its axial direction towards the implant to simulate the strike of the impact rod [14].

3.5 Dynamic Explicit Step

With the boundary conditions in place, a dynamic explicit step was created to examine the acceleration response of the system over time. In experiments, 0.0005 seconds captured a full strike, so this was chosen as the duration of the step. The primary outcome variable measured from experiments is the acceleration of the impact rod. The average acceleration of the nodes in the impact rod in the x-direction (axial direction of the rod) was requested as a history output to compare with the data obtained from ASIST measurements. The time interval of the output was 3.4 microseconds to match the output of the ASIST for easy comparison. This resulted in a plot of the impact rod acceleration over the time of the strike. The ASIST data could be plotted in a similar way once the data was converted from voltage (measured from the device) to acceleration.

3.6 Mesh

Tetrahedral quadratic elements were used to mesh the model. Although quadratic elements add computation time, they can represent the curves of the geometry better than a linear element. A mesh dependence study was done to determine the size of elements and find the ideal balance between accuracy and computation time. The critical areas of the system (Figure 3.4) were the neck of the abutment and the interface between the impact rod and abutment, and so the mesh of both parts was refined. Some preliminary tests were done with local mesh refinement on the implant/abutment neck, but the differences in computation time between local refinement at the neck and global refinement of the part was low, and so the global refinement of the part was the chosen method.

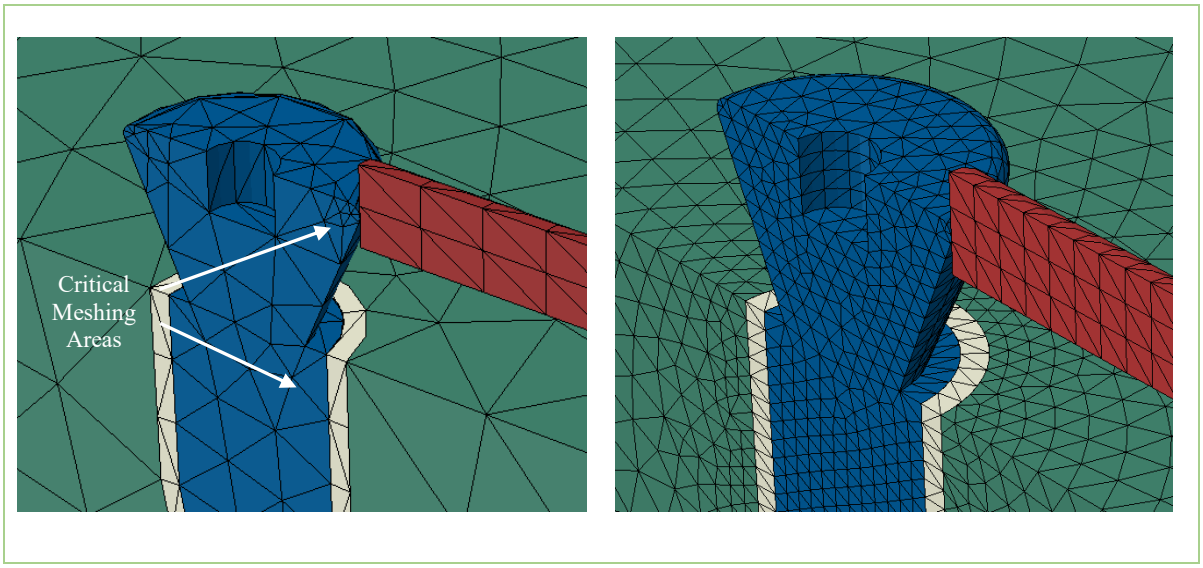

Figure 3.4: Mesh Refinement

The interface and edge of the bone block connected to the interface were also seeded to match the edge of the implant, and then the bone block was allowed to get coarser closer to the outer edges. The critical mesh seed was varied between 1.5 and 0.25 mm and the maximum acceleration of the impact rod in its axial direction was extracted as the converging variable. The maximum acceleration was plotting with respect to the mesh seed in Figure 3.5.

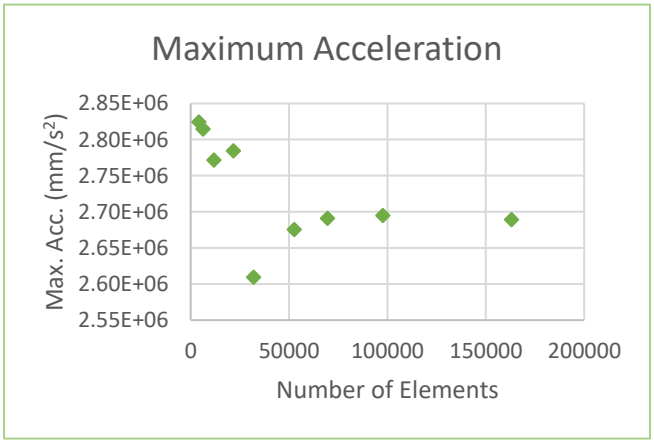

Figure 3.5: Maximum Acceleration of the Impact Rod as a function of Mesh Density

The acceleration appeared to converge within 1% after an element size of 0.4 mm when the number of elements was 52549. At this point, the acceleration was no longer a function of the mesh resolution so the element size at the critical areas was prescribed at 0.4 mm for the remaining simulations.

3.7 Comparison to Experimental Data

Four Straumann bone-level RC-4.1 mm implants were installed into Sawbones artificial bone blocks with the same dimensions as the geometry used in the model. 6 mm healing abutments were attached to each implant and each installation was measured using the ASIST. Acceleration versus time data from both the experiment and the FE model were used to obtain ASC measures using the ASIST analytical model described in Section 2.5.2 for comparison.

With each ASIST measurement, the impact rod strikes the abutment 16 times and records the acceleration response for each strike. Some strikes are automatically filtered out if they are too far outside of the possible response expectations. Each block was measured 5-6 times and all the valid strikes for each measurement were used to find the average ASC value. The experimental results are shown in Table 3-1 for each measurement taken on each block with the average of the 23 ASC measurements being 15.8 (SD = 1.4). Note that the four replicate bone blocks were meant to be identical; however, variations between the installations were noted as seen in Table 3-1. The average ASC values for each block, and the two most prominent vibration frequencies obtained from the analytical model are recorded in Table 3-2. The last row of Table 3-2 is the comparable values found from the acceleration response taken as an output from the FE model.

Table 3-1: ASC Measurements of an RC 4.1 mm Implant With 6 mm Abutment in 40 pcf Polyurethane Block

Experiment	Measured ASC Values						Average ASC	Standard Deviation
Block 1	16.3	16.5	16.5	16.4	16.5		16.4	0.1
Block 2	13.7	13.4	13.7	13.4	13.7	13.6	13.6	0.1
Block 3	16.5	17.1	17.5	15.9	15.8	17.2	16.7	0.7
Block 4	16.7	16.8	16.9	16.0	16.8	16.9	16.7	0.3
Average				15.8				1.4

Table 3-2: Comparable Values from Experimental and Model Data

Test No.	ASC	First Mode Frequency (rad/s)	Second Mode Frequency (rad/s)
Block 1	16.4 ± 0.1	14149 ± 36	194657 ± 979
Block 2	13.6 ± 0.1	13530 ± 57	191561 ± 2505
Block 3	16.7 ± 0.7	13943 ± 61	181030 ± 2632
Block 4	16.7 ± 0.3	14470 ± 51	199734 ± 750
FEA	15.7	13852	188737

It can be seen in Table 3-2 that each comparable value (ASC and both prominent frequency modes) found from the FE model is between the highest and lowest values from the experiments. This suggests that the FE model is able to provide a good representation of the dynamic behavior of the physical system. Comparison between the FE model response and experimental data can be better visualized in Figure 3.6 where the black line was generated from the impact rod of the model, and each colored line is a strike from the ASIST. The four colors represent the four replicate installations of the experiment, and each color has between 39 and 70 lines representing the individual valid strikes. The coefficient of determination (R^2) value for the model's acceleration response was 0.95 when compared to all the data showing excellent agreement between the two.

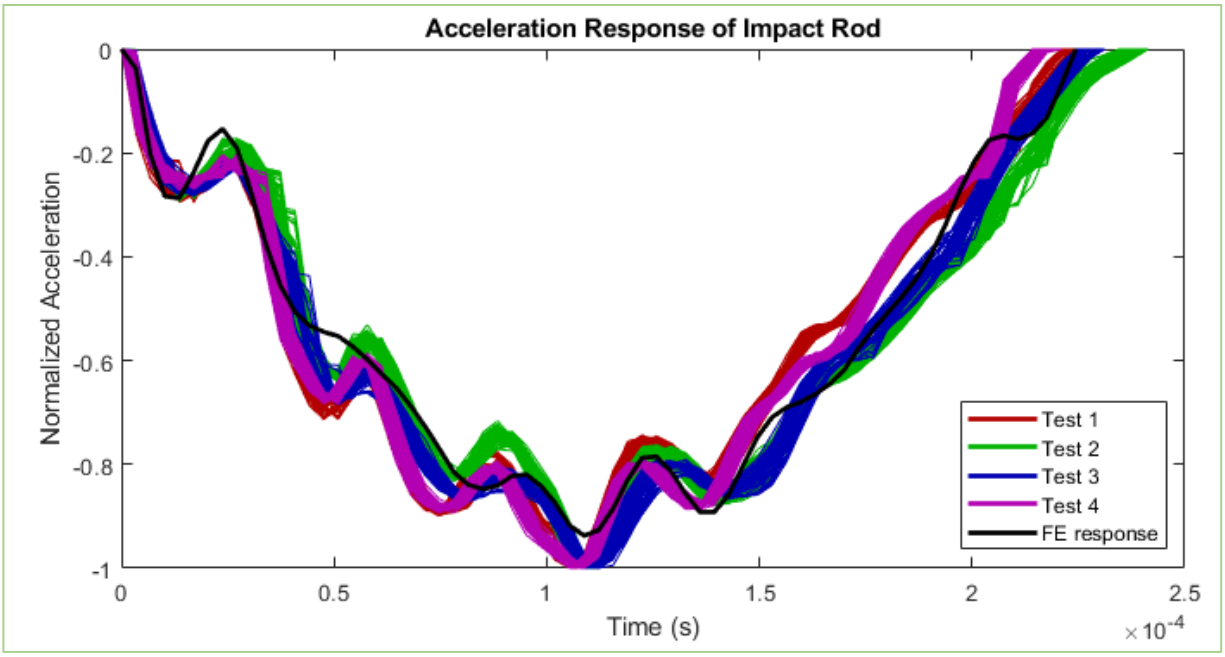

Figure 3.6 Comparison of Acceleration Responses of Finite Element Model and Experimental Data

3.8 Sources of Error

In this comparison, there are sources of error in both the ASC measurements taken from the bone blocks, and the ASC measurement from the simulation results. In the experimental measurements, error can occur in the creation of the test pieces. The implants were not inserted by professional dental surgeons, and so there may be differences between the installations in drilling the holes and installing the implants. To minimize variations, a torque wrench was used to insert each implant, and the process of drilling was controlled using a drill press and standardized drilling procedure. These samples were meant to represent second stage osseointegration and were held in by super glue. Because of slight differences in drilling, there may be different amounts of glue in each sample or possibly different amounts of surface contact in each sample. There may also be differences in the ASIST measurements due to the acceleration measurement process. A difference in the clamping direction, or in the angle at which the impact rod is held could affect the acceleration response. Sensitivity of the results to these two factors as well as drilling depth will be examined in the next chapter. Errors due to the handpiece accelerometer and recording hardware are not available to be examined here but could also contribute to differences in the measurements.

In the FE model, error could result from the simplification of the geometry of the model. The interface between the bone block and the implant was represented as a layer of solid homogeneous material, which differs from the real interaction of a threaded implant glued into a medium. The implant and abutment were modelled as a single piece, which differs from both the analytical model and the physical system where they are separate components. The contact definitions in the model also differ from the physical samples. Tying the implant into the medium, would remove any effect of insertion torque present in the sample. Since the displacement of the model was so small, each material was defined as linearly elastic with the Young's Modulus of the block defined as the average between the compressive and tensile modulus stated by the supplier. These assumptions may be small sources of error. The material properties of the implant (titanium) and the impact rod (steel) were obtained from a materials database which may not necessarily be accurate to the components used in the experiment. There are also sources of error that come from the FE method. The calculations are not exact solutions but depend on mesh refinement, mesh parameters, and calculation methods.

The last category of error is errors due to the numerical optimization approach to match the analytical model to the measured (or simulated) acceleration response and determine an ASC value. A custom Mathematica code is used to curve fit a solution to the mathematical model to the data. There is some error that is caused by differences between the data and the analytical model curve which may affect the final result. The result is the value of the interface stiffness used in the mathematical model that creates the curve closest to the inputted acceleration response. The relationship between this value and the inputted curve is complex, and it is difficult to directly compare the errors present in the acceleration response to the error present in the ASC value.

3.9 Summary

An FE model was developed for a single implant/abutment system and validated using experimental measurements. The geometry of the model was simplified by removing the threads of the implant and combining the implant and abutment into a single part. The dynamic model was set up to represent a single strike of the ASIST impact rod, and the acceleration response of the rod was extracted and compared to the experimental response. Variation between strikes in the experimental data was noted and will be investigated using the model in the next chapter.

Chapter 4 : Examining Variability in Similar Experiments using FE Models

The experimental acceleration responses that were compared to the FE model in Chapter 3 are replotted below (without the FE model response) in Figure 4.1. Some variability can be seen between each experiment. Even though each test was done on the same density of bone block, with the same model of implant and abutment, using the same implantation method, there are slight differences in the response that must be explained through other variables. This chapter aims to explain the range of variability in the experimental data by examining the effect of four main factors on a simulated response: the angle of the strike measured from the horizontal, the direction of the strike compared to the clamping force on the block, the depth of the hole drilled for the implant, and the thickness of the interface layer.

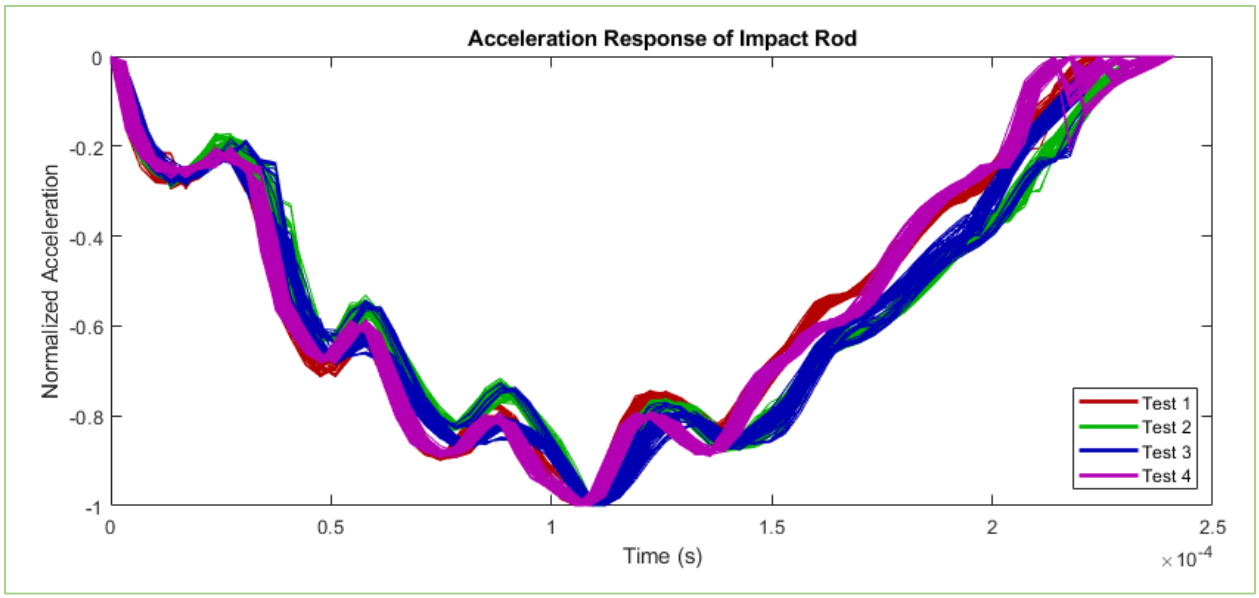

Figure 4.1: Acceleration Responses of Experimental Data

The four factors considered can all vary slightly between experiments, so it is important to understand their effect on the acceleration response and overall stability measure. The first two sources of variability are modelled by changing the striking angle of the impact rod and changing the surface of the clamping boundary condition, respectively. Variability in hole depth is modelled by decreasing the depth of the hole so that the implant protrudes slightly. The width of

the interface layer around the implant is also tested as a variable to determine if this affects the models results in this case.

4.1 Modelling the Factors

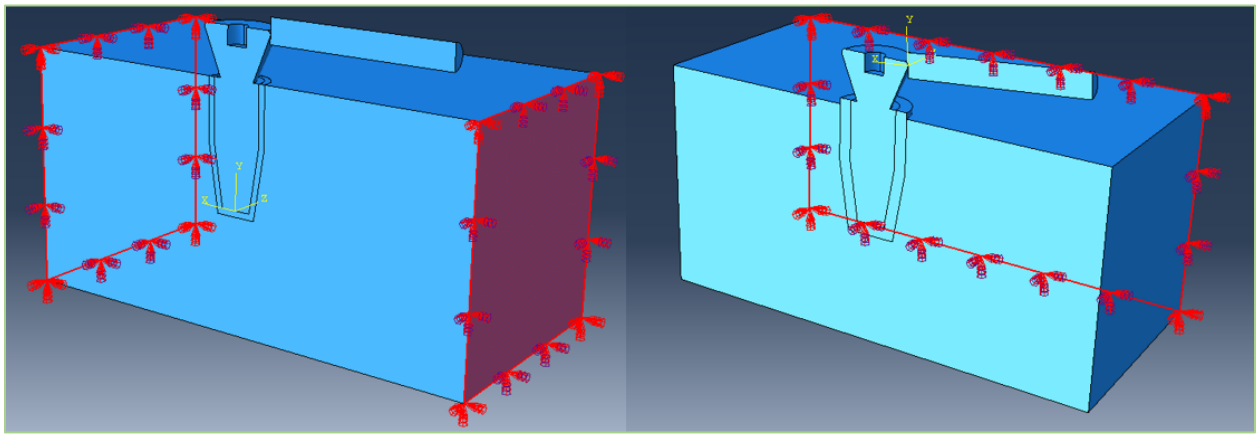

Figure 4.2: Simulation of Four Experimental Variables Each Modelled with a "Low" Condition (Left) and a "High" condition (Right)

This series of FE simulations was treated as a 2^4 factorial experiment. Each of the four factors were treated as binary with a “low” value (Figure 4.2 [Left]) and a “high” value (Figure 4.2 [Right]). This created an experiment with 16 simulations that could show if each variable had an effect on the output. The output of these simulations was an acceleration over time plot which was evaluated using a custom Mathematica code to extract an ASC value. The angle of impact was either 0 or 5 degrees, as this has been reported as the optimal range for ASIST measurements [82, 13]. The interface thickness was set as either 0.5 or 1.0 mm [72, 73] and the hole depth was such that the implant either fit perfectly or protruded 1 mm. The clamping direction was either perpendicular or parallel to the impact direction. In Table 4-1 below, each variable is given either -1 for the lower value or 1 for the higher value except for the clamping direction where -1 refers to the perpendicular direction and 1 to the parallel direction. The design of this experiment is shown geometrically in Figure 4.3.

Table 4-1:Factor Combination in Each Simulation

Simulation Number	FACTORS				Run Label
	Impact Angle (A)	Interface Thickness (B)	Hole Depth (C)	Clamping Direction(D)	
1	-1	-1	-1	-1	(1)
2	1	-1	-1	-1	a
3	-1	1	-1	-1	b
4	1	1	-1	-1	ab
5	-1	-1	1	-1	c
6	1	-1	1	-1	ac
7	-1	1	1	-1	bc
8	1	1	1	-1	abc
9	-1	-1	-1	1	d
10	1	-1	-1	1	ad
11	-1	1	-1	1	bd
12	1	1	-1	1	abd
13	-1	-1	1	1	cd
14	1	-1	1	1	acd
15	-1	1	1	1	bcd
16	1	1	1	1	abcd

Each combination of the high and low configurations of these variables was simulated once. Since each simulation is generated from a computational model, repeated simulations do not provide any additional information; we only have a single replicate for each case.

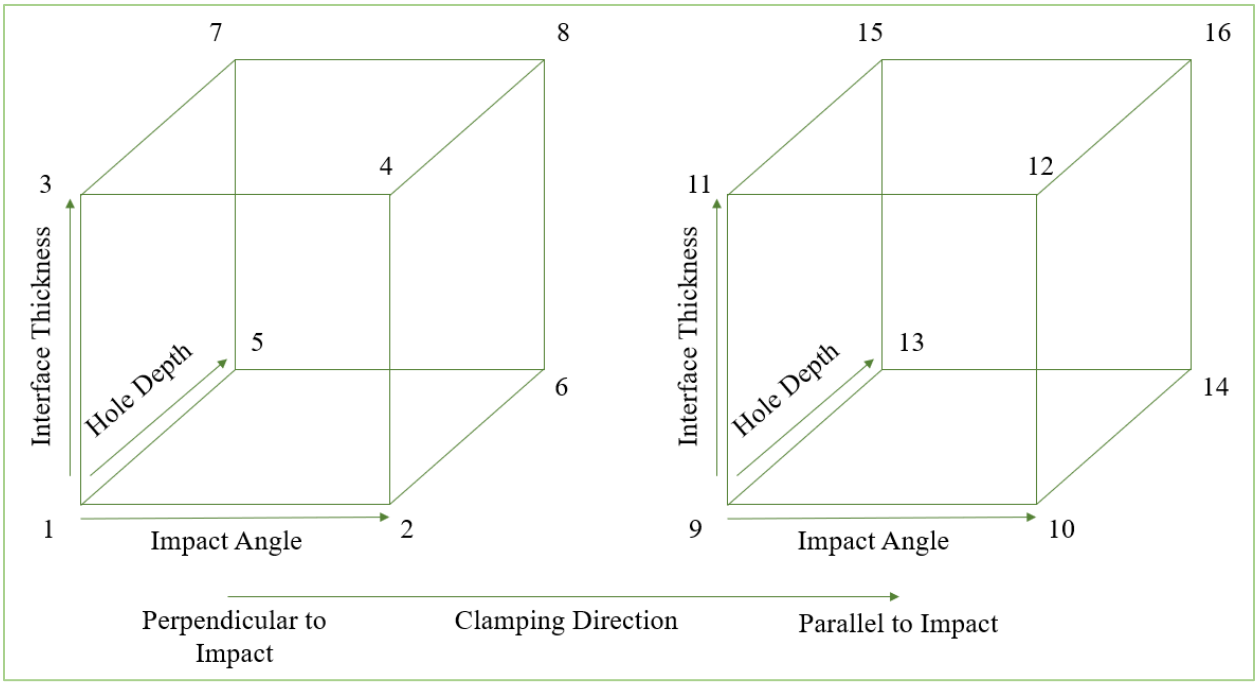

Figure 4.3: Design of Unreplicated Factorial Simulation Series

4.2 Results

The acceleration responses from the simulations are plotted in Figure 4.4. Each of the figures (a – d) shows the responses separated into the two configurations of a single variable to visualize the effect of that variable on the response. The most obvious difference is due to the clamping direction shown in Figure 4.4(d). Each of the responses with parallel clamping have a slightly longer contact time (i.e., lower first mode frequency) and a slightly lower amplitude. Implant protrusion also appears to result in a longer contact time, but a higher impact angle may result in a shorter contact time. The interface thickness does not appear to have a large impact on the result.

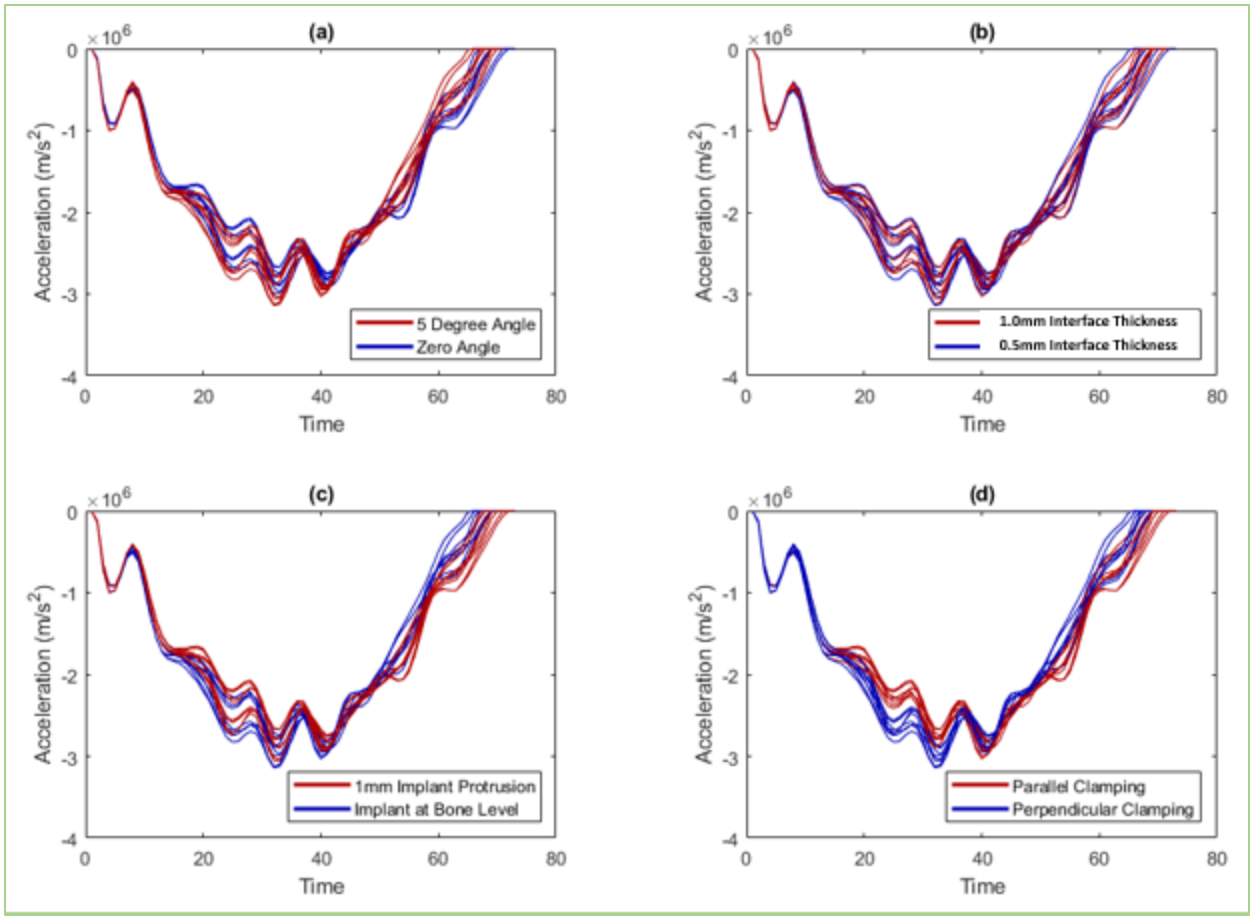

Figure 4.4: Acceleration Responses Extracted from Simulations to Show Variation due to Each Variable. a) Impact Angle. b) Interface Thickness. c) Implant Protrusion. d) Clamping Direction.

Each response was curve fitted using a custom Mathematica code to extract an ASC value that estimates the stability of the implant. These values are shown in Table 4-2 for each simulation. From these values, we have a range of ASC values that can be explained by human error/inconsistency in experiments. This range is 11.5-18.9 for this set of parameters. The range of ASC values from the experimental tests is 13.6-16.7, which falls within this predicted range.

Table 4-2: ASC Results of Simulations of Variability in Experiments

Simulation Number	Run Label	Impact Angle (degrees)	Interface Thickness (mm)	Protrusion (mm)	Clamping Direction	ASC
1	(1)	0	0.5	0	Perpendicular	15.7
2	a	5	0.5	0		18.9
3	b	0	1.0	0		16.0
4	ab	5	1.0	0		17.5
5	c	0	0.5	1		13.4
6	ac	5	0.5	1		15.1
7	bc	0	1.0	1		13.7
8	abc	5	1.0	1		15.6
9	d	0	0.5	0	Parallel	13.2
10	ad	5	0.5	0		15.2
11	bd	0	1.0	0		13.3
12	abd	5	1.0	0		14.5
13	cd	0	0.5	1		11.5
14	acd	5	0.5	1		12.6
15	bcd	0	1.0	1		11.8
16	abcd	5	1.0	1		12.9

The effects of each variable and each interaction of variables was calculated and reported in Table 4-3. From these values, the normal probability plot of the effects was generated (Figure 4.5) to determine which factors were significant. The points A, C, and D (corresponding to impact angle, hole depth, and clamping direction) lie far from the fitted line, and so they are significant. Since the interface thickness (B) is not a significant factor, this experiment can be treated as an experiment with three factors and two replicates. The second replicate comes from the samples with all the same factors but a different interface thickness.

Table 4-3: Factor Effect Estimates and Sums of Squares for Variation Between Experiments

Factor	Effect Estimate	Normal Probability (Z-Value)	Sum of Squares	% Contribution
A	1.713	1.834	11.731	19.082
B	-0.037	0.000	0.006	0.009
C	-2.213	-1.282	19.581	31.852
D	-2.613	-1.834	27.301	44.410
AB	-0.288	-0.728	0.331	0.538
AC	-0.263	-0.524	0.276	0.448
AD	-0.363	-0.967	0.526	0.855
BC	0.387	1.282	0.601	0.977
BD	0.038	0.341	0.006	0.009
CD	0.363	0.967	0.526	0.855
ABC	0.338	0.728	0.456	0.741
ABD	0.087	0.524	0.031	0.050
ACD	0.013	0.168	0.001	0.001
BCD	-0.087	-0.168	0.031	0.050
ABCD	-0.138	-0.341	0.076	0.123

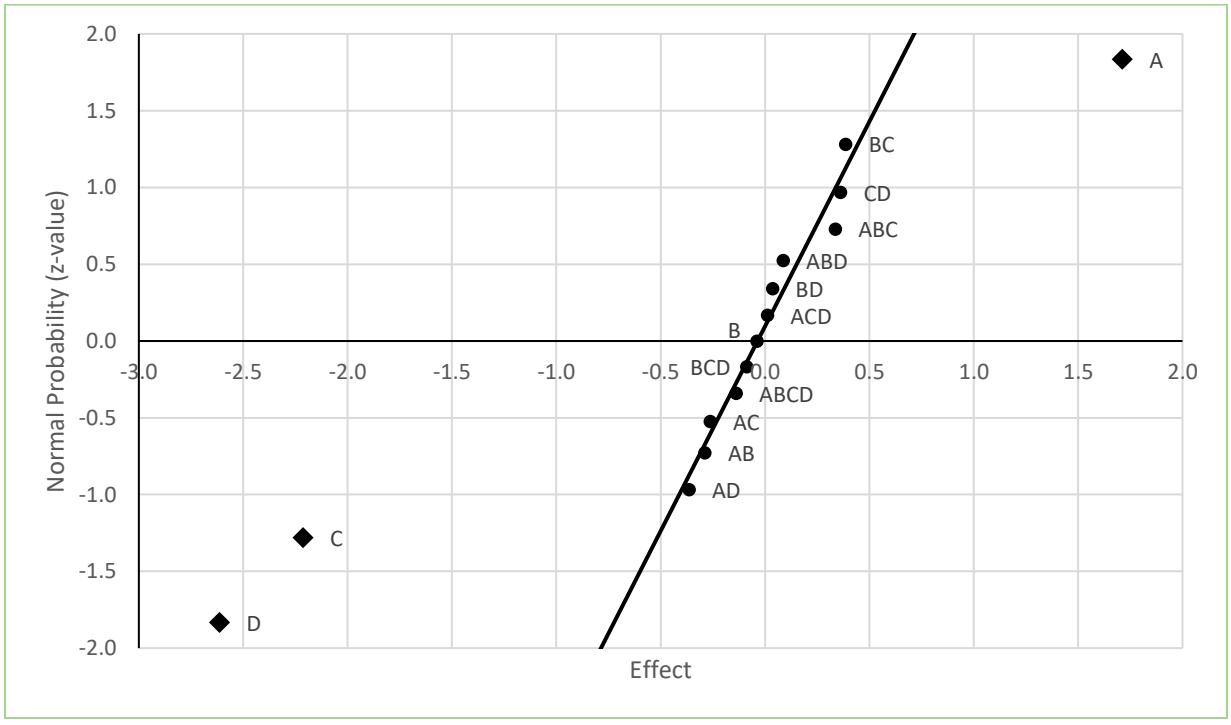

Figure 4.5: Normal Probability Plot of the Effects for the Variation Between Experiments

The new effects, and contributions were calculated for the three significant variables and their interactions in Table 4-4. Factors A, C, and D are still significant with high contributions to the ASC value, while none of their interactions are significant.

Table 4-4: Factor Effect Estimates and Sums of Squares for Variation Between Experiments (Ignoring Interface Thickness)

Factor	Effect Estimate	Normal Probability (Z-Value)	Sum Of Squares	% Contribution
A	0.856	1.465	11.731	19.082
C	-1.106	-0.792	19.581	31.852
D	-1.306	-1.465	27.301	44.410
AC	-0.131	0.000	0.276	0.448
AD	-0.181	-0.366	0.526	0.855
CD	0.181	0.792	0.526	0.855
ACD	0.006	0.366	0.000625	0.001

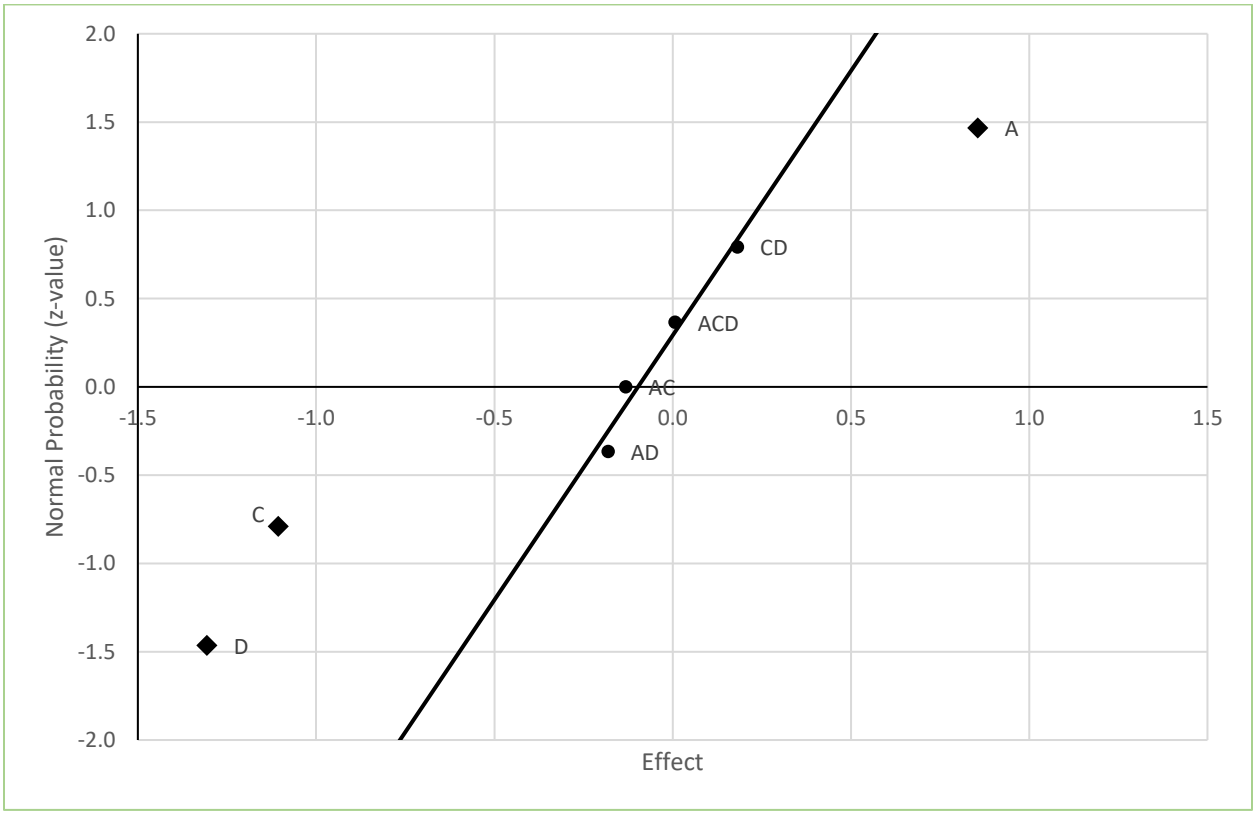

Figure 4.6: Normal Probability Plot of the Effects for the Variation Between Experiments (Ignoring Interface Thickness)

The average ASC values for the high and low of each condition are plotted in Figure 4.7. The simulations predict the largest difference to be due to a difference in clamping direction. Changing the clamping from perpendicular to parallel, could increase the measured ASC value of the same system by 2.6 (Figure 4.7[c]). An improperly drilled hole in which the implant protrudes by one millimeter could decrease the ASC value by 2.2 (Figure 4.7[b]) and striking the abutment at an angle of 5 degrees could increase the ASC value by 1.7 (Figure 4.7[a]).

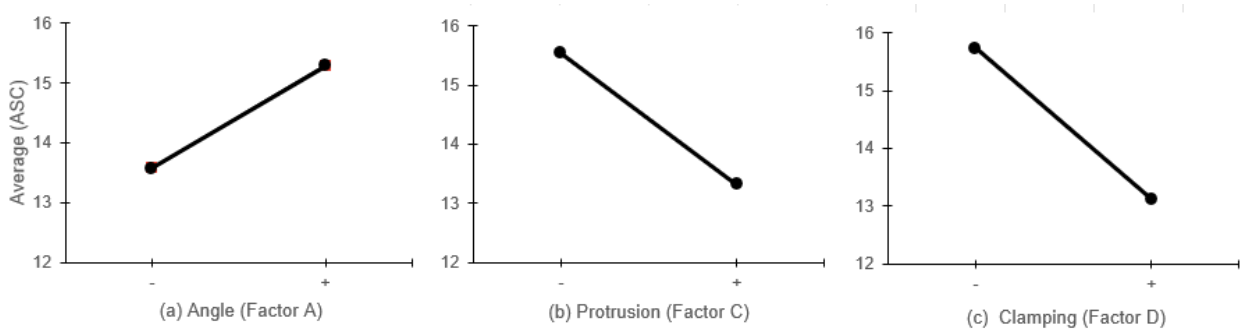

Figure 4.7: Main Effect Plots for (a) Impact Angle. (b) Protrusion. (c) Clamping Direction.

4.3 Discussion

The ASC measurements from the ASIST for this particular experiment (RC 4.1 mm implant with 6 mm healing abutment implanted into 40 pcf polyurethane block) have a mean and standard deviation of 15.8 ± 1.4. These experiments were all reported as being done with a 0-degree angle, no implant protrusion, and being perpendicularly clamped. The mean value of all four experiment runs agrees well with the simulation value of 15.7, however each block has its own average that may not agree with this value. Figure 4.8 shows the measured ASC values for each round of strikes from the ASIST. The means for each testing block are shown in different colours. Since the implants are not inserted by professional dental surgeons, and the recommended angle for the ASIST handpiece is between 0 and 5 degrees, it is possible that the implants have some small level of protrusion, and the impact rod has some non-zero angle. The mean of block 2 is lower than the others. This could possibly be explained by the implant protruding slightly from the surface of the block. It could also be that the block was mistakenly clamped in the parallel direction for these experiments. The remaining results on the remaining blocks are all slightly above the mean, and above the value predicted by the initial simulation. This could be explained by a slight impact angle due to the device being handheld, or the geometry of the hand piece preventing a perfectly

horizontal strike. If a simulated 5-degree angle resulted in a change of 1.7 to the ASC, then angles close to this would explain the difference between the simulated value of 15.7, and the measured values of the ASC ranging between 15.8 and 17.5.

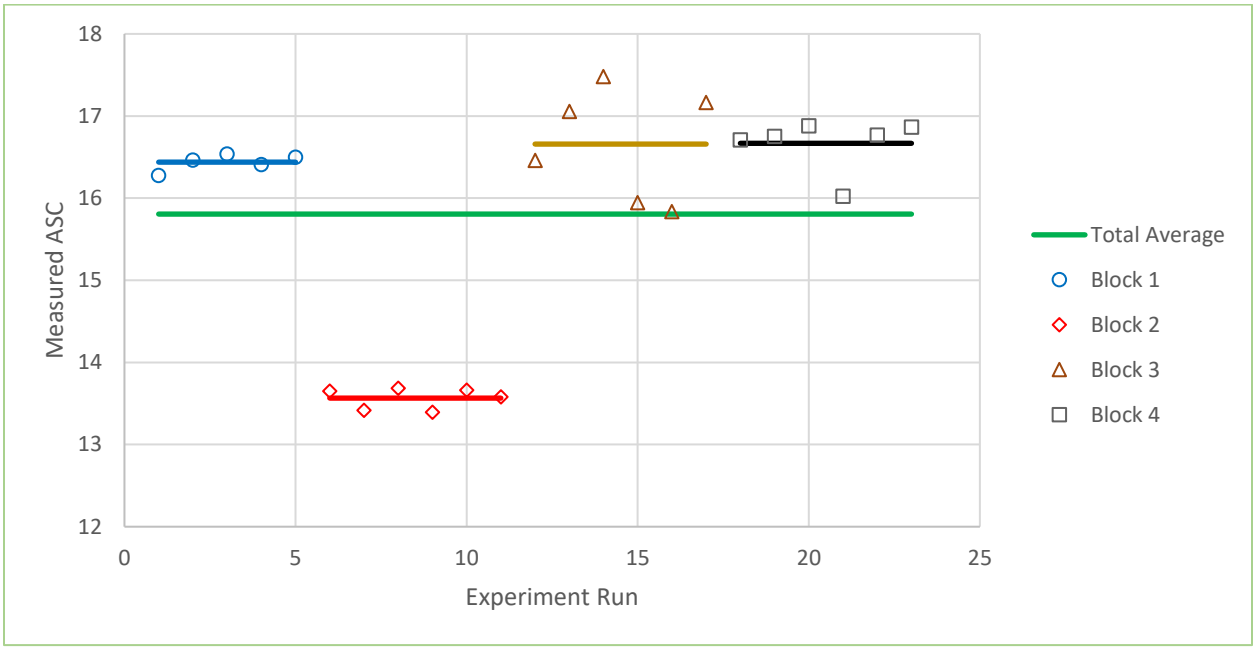

Figure 4.8: Measured ASC for Each Experiment Sample

Another factor that was not investigated in this chapter is that the drilling process may have been different in blocks one and two than blocks three and four. Two different researchers prepared the samples according to the Straumann implant recommended procedure. This drilling procedure differs for "hard bone" or "soft bone". The 40 pcf sawbones are generally considered "hard bone" and so there should be no discrepancy, however slight operator differences may still exist. Additionally, in other experiments with lower density blocks such as 20 pcf or 30 pcf Sawbones, there may be different choices made on which specific method to use. This could create another difference between samples that have been prepared by different researchers.

Chapter 5 : Effect of Model Assumptions at the Bone-Implant Interface

In previous studies, the bone-implant interface has been represented as a frictional contact between the implant and the bone [18, 83, 84]. In the current model discussed thus far, this interface has been modelled as a separate layer of material with its own material properties. This separate layer method has also been done previously [72, 73, 85] and this chapter will investigate pros and cons of each method. The primary purpose of this study is to develop a modelling process that will lead to a model of a dental implant system undergoing impact loading in such a way that the acceleration response of the impact rod will resemble the response from the ASIST when measuring a similar system. This model must be versatile enough to represent a new dental implant held in place by primary stability, or one that has undergone osseointegration and has secondary stability. These two separate conditions represent different properties of the interface, and so this chapter will examine whether a frictional contact condition or an interface material will better represent these conditions.

5.1 Modelling the Interfaces

A frictional contact between an implant and the bone has been defined previously [18, 83, 84] with a friction coefficient of 0.2-0.61. Using a frictional interface allows the implant to move due to sliding with respect to the bone. A lower coefficient of friction (COF) should result in more movement and should represent an implant with lower stability (less osseointegration). To examine the relationship between the COF and the calculated ASC value for the Straumann RC 4.1 mm implant and 6 mm healing abutment, the system was simulated with tangential COF values ranging from 0 to 5. The block geometry was modified so that it was directly in contact with the implant with no material in between and the friction condition was applied to the BII.

A more common approach to modeling osseointegrated implants is to model the BII as an interface material with its own material properties [72, 73, 85, 76] as described Chapters 3 and 4. This material layer would be between the implant and bone and, if its surfaces were tied to the implant and bone, there would be no sliding taking place on the surfaces of the interface. The implant's movement would be due to the deformation of the interface, therefor it is expected that increasing the stiffness of the interface material would increase the implant stability. The Straumann RC 4.1

mm implant and 6 mm healing abutment system was simulated with an interface of 0.5 mm thickness and a Young's modulus ranging between 43.975 and 1055.4 MPa, which corresponds to 5% and 120% of the modulus of the 40 pcf bone block being used for the surrounding substrate material.

5.2 Frictional Interface

Eight values of the COF were modelled between 0 and 5 (0.00, 0.05, 0.10, 0.40, 0.60, 0.80, 1.50, and 5.00). The impact rod acceleration response for each value is shown in Figure 5.1. In this figure, the second mode frequency of the signal appears to be very similar for all friction coefficients where the local peaks occur at similar times. However, the damping in model, which is particularly evident in the second mode, appears to increase with increasing friction. Further, the total contact time appear to be inversely related to the friction coefficient. The peaks are less pronounced, and the time at which the acceleration reaches zero is shorter as the friction is increased.

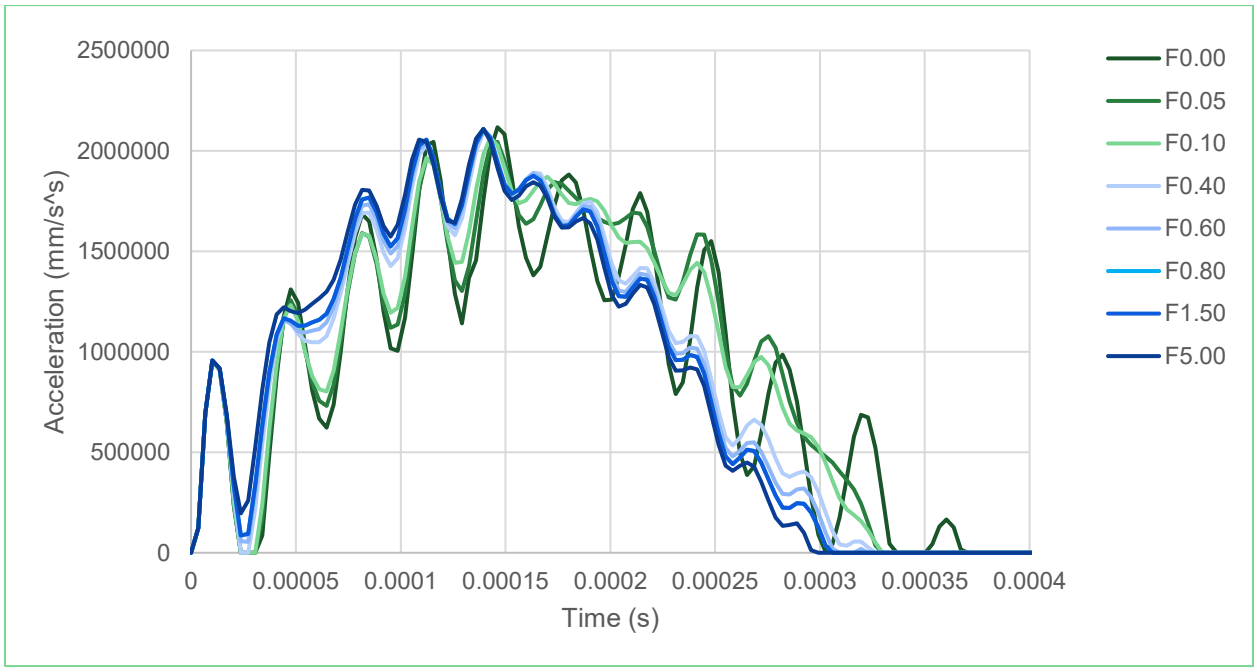

Figure 5.1: Acceleration Responses of a Dental Implant Using a Friction Coefficient to Model the BI Interface

Each resultant acceleration response was fit with the analytical model as discussed in previous chapters to obtain an ASC value that is used to quantify the apparent interface stiffness of the

system. The ASC values for each COF are plotted in Figure 5.2. The ASC values for the tested range of COFs were all between 4.2 and 6.0. The ASC values appear to increase with respect to the COF, however after a COF of 0.8, the ASC does not change significantly.

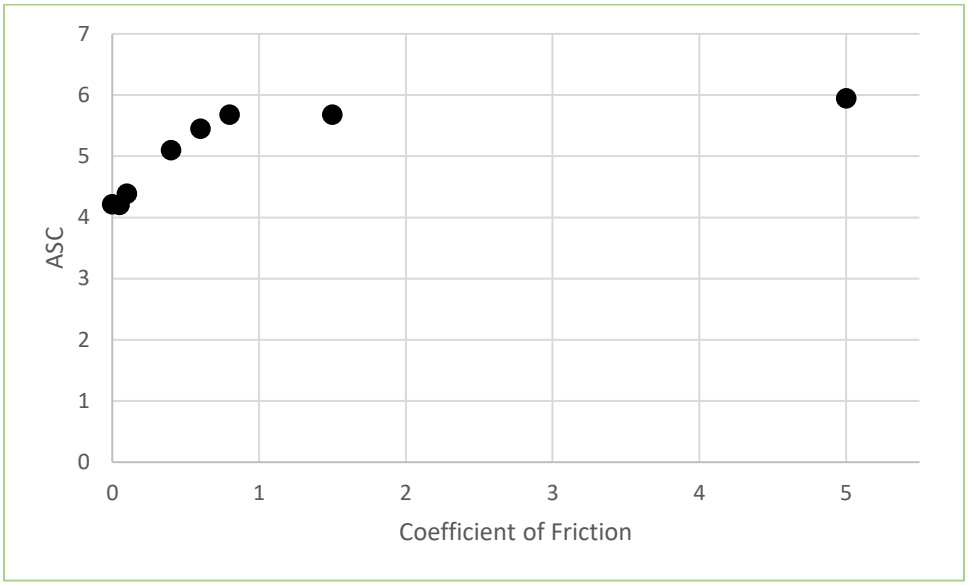

Figure 5.2: Extracted ASC for Each Model with Varying Coefficients of Friction.

5.3 Elastic Material Interface

Similar simulations were done using an interface material with ten different moduli of elasticity between 43.975 and 1055.40 MPa (5% - 120% of the Young's modulus of the surround substrate). The acceleration responses for each of these values is shown in Figure 5.3. There is clearly more variation between these responses than when using a frictional interface (Figure 5.3). An increase in the modulus of elasticity results in a smaller amplitude of the second mode frequency, but also increases the value of the second frequency; the local peaks are less pronounced and closer together. Changing the modulus also has a more dramatic impact on the first mode frequency. Both the contact time and the amplitude change significantly with the change in modulus. The contact time decreases, and the amplitude increases as the modulus increases.

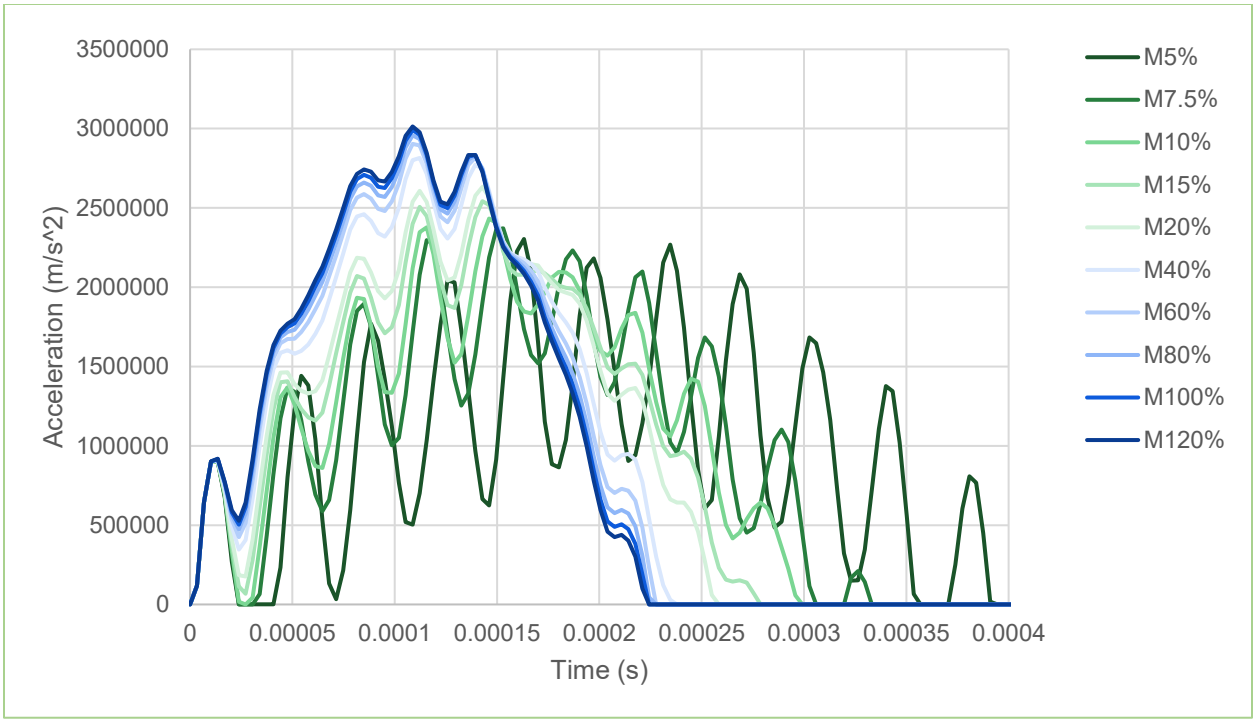

Figure 5.3: Acceleration Responses of a Dental Implant Using an Elastic Material Layer to Model the BI Interface

The trends shown in the response plot align with the expectation that a stiffer interface material will result in a lower contact time since the implant is not displaced as much by the impact force. The peak acceleration is higher because the restoring force on the implant is greater due to the stiffer interface.

Each resultant acceleration response was fit with the analytical model in the same way as the COF responses to obtain an ASC value that is used to quantify the interface stiffness of the system. The ASC values for each modulus of elasticity are plotted in Figure 5.4. The ASC values for the tested range of moduli were between 2.8 and 18.6. The ASC is always increasing with increasing modulus and doesn't appear to plateau within the tested range of values.

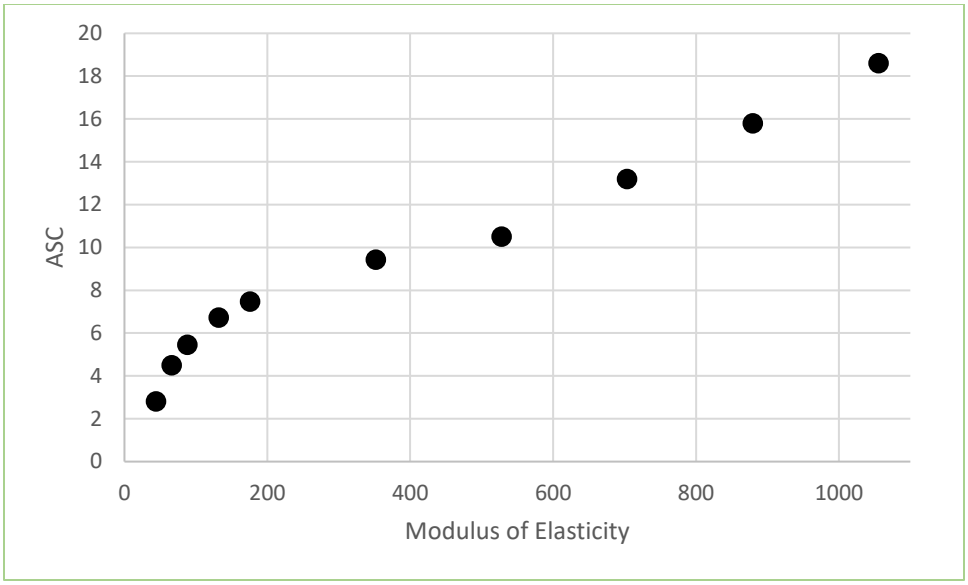

Figure 5.4:Extracted ASC for Each Model with Varying Moduli of Elasticity

5.4 Evaluation of Interface Methods

As part of a parallel study, benchtop tests were done using implants inserted into Sawbones blocks to simulate implants installed in bone. Samples were made either with or without glue to simulate secondary or primary stability, respectively. The measured ASC values for the RC 4.1 mm implant inserted into the 40 pcf block were between 3.4 and 7.6 for primary stability (without a glue bond at the interface), and between 13.4 and 17.5 for secondary stability (bonded with super glue at the interface). These ranges are show in Figure 5.5 to highlight the ranges of ASC values that are of interest for modelling using the tested interface methods.

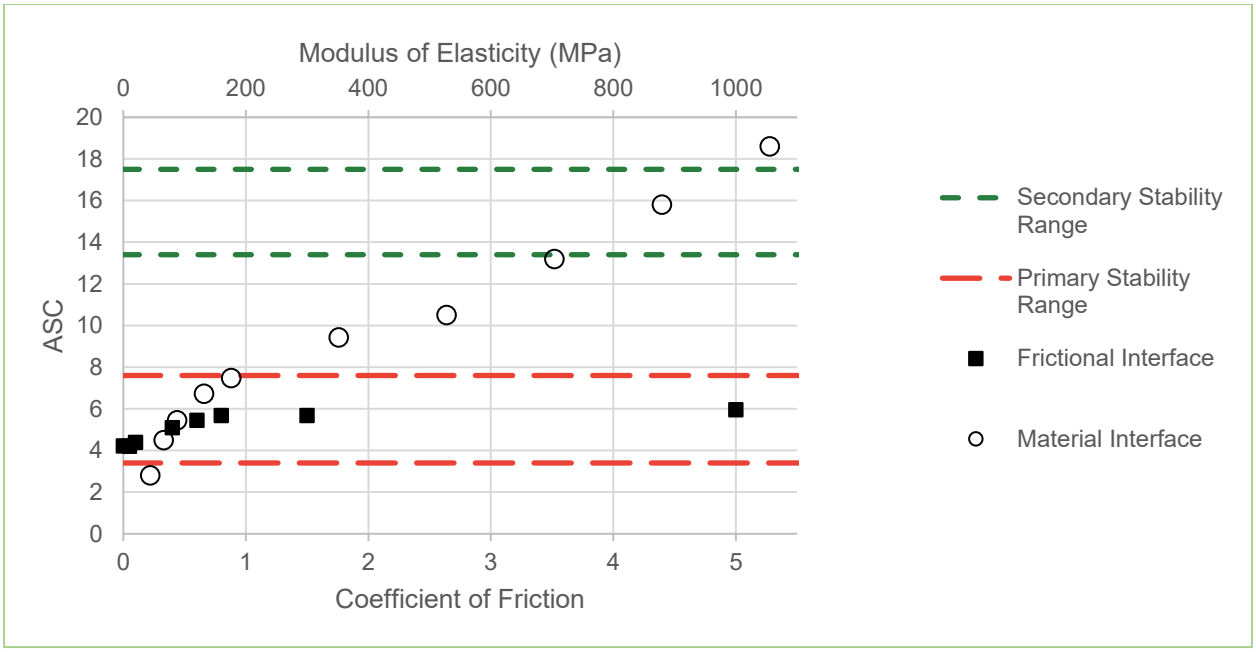

Figure 5.5: ASC Ranges of Dental Implant Simulations Modelling the BI Interface as Either a Frictional Contact, or an Elastic Material Layer.

It is evident from Figure 5.5 that adjusting the COF of a frictional interface parameter will not sufficiently capture the full range of ASC values measured in the primary stability experiments, or any of the ASC values measured in the secondary stability measurements. A frictional interface is not a suitable model for representing the range of interface stiffness values that are relevant in the ASIST stability measurements of the RC 4.1 mm implant inserted into 40 pcf bone. Alternatively, using an appropriate elastic material with 0.5 mm thickness can approximate the interface between the implant and the bone within the ranges measured in experiments. By adjusting the modulus of elasticity, the system can be tuned to represent either primary or secondary stability and give a resulting acceleration response resembling the response of the ASIST used in an experimental context.

A simulated interface stiffness of 879.5 MPa (equal to that of the surrounding bone) gives a lower ASC value than the highest boundary of the secondary stability range. Conceptually this simulation should be equivalent to perfect osseointegration since the interface resembles bone, and the surfaces are tied, but the elasticity value that would give an ASC value closer to this upper bound is between 100% and 120% of the surrounding bone. Some of the probable causes for this are: the

simplified implant geometry, the stiffness of the superglue being stiffer than the surrounding bone, uncertainty in the polyurethane properties, changes in experimental procedure and/or sample preparation, and curve fitting discrepancies. The next simulations discussed will use a modulus of 106% of the bone modulus. This is estimated by interpolating between the ASC values of the 100% and 120% cases to find a value that would match the ASC of the stiffest ASIST measurement (17.5).

Chapter 6 : Validation of the Modelling Process

In the previous chapters, the model was developed using a single implant/abutment system (Straumann RC 4.1 mm implant and 6 mm healing abutment). This was done to develop the modelling process and to understand the effect of different factors of the system in the model response. However, in clinical practice, a variety of implants and abutments/superstructure can be used, and clinicians can encounter varying bone quality across patients. Thus, it is important to understand the behavior of systems with different parameters and conditions, particularly within the context of implant stability measurement using the ASIST. As described in Section 2.5.4, experimental benchtop data is available for four different implant-abutment combinations from the Straumann bone-level implant system (RC 4.1 mm implants with 6 mm and 4.5 mm HA; NC 3.3 mm implants with 3.6 mm and 3.3 mm HA). Each of these implant-abutment combinations were tested in four different uniform densities of Sawbones (40, 30, 20, and 10 pcf). FE models were created following the procedures outlined in Chapter 3-5 to simulate each of these experimental conditions to further validate the modeling approach and to understand the effect of implant/abutment geometry and bone density on the resulting stability measurements.

In the models presented in this chapter, the naming convention uses two letters to represent the implant model, the block density in pcf, and the abutment diameter (without a decimal place) each separated by an underscore. For example, the RC implant with a 4.5 mm abutment embedded in a 40 pcf block is labeled as RC_40_45. Each sample was modelled with an interface elastic modulus of 106% that of the surrounding bone in an effort to create models that represented complete osseointegration as mentioned in Chapter 4.

6.1 Examination of Simulated Acceleration Responses

Figure 6.1 shows the simulation responses of each implant/abutment system. It can be clearly seen that increasing the density and modulus of elasticity of the bone by selecting a different Sawbones block can greatly increase the contact time and lower the amplitude of the response.

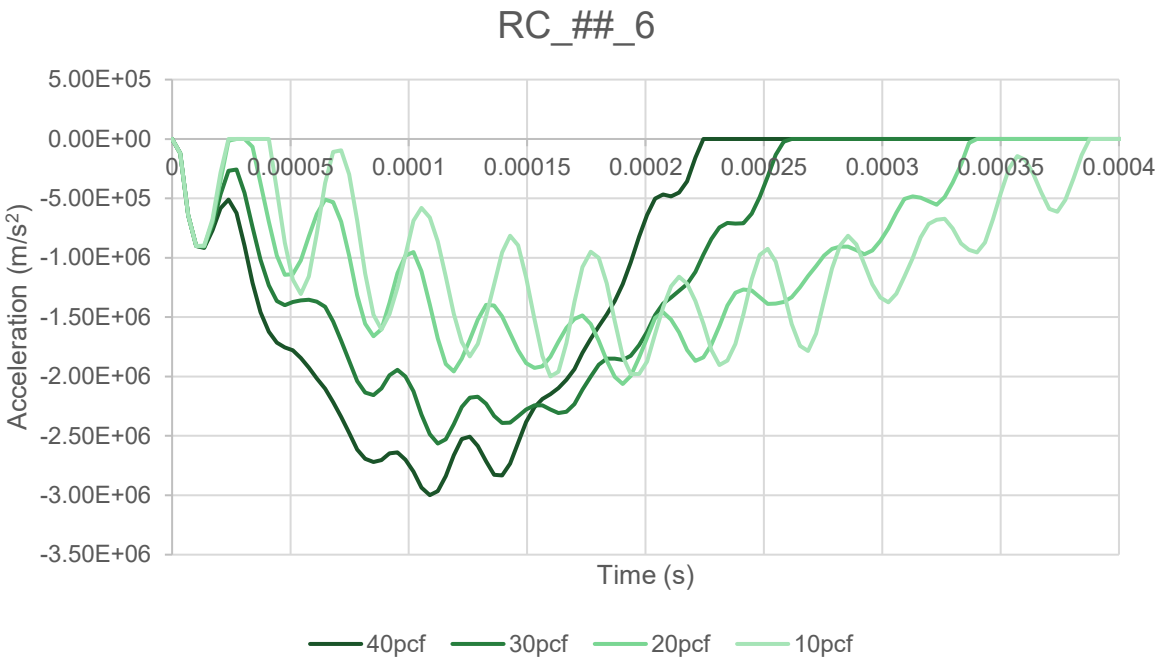
RC_##_6
5.00E+05
0.00E+00
-5.00E+05
-1.00E+06
-1.50E+06
-2.00E+06
-2.50E+06
-3.00E+06
-3.50E+06
Acceleration (m/s²)
0
0.00005
0.0001
0.00015
0.0002
0.00025
0.0003
0.00035
0.0004
Time (s)
40pcf
30pcf
20pcf
10pcf

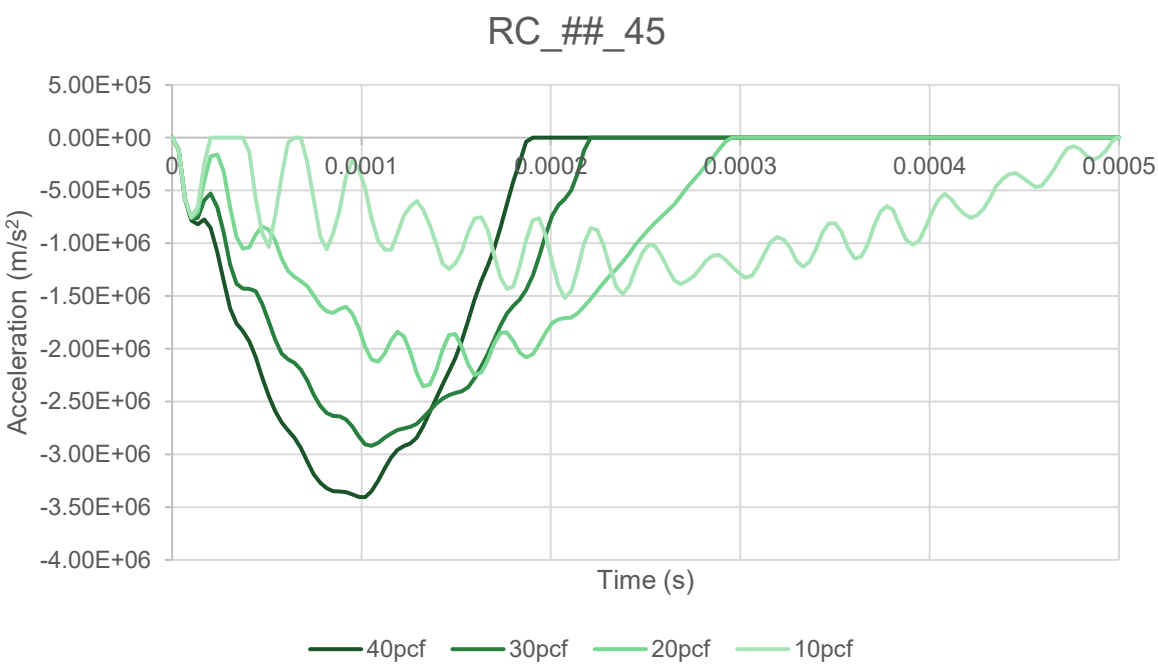
RC_##_45
5.00E+05
0.00E+00
-5.00E+05
-1.00E+06
-1.50E+06
-2.00E+06
-2.50E+06
-3.00E+06
-3.50E+06
-4.00E+06
Acceleration (m/s²)
0
0.0001
0.0002
0.0003
0.0004
0.0005
Time (s)
40pcf
30pcf
20pcf
10pcf

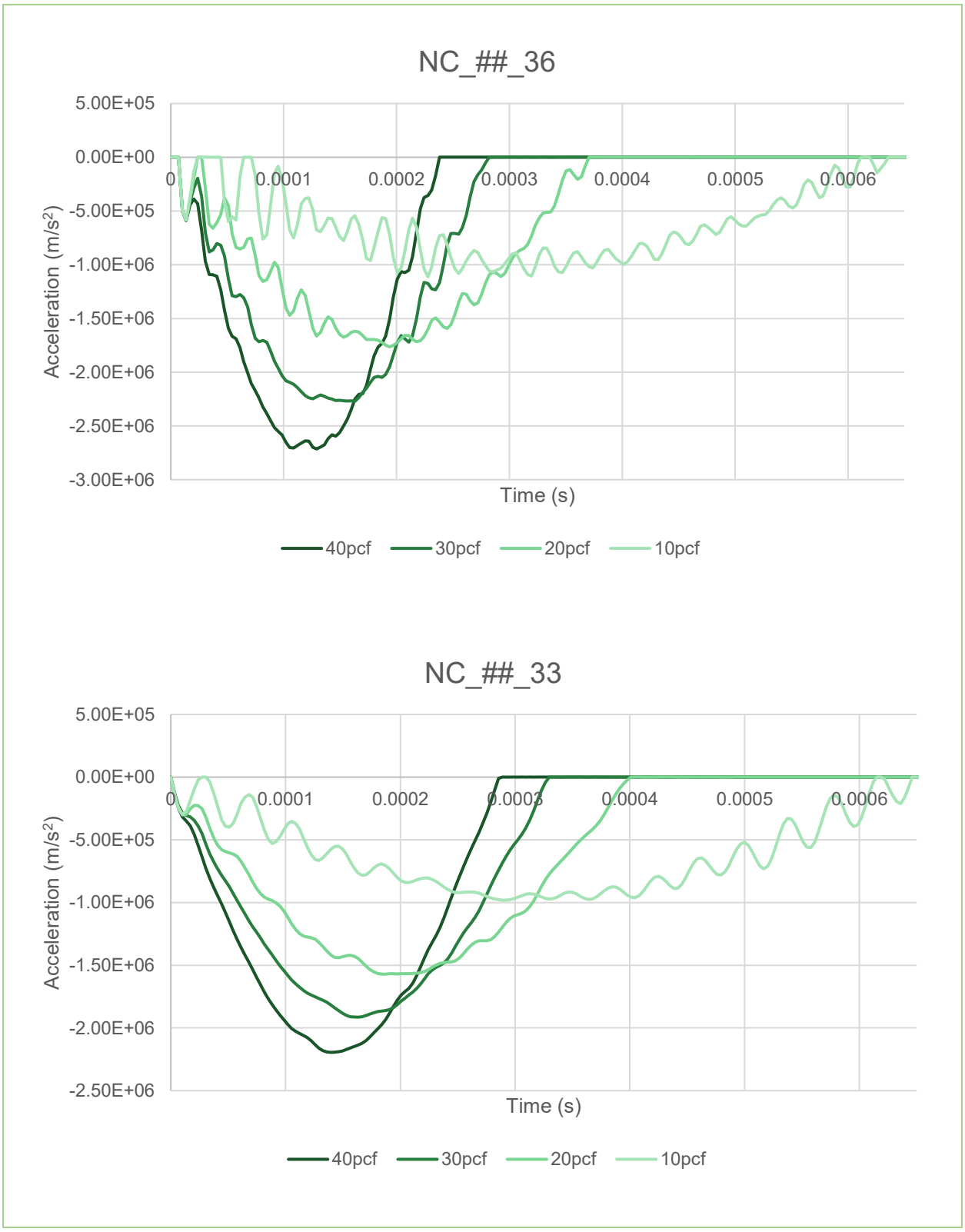

Figure 6.1: Simulated Acceleration Responses of Each Implant/Abutment System in Five Different Test Blocks

Each acceleration response curve was fit to the analytical model to extract the ASC and interface stiffness per unit area. In Figures 6.2 and 6.3 are the extracted ASCs and interface stiffnesses of each model. The trends of each plot are as expected with both the stiffness and ASC increasing as the block density increases.

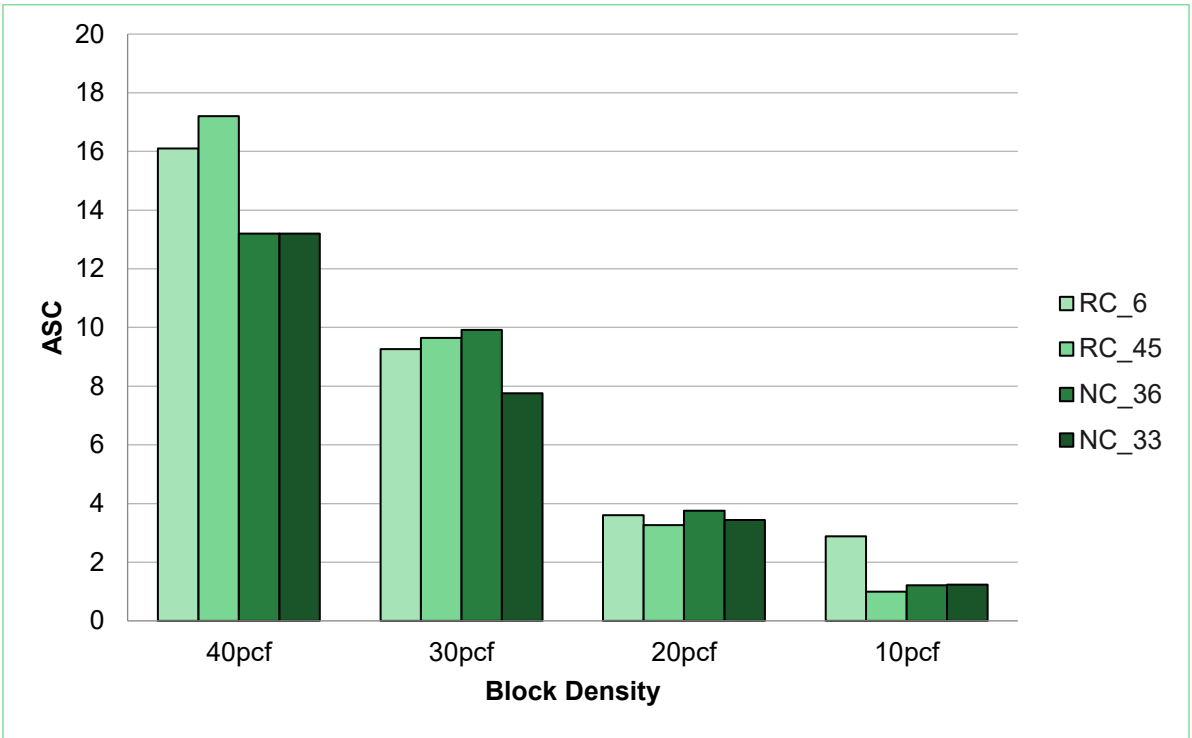

Figure 6.2: Extracted ASC from Simulations of Each Abutment/Implant System in Four Different Test Blocks

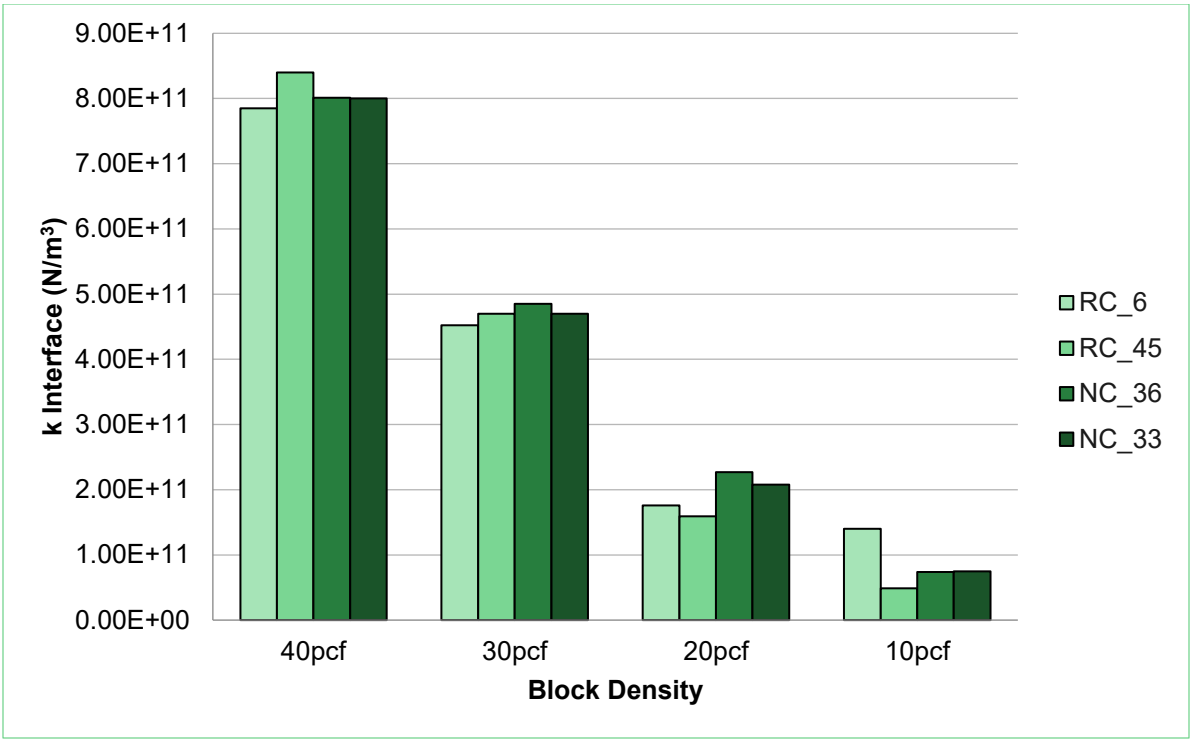

Figure 6.3: Extracted Interface Stiffness from Simulations of Each Abutment/Implant System in Four Different Test Blocks

Two-way ANOVA was used to check whether the ASC or interface stiffness (per unit area) was influenced by the implant or the block properties. For the ASC, the p-value for the block type was 3.74E-8 ($p < 0.05$) and for the implant 0.018 ($p < 0.05$) showing that the changing block properties was highly significant to the ASC and the type of implant had a statistically significant effect on the ASC. For the stiffness per unit area, the p-values were 1.52E-9 ($p < 0.05$) and 0.559 ($p > 0.05$) for the block type and implant respectively, showing that changing the block type is highly significant with regard to the stiffness, but the implant does not significantly affect the stiffness per unit area value. The full ANOVA Tables are recorded in Appendix B.

These results show that both the ASC and the stiffness value are affected by the properties of the implant medium, but the stiffness per unit area is independent of the type of implant used where the main difference between the implants was the diameter. The analytical model assumes a uniform stiffness applied over the surface of the implant. It makes sense that the stiffness per unit area is independent of the implant, since the FE model used the same thickness, density, and Young's modulus for each implant/abutment geometry. While the stiffness per unit area was not affected by a change in implant, the effective stiffness (reflected in the ASC) was significantly

related to the implant geometry. Larger implants with a larger surface area will generally have a higher stability from the same interface properties since that interface is in contact with a larger area. This is why the implant type is a significant variable for the ASC, which is a measure of the stability, but not for the interface stiffness per unit area.

By showing that the extracted stiffness is independent of the implant, the simulations affirm that the ASIST can be used to compare the stability of two different implants regardless of the effects of their geometry on the signal response. The ASC incorporates the geometry into the measure of the stability but first extracts the interface properties that are unbiased by the geometry.

Each implant was simulated with two different abutments that were only compatible with the implant they were designed for. Using ANOVA on the abutment effects was not possible because there were not enough degrees of freedom in the data since repeating the simulation did not provide new data, and the abutments could not be used on the implant it was not designed for. A paired t-test was done to test if changing between the larger and smaller abutments available for each sample had an effect of the ASC or interface stiffness extracted from the simulation data. The data sets used were the differences between the ASC or interface stiffness of the larger and smaller abutments for simulations with the same density and implant. In order to use paired t-tests, the data sets were tested to see if they could be modelled as having normal distributions. Both data sets passed the Shapiro-Wilk test with a p-value between 0.1 and 0.5 ($p > 0.05$) allowing the assumption of normality. In these tests, the null hypotheses that the change in both measured ASC and stiffness per unit area between two different abutments is zero was not rejected; both tests resulted in a large p-value ($p >> 0.05$) which showed insufficient evidence to reject the hypotheses. For the ASC the p-value was 0.573, and for the stiffness the p-value was 0.340.

The above tests reinforce the value of the ASIST in measuring the implant stability independently of the geometry of an attached abutment. This was a clear issue with previous methods described in Chapter 2.4.

6.2 Comparison with Experimental Data

Figure 6.4 shows the experimental acceleration responses of each implant/abutment system in each of the four uniform densities as well as the corresponding simulation response. The experimental

responses for four replicate installations of each setup are shown in colour, with the simulated responses in black.

From the plot in figure 6.4, the general fit between the simulation response and the experimental data is better for high density than low density. The majority of the simulation response curves fall within the range of experimental data. However, the low-density blocks gave a wider range of response curves during experiments and compared to the simulated response, gave a shorter contact time. Variation within each experiment is likely due in part to the factors discussed in Chapter 4. clamping conditions, impact angle, and installation procedure could all contribute to the variation in the responses. In particular, the low-density blocks have fewer samples since the implant installation was not always successful and the fragile block would sometimes not sufficiently hold the implant. The second mode behavior between the two responses were very consistent. The average ASC for all the experimental data and the ASC extracted from each simulation is presented in Table 6-1 along with the difference between the two. The average difference between the simulated and experimental ASC was 0.37 indicating that the behavior of the simulation was consistent with the experimental data.

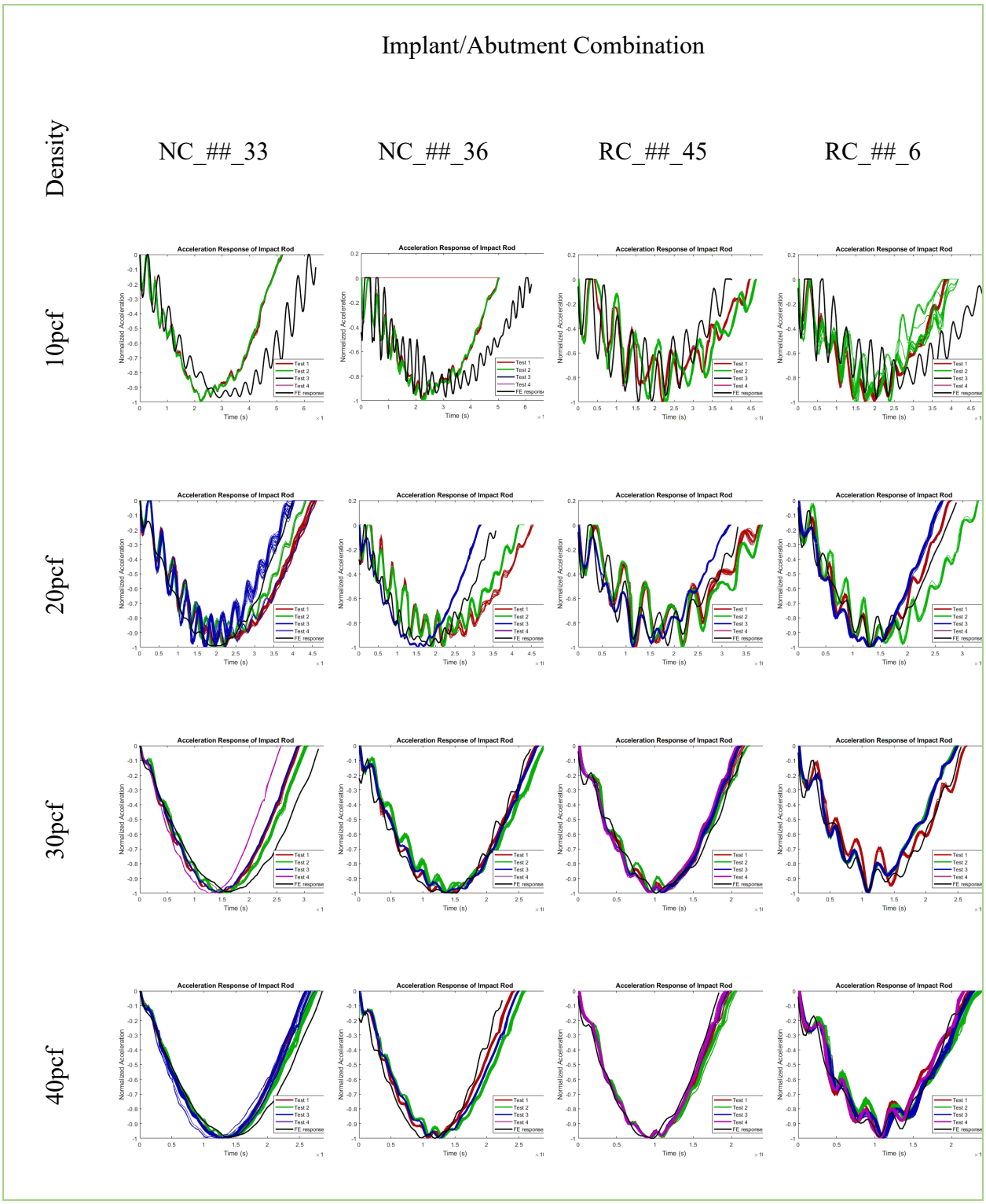

Figure 6.4: Plots Comparing Simulations of Each Block Density used for Four Implant and Abutment Systems to Their Corresponding Experimental Responses

Table 6-1: Comparison of ASC and K interface between Simulated and Experimental Data

Simulation ID	Simulation k interface ($\times 10^{11}$ N/m^3)	Simulation ASC	Average Experimental ASC	ASC Difference $(FE - Exp.)$	ASC % Difference $100\% \times \left(\frac{FE - Exp.}{Exp.}\right)$
RC_40_6	7.85	16.1	15.81	0.29	1.9
RC_30_6	4.52	9.26	9.26	0.00	0.0
RC_20_6	1.76	3.60	4.20	-0.60	14.0
RC_10_6	1.40	2.88	2.34	0.54	23.3
RC_40_45	8.40	17.2	16.92	0.28	1.7
RC_30_45	4.70	9.64	9.37	0.27	2.9
RC_20_45	1.59	3.26	4.05	-0.79	19.6
RC_10_45	0.49	1.00	1.73	-0.73	42.1
NC_40_36	8.01	13.2	15.09	-1.89	12.5
NC_30_36	4.85	9.92	9.18	0.74	8.1
NC_20_36	2.27	3.75	2.82	0.93	32.8
NC_10_36	0.74	1.21	2.02	-0.81	40.0
NC_40_33	8.00	13.2	14.93	-1.73	11.6
NC_30_33	4.70	7.76	10.07	-2.31	23.0
NC_20_33	2.08	3.44	2.87	0.57	20.0
NC_10_33	0.75	1.23	1.98	-0.75	38.0

The simulations with the greatest percent differences were the 10 pcf samples. The preparation of samples in these blocks was not always successful due to the lack of integrity in the material. The blocks were modelled as a uniform elastic material which may not have accurately portrayed the porous structure that is more apparent in the low-density samples.

The other simulation responses generally fell within, or close to the range of experimental responses. The simulations could likely be made more accurate by tuning the interface materials to obtain responses that more closely match the behavior of the experimental data. Using an elastic modulus of 106% of the surrounding bone modulus, has created responses for most cases that obtain an ASC that matches to the mean of the experiment ±1.0. By using the simulation as a model to find the ASC of a certain system, the overall fit of the simulation model to all the available data is good with an R^2 of 0.94.

6.3 Summary

This chapter provides validation of the modelling process, and insight into the analytical model of the ASIST. This analysis provided evidence that the ASC and stiffness per unit area found by

matching to the analytical model are both sensitive to the properties of the installation medium, but the stiffness per unit area is not sensitive to the implant/abutment system. The ASC is sensitive to the geometry since it incorporates contact area between the bone and implant into the measure of the stability, but the analytical model first extracts the interface properties so that the stiffness measurement is not biased by the inertial properties of the implant/abutment system.

The simulation responses were compared to experimental data, and the majority of the simulations achieved a response within the range of what was seen experimentally. The most notable exception was the samples involving 10 pcf polyurethane foam. The differences here were likely due to lack of integrity in the blocks causing difficulties with implant installation, and the material property assumptions in the simulated model that the block was a uniform elastic material when in reality the block is porous and not perfectly elastic.

Chapter 7 : Towards the development of simulations for clinical scenarios

Thus far, the FE model has focused on the Straumann bone-level implant with an attached healing abutment, installed in a uniform material bone block. To expand the applicability of the model, several clinical factors should be included. First, it is expected that implants installed in either the mandible or maxilla will be inserted into bone with both trabecular and cortical regions [51, 45]. The bone at potential implant sites has a layer of cortical bone of approximately 1 mm thickness which can vary depending on specific location, patient age, and health-related factors. Thus, a bi-layer bone model should be considered. Secondly, one of the primary mechanisms of clinical implant failure is bone resorption around the implant [86, 87, 88, 89]. Thus, it is important to investigate the effect of bone resorption on the resulting acceleration response and stability measurement of the system. Finally, in a clinical scenario, the implant-healing abutment system is applicable only for the initial healing period, after which a final abutment and prosthetic crown in attached to the implant [90]. Thus, it is important to include a prosthetic crown into the model in order to understand the response of the system and the expected stability measurement with this added component.

In this chapter, the developed FE model will be expanded to incorporate laminated bone blocks that are used to more closely represent bone by using a layer of dense material (representing cortical bone) on top of a layer of low-density material (trabecular bone). Further, varying levels of bone resorption at the bone surface will be simulated to predict how the ASIST response might change as bone loss occurs. Finally, a simplified dental crown geometry placed on top of the abutment/implant structure will be simulated. With these improvements to the model, it can then be used to predict what the responses might look like in a clinical setting under varying conditions.

7.1 Modelling a Composite Bone Block

The laminated Sawbones polyurethane foam block is made up of a 3 mm layer of 50 pcf foam overlaying a 17 mm layer of 20 pcf foam. Blocks with a 3 mm layer were chosen to simulate composite bone rather than a more clinically realistic 1 mm layer due to their availability. Modelling this new system was done by splitting the previous block geometry into two parts in Solidworks, importing the new geometry to ABAQUS, and tying together the inner surface of the two layers. This allowed the two layers of the block to be given different properties according to the specifications for each type of foam reported by the manufacturer. The values for density, Young's modulus, and Poisson's ratio of the 50 pcf foam were 0.80 g/cm^3, 1308.5MPa, and 0.3 respectively. For the 20 pcf foam, these values were 0.32 g/cm^3, 247MPa, and 0.3. The new model is shown in Figure 7.1. The interface layer has also been separated so that its properties can be

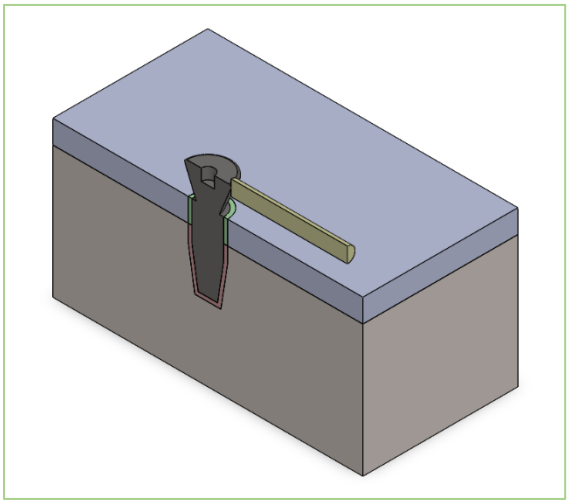

Figure 7.1:Simplified Dental Implant Model Embedded in a Composite Material

representative of the bone implant interface for each bone type, where it is assumed that the BII in the cortical region would be proportionally stiffer than in the trabecular region, similar to the surrounding substrate material [91, 92]. The result of this simulation is compared to the experimental benchtop ASIST measurements of the 20/50 pcf laminated block with the same implant and abutment (RC 4.1 mm with 6 mm HA as a representative example) in Figure 7.2. The resemblance between the simulated response (black) and the other responses is clear from the similar contact time and behavior of the second frequency.

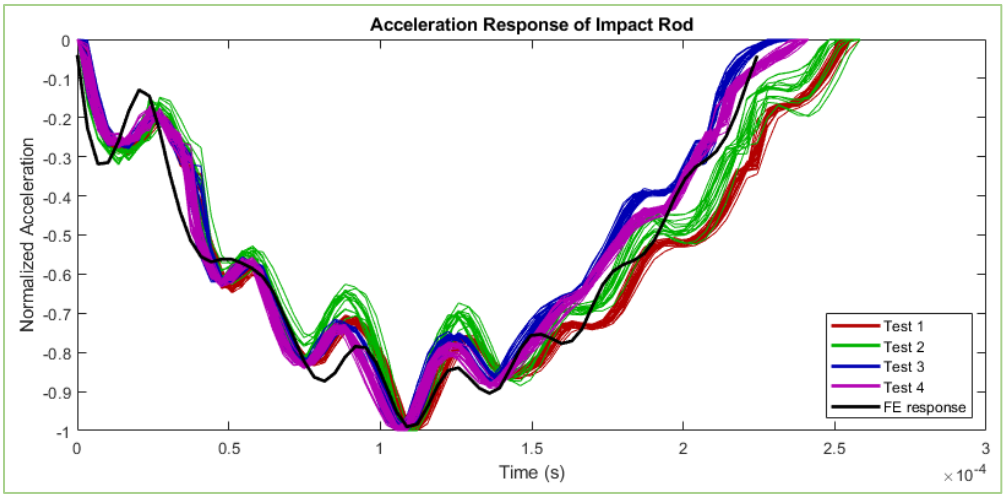

Figure 7.2: Acceleration Response of an Impact Loaded Dental Implant Simulation Compared to Experimental Data

To curve fit the responses from a composite block and extract the ASC, the analytical model must be adjusted to incorporate the two different materials present in the block. The top layer will have a different stiffness than the bottom layer. In the new analytical model, this is represented as a coefficient α to represent the ratio between the two stiffnesses. The schematic in Figure 7.3 shows the new system with a stiffer top layer of bone of thickness l_c and interface stiffness of αk_i.

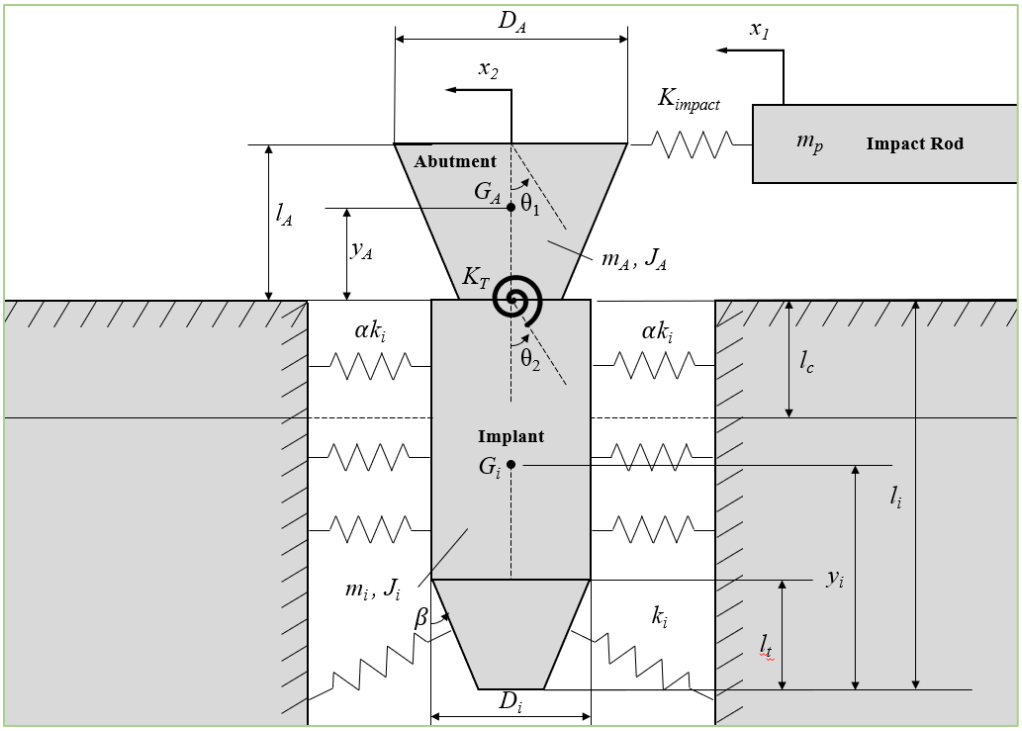

Figure 7.3:Schematic of the 4-DOF model of the Dental Implant and Abutment System Embedded in a Composite Material

The adjustments made to the analytical model will allow the evaluation of k_i in the new system. This value still needs to be normalized using the surface area of the implant to be compared between implants. However, the system now has two stiffness values to incorporate into the overall stability coefficient. This can be done by adjusting the formula for the ASC in such a way that the effective stiffness is a combination of the stiffness from both layers over each contacted surface. Using a value α as the ratio between the stiffnesses limits the number of unknown variables that are matched to the analytical model and allows the same ASC formula to apply to both composite and uniform materials by making α equal to 1 or higher than 1. The previous equation, and new ASC equation are shown below.

$$ASC_{Uniform\ Stiffness} = \frac{K_{eff}}{K_{nom}} = \frac{2 \times l_i \times d_i \times k_i}{4 \times 10^6 N/m}$$

$$ASC_{Composite\ Stiffness} = \frac{K_{eff}}{K_{nom}} = \frac{2 \times (l_i - l_c) \times d_i \times k_i + 2 \times l_c \times d_i \times \alpha k_i}{4 \times 10^6 N/m}$$

$$= \frac{2 \times d_i \times k_i \times (l_i + (\alpha - 1) l_c)}{4 \times 10^6 N/m}$$

The reported properties for the Sawbones samples included tensile and compressive moduli, which thus far have been combined in the simulations into one approximate elastic modulus for the bone substrate, and 106% of this value for the interface material (due to the discussion in Chapter 5.4). Using the calculated values for 20 pcf and 50 pcf interface material (262 MPa and 1387 MPa), the ratio of the elastic modulus between the two layers of the composite block is 5.30. The experimental tests and simulation response have been processed (Table 7-1) using both α equal to 1 assuming a uniform block, and α = 5.30 assuming that the ratio between elastic modulus is the same as the ratio between the related interface stiffnesses. Two replicate benchtop experimental samples were tested with the ASIST for comparison. The samples labelled with "A" and "B" in the tables and figures below are the experimental samples.

Table 7-1:ASC and Interface Stiffness Measurements of an RC Implant With 6mm Healing Abutment in 20/50 pcf Polyurethane Block

	α=1		α= 5.30		
Sample	k_i ($\times 10^{11}$ N/m^3)	ASC	k_i ($\times 10^{11}$ N/m^3)	αk_i ($\times 10^{11}$ N/m^3)	ASC
RC_2050_6	4.89	10.0	1.83E+11	9.68E+11	8.6
RC_2050_6A	5.23	10.7	2.02E+11	1.07E+12	9.5
RC_2050_6B	5.53	11.3	2.06E+11	1.09E+12	9.7

Using an α value of 1 gave a consistently higher ASC than the adjusted α of 5.3. An average difference of 1.4 between the stability measurements of each method shows that treating the surrounding material as a uniform material can bias the result making it have a higher stability measurement value. Using the adjusted α value gave results close to what would be expected. The stiffness per unit area of the bottom of the block (k_i) was expected to be similar to the interface of a uniform 20 pcf block, and the stiffness per unit area at the top (αk_i) was expected to be higher than the 40 pcf block. The mean interface stiffness value with 20 pcf blocks was approximately 1.93E11 N/m^3 and for the 40 pcf blocks, the stiffness was 8.07E11 N/m^3 (Chapter 6). These stiffness values show that using an α value of 5.30 will produce values close to the expected trends. The simulation was repeated for each of the available implant/abutment systems and compared to the experimental data (Figure 7.4 and Table 7-2).

NC_20/50_33

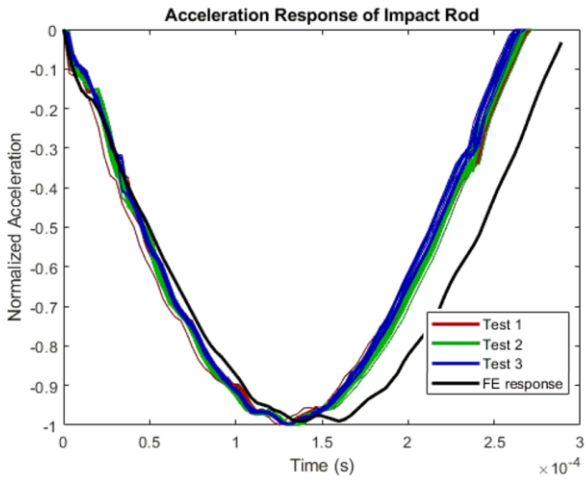

NC_20/50_36

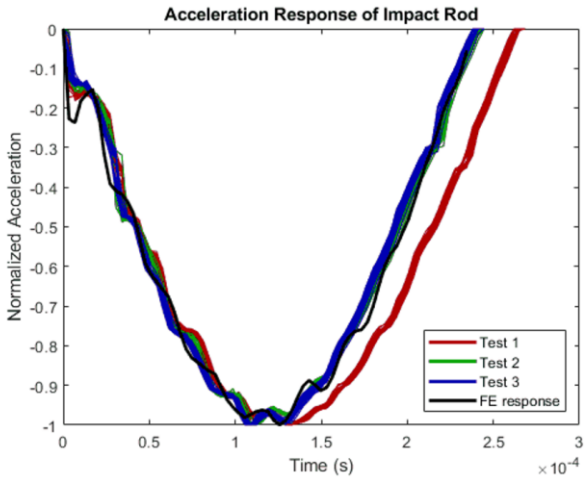

RC_20/50_45

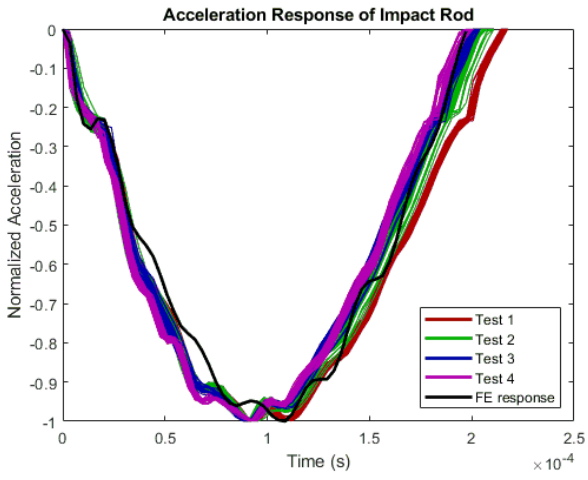

RC_20/50_6

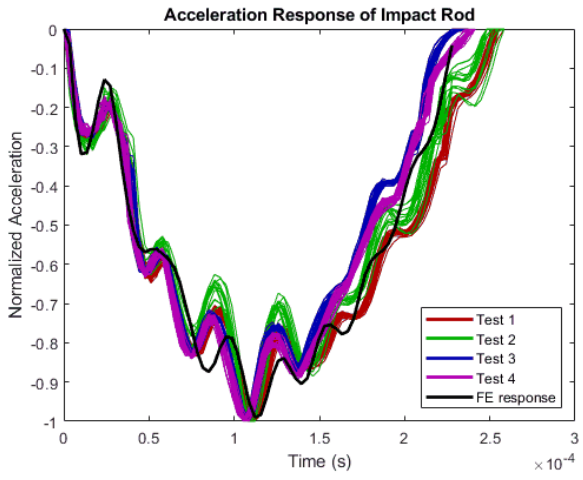

Figure 7.4: Plots Comparing Simulations of Four Implant and Abutment Systems installed into Composite Sawbones Blocks to Their Corresponding Experimental Responses

Table 7-2: ASC and Interface Stiffness Values Obtained from Simulations and Experimental Data

	α= 1		α = 5.3		
	k_i ($\times 10^{11}$ N/m^3)	ASC	k_i ($\times 10^{11}$ N/m^3)	αk_i ($\times 10^{12}$ N/m^3)	ASC
RC_2050_6	4.89	10.0	1.83	0.97	8.6
RC_2050_6A	5.23	10.7	2.02	1.07	9.5
RC_2050_6B	5.53	11.3	2.06	1.09	9.7
RC_2050_45	5.36	11.0	1.71	0.91	8.0
RC_2050_45A	5.54	11.4	2.15	1.14	10.1
RC_2050_45B	5.60	11.5	2.13	1.13	10.0
NC_2050_36	6.87	11.3	2.43	1.29	9.2
NC_2050_36A	7.15	11.8	2.58	1.37	9.7
NC_2050_33	6.20	10.2	2.20	1.16	8.3
NC_2050_33A	6.12	10.1	2.01	1.07	7.6

In most of the experimental samples, the resultant ASC values from both calculation methods are higher than the simulation values indicating that the material interface may need to be tuned further to accurately depict the behavior of the experimental samples. The ASC value using an alpha value equal to 5.3 is consistently lower than the results when alpha is 1. This further reinforces the idea that assuming a uniform material can make a measurement appear higher than the actual stability.

7.2 Modelling Bone Resorption

Bone resorption over the first year of life for a dental implant can average about 1 mm with an increase of 0.1 mm annually after the initial healing process [86]. One report found an average resorption of 0.3 mm in the first year, with annual resorption of 0.06 mm annually afterwards [87], and another found an average of 0.86 mm in the first 2 months [88]. The most important factor that influences the bone loss around an implant is oral hygiene, with implant overloading being another significant factor [87]. A more recent study found that the habit of smoking, and the implant location can also significantly affect the failure of an implant [89]. Since bone resorption is a common mode of implant failure, it would be useful to measure bone resorption in a quick non-invasive way or observe warning signs of bone resorption before symptoms appeared that require an x-ray. By modelling the bone resorption around a dental implant and extracting the

acceleration of an impact rod striking the implant, the ASIST measurement of a similar implant undergoing resorption can be predicted.

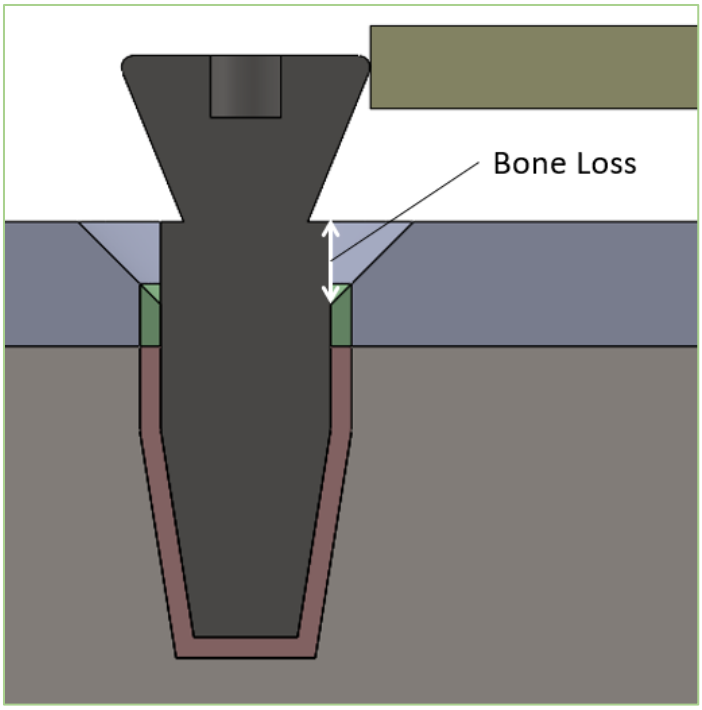

Figure 7.5: Bone Loss Modelled Around a Dental Implant

For this set of simulations, the bone loss was modelled between 0 mm and 2 mm in 0.5 mm increments. This was modelled on the composite bone block model since this may better represent the cortical and trabecular layers of bone found in a clinical setting. The block was cut at an angle of 45 degrees down and towards the implant as shown in Figure 7.5 with the value of the bone loss being the depth of the cut, or the height of the implant protruding above the bone contact point [86]. This shape is similar to the bone loss observed in scans, and a previous finite element modelling study [86]. This series was done with the RC 4.1 mm implant and 6 mm healing abutment. The resultant acceleration response is shown in Figure 7.6. From the plot, it is clearly seen that increasing the bone loss increases the contact time and lowers the amplitude of the signal. The local peaks after 0.00015 s are more distinct with greater bone loss, but the actual frequency of the local peaks appears unchanged.

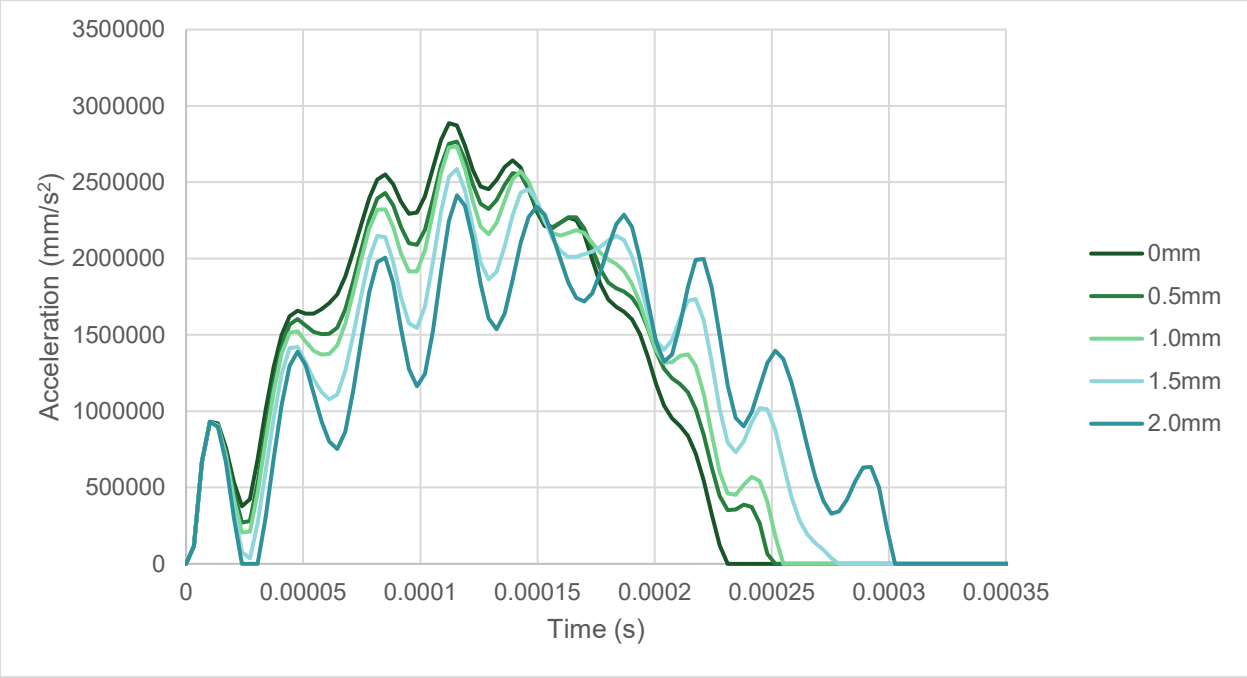

Figure 7.6: Acceleration Response of a Simulated Dental Implant System with Varying Levels of Bone Loss

After curve fitting each strike response, the ASC values and the extracted interface stiffness values were recorded in Table 7.3. To predict how bone resorption might reveal itself in the response of an implant, the curve fitting was done similar to Chapter 7.1, using an alpha value equal to 5.30 (the assumed ratio between the layer stiffnesses) and a top layer thickness of 3 mm. Even though the thickness of the top layer, and contact area are changing at the implant, the curve fitting is done assuming no resorption to examine the evidence of bone resorption that can be seen in the response with no knowledge of the issue.

Table 7-3: ASC and Interface Stiffness Extracted from Simulations with Varying Degrees of Resorption

Resorption (mm)	k_i ($\times 10^{11}$ N/m^3)	αk_i ($\times 10^{11}$ N/m^3)	ASC
0.0	1.83	9.68	8.6
0.5	1.59	8.45	7.5
1.0	1.49	7.87	7.0
1.5	1.18	6.27	5.6
2.0	0.92	4.86	4.3

It is clear from the table that bone resorption causes a reduction in the ASC and therefor a reduction in the implant stability. With an average decrease of 2 in the ASC per millimeter of resorption, the ASIST appears to give relevant measurements to monitor the health of implants even after full osseointegration. A decrease in the ASC could be evidence of bone loss that could otherwise only be seen through x-rays.

7.3 Modelling a Dental Crown

When an implant has healed enough to support loading, the healing abutment is removed, and a crown is placed. As the ASIST is meant to be used for the life of the implant, even after the crown has been placed, it is important to characterize the dynamic response of the implant-abutment-crown system as well. In the laboratory setting, prosthetic dental crowns were manufactured and tested using the ASIST. A premolar on the RC 4.1 mm implant was simulated in the FE model and compared with the benchtop experiments.

An STL file of the premolar was available from the manufacturing process, but the geometry needed to be modified in order to mesh adequately in the model. The original model (Figure 7.7) had many small edges, which would have resulted in a large number of elements and a very high computation time for the model when meshed.

Figure 7.7: Original Crown Model

To make the model more computationally reasonable, the crown was processed using Geomagic Design X (3D Systems) to make the surface smoother. The resulting model (Figure 7.8) had a more uniform surface with edges of approximately 0.25mm in length. The hole in the center was adjusted to fit around a final abutment that is attached to an implant with a small screw. This abutment, screw, and implant were simplified by making them into one piece (assuming rigid connections) that fit snugly inside the crown.

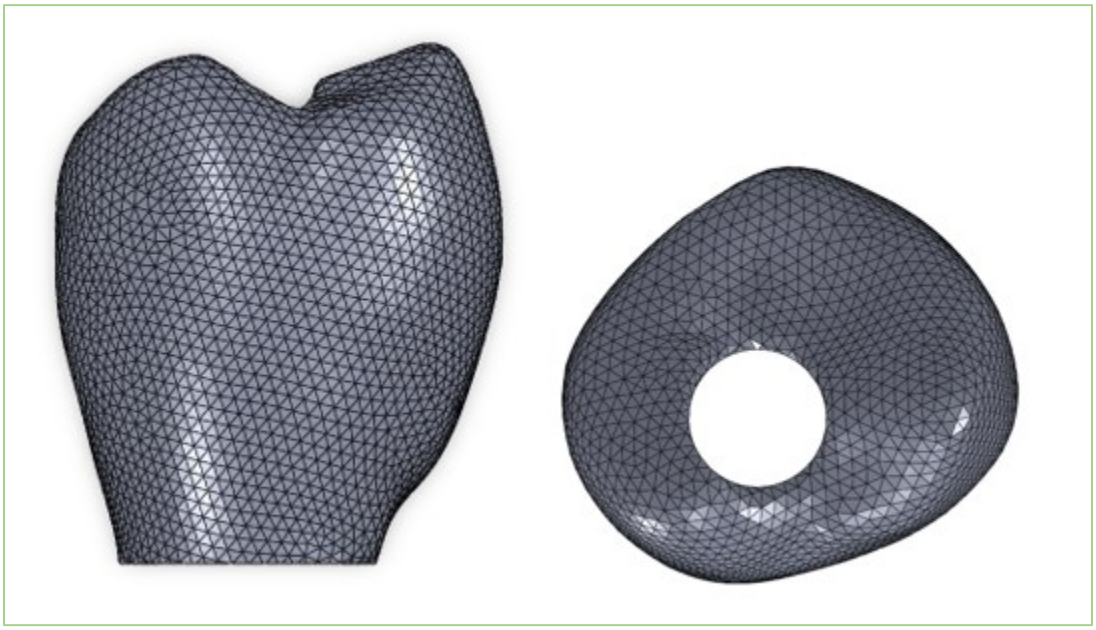

Figure 7.8: Processed Crown Model

A dental crown can be made up of several different materials such as porcelain or zirconia-based ceramics [93, 94]. The specific material of the available crowns that were used for lab measurements was Katana STML Zirconia. Limited material properties were provided by the manufacturer, so for the simulation, the elastic modulus was set to 29000 MPa, and Poisson's ratio to 0.38 as reported in a recent study [94]. The density of the crown was defined based on mass measurements done on the physical provided crown, and the volume of the crown as determined by the ABAQUS software. The density was set to 5.73 g/cm^3.

The implant/abutment system was adjusted to reflect the approximate geometry of an implant with the final abutment that would be glued on to the crown. In this model, rather than a glue material, the surface of the abutment was tied to the crown in ABAQUS. The previous impact rod geometry had a flat end that impacted the curved surface of the abutment. With the more complicated mesh of the crown, and the relatively flatter surface, initial tests had problems where the edges of the rod were striking the implant and causing large distortions at the edge and noise in the signal. To prevent these effects, the rod was adjusted to have a rounded end (but similar volume) to uniformly distribute the stress on the end of the rod. The new assembly with the final abutment and rounded impact rod is shown in Figure 7.9.

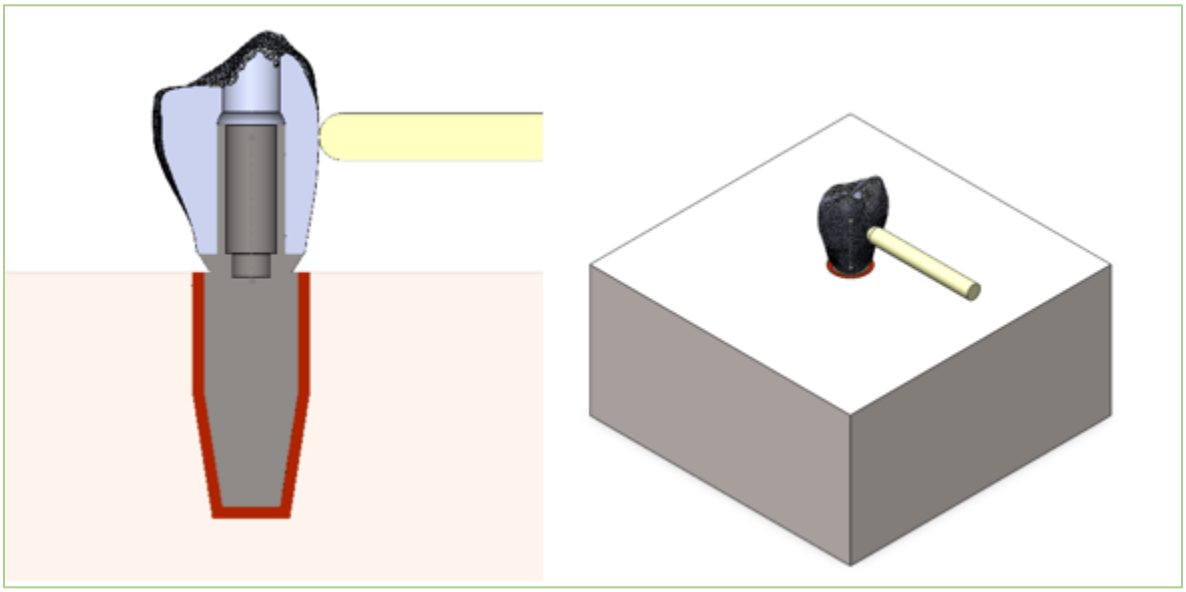

Figure 7.9: Dental Crown Assembly

When testing the implants with healing abutments, the impact rod was positioned directly in line with the top edge of the abutment. The surface of the crown lacks distinct features that can be used for positioning, and the top edge did not produce viable data in experimental tests. The position of the impact rod in experimental tests was reported as 3.0-5.0 mm from the top edge, and so a range of simulations were done with strike distances between 2.5 mm and 5.5 mm measured from the top peak of the crown. The acceleration responses shown in Figure 7.10 show trends of increasing contact time with decreased distance from the peak; a higher strike point gives a longer response (lower first mode frequency). There is also a change in the number of second mode peaks in the response. The signals from strikes that are 3.5 and 2.5 mm from the top give responses that have four second mode peaks in the signal, but strikes farther from the top give only three second mode peaks.

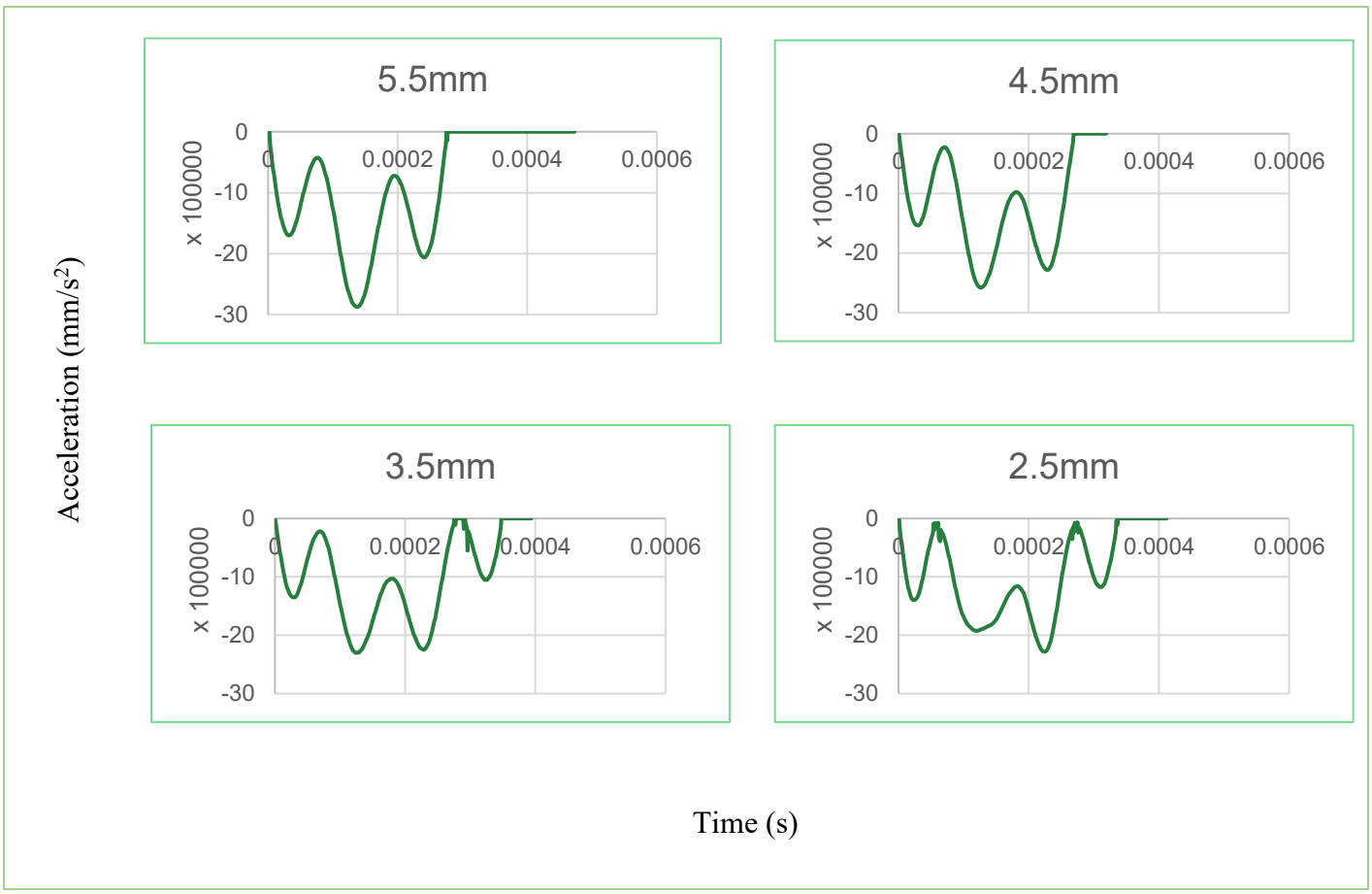

Figure 7.10: Acceleration Response of an Impact Rod Striking a Premolar Dental Crown at Various Distances from the Peak

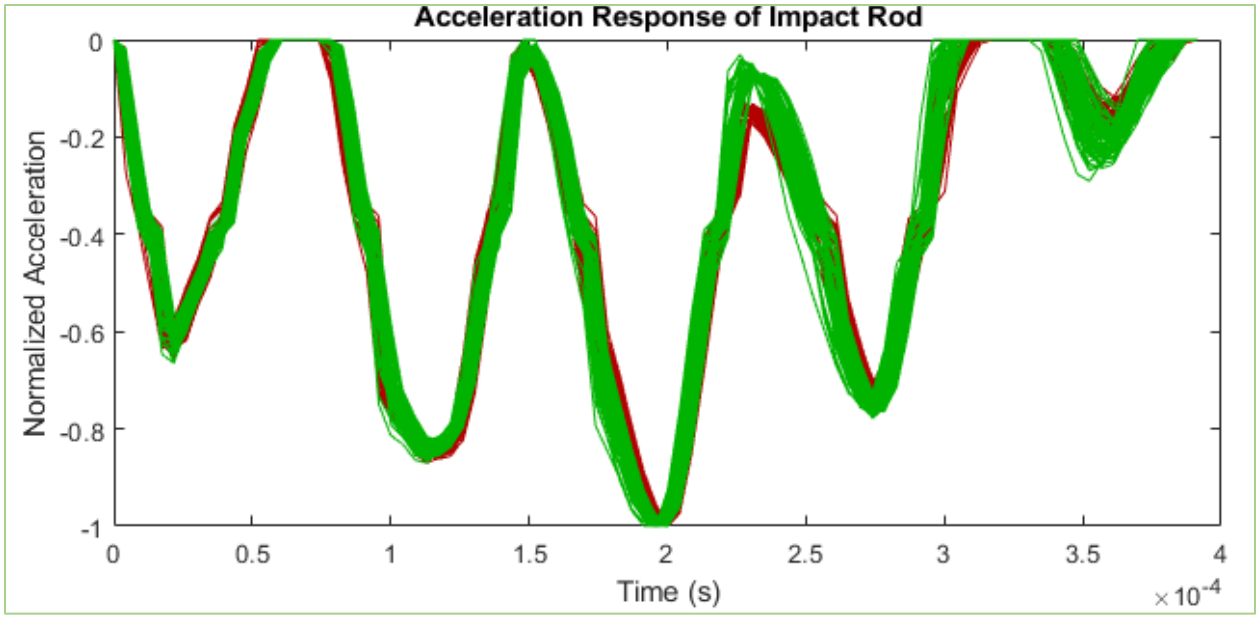

Figure 7.11: Acceleration Response of Experiments Using a Premolar Crown and RC Implant

The responses acquired from the experimental measurements (Figure 7.11) each showed five second mode peaks and had a longer contact time than any of the simulations. When fit with the analytical model, the experimental ASC was 17.4 for one sample and 18.1 for the second sample. The analytical model was adjusted to incorporate the mass and geometry of the crown and to account for a striking height. The ASCs for the simulations are in Table 7-4. The ASC follows a similar trend to the contact time, increasing as the strike distance from the top of the crown decreases.

Table 7-4: ASC's Extracted from Premolar Model

Distance from Crown Peak (mm)	ASC
5.5	13.8
4.5	13.9
3.5	15.8
2.5	22.2

The extracted ASCs from the four simulations had a large range and appeared to change with striking height. This is contrary to the desired result since it means that different measurements can be obtained on the same implant with the same interface conditions. Since the implant and

bone block are the same as the RC_40_6 experiments tested previously, and the ASC should not depend on the geometry of the abutment, the ASC should be the same as the values obtained in those experiments averaging 15.8. Although this is the value obtained when the striking height is 3.5mm from the top, the trend of the ASC changing with strike height implies that the analytical model imperfectly captures the behavior of the crown system. If the ASIST were to be used to test crowns in a clinical setting, a change of 3mm in height could result in a change of ASC of 8.4 even though the interface may not have changed at all. The significance of this difference is shown from the interface simulations in Chapter 4. A difference in the ASC of 8.4 is approximately equivalent to the stiffness changing from 40% of the surrounding bone stiffness to 120% of the surrounding bone stiffness. This is a large difference when monitoring the healing process of the BI interface in a clinical setting. Using a striking height of 3.5mm from the crown peak appears to give a reasonable ASC but if the ASIST handpiece is meant to be handheld, the amount of precision required may be unrealistic. Therefore, the variation must be addressed in the analytical model and improving the accuracy with respect to the striking location on a crown.

7.4 Summary

This chapter provides preliminary work towards modelling important clinical scenarios. Clinically, dental implants are installed into bone made up of both trabecular and cortical regions. Modelling this property allowed the examination of how an assumption of uniformity may influence the ASC value and cause a bias in the stability measurement. Bone resorption is a clinically relevant problem that was modelled by changes in the bone block geometry. The changes in the stability due to this resorption were examined to understand how the ASIST measurements could be used to detect evidence of the problem before notable symptoms developed. An average decrease of 2 in the ASC per millimeter of resorption was found in the simulation responses. Since the ASIST does not require special components attaching to the implant, it can be used on a patient with a dental crown. A dental crown system was modelled to examine the acceleration response, and the effect of strike height on the stability measurement. Large changes in the ASC occurred due to variation of the striking height. This sensitivity is a problem to address in future work if the ASIST is to be a handheld device where the precision in striking height cannot be easily controlled.

Chapter 8 : Summary and Conclusion

8.1 Summary

This research presents the development of a Finite Element (FE) model that represents the function of the Advanced System for Implant Stability Testing (ASIST). This system uses impact loading and a 4-Degree of Freedom (DOF) analytical model to determine the stiffness of the bone-implant interface (BII) of dental implants in a non-invasive procedure. The FE model allows further understanding of the factors present in the system and allows the prediction of measurements on systems that cannot be tested in an experimental setting.

The simulations developed in this work are for a dynamic system excited by impact loading. The impact rod of the ASIST handpiece is modelled as a cylinder which is given an initial velocity towards the top of an implant/abutment structure. This structure is held in place by a material representation of the BII which connects the implant surface to surrounding bone. Just like the ASIST, the output of the model is the acceleration response of the impact rod. The acceleration response is matched to the analytical model to extract the ASIST Stability Coefficient (ASC) and the interface stiffness.

This research builds upon previous work in developing the ASIST for Bone Anchored Hearing Aid (BAHA) implants, and current work testing the ASIST on dental implants. This work provides further understanding of the physical system and its dynamic behavior by investigating variables related to lab testing procedure such as the impact angle or clamping conditions that can affect the measurements from the ASIST.

The simulations done in this work provide further evidence that the ASIST can be used to compare the stability of different implants based only on the BII, without being biased by the effects of implant or abutment geometry on the vibration behavior. By modelling four different implant/abutment systems with five different artificial bone blocks, the model was used to validate ASIST measurements taken on similar samples experimentally. The model was also used to examine the response of a crown attached to an implant and the impact of striking height on the signal.

The FE model also creates the opportunity to investigate systems that are more difficult to test in an experimental setting such as the degree of osseointegration. The model was used to measure a sample at many points that represent a system with full bone-implant bonding, or with very weak bonding. The model was also used to test simulations that more closely represent dental implants in a clinical setting by incorporating bone resorption into the model.

8.2 Research Contributions

- A FE model was developed to examine the dynamic response of an osseointegrated dental implant undergoing impact loading.
- The model was used to explain variations in experiments using the ASIST, and possible variables that could influence the stability measurements made by the ASIST.
- The modelling of the BII was done using a material interface and frictional interface to test the versatility of each method in the presented model. An elastic material interface allowed the tuning of the model within the ranges of both primary and secondary stability measurements taken in an experimental setting.
- The modelling process was used to create simulations of four different implant/abutment systems embedded in five different materials to compare the dynamic responses of each system.
- The models showed evidence that the stability measurements of the ASIST were not dependent on the properties of the implant or abutment but relied on the properties of the BII and surrounding material.
- The modelling process in most cases was able to provide an ASC within 1 of the experimental measurement and modelled the systems with an R^2 of 0.94.
- The model was expanded to include a dental crown, a composite surrounding material, and bone resorption.
- The model was able to highlight the sensitivity of the ASC to the striking location of the dental crown.
- The analytical model was adjusted to incorporate the stiffness of each layer of the composite surrounding material which showed that assuming a uniform material may result in the appearance of a higher stiffness.

- Bone resorption was shown to create a similar effect to lower stiffness in the BII.

8.3 Limitations

This work and the model developed in it have several limitations to be addressed in future applications. The material properties used in the model for the SawBones blocks were all approximated using the tensile and compressive moduli given on the Sawbones website. In the model, these materials were assumed to be linear elastic, isotropic, and have a Young's modulus equal to the average of the two given values. The material interface was a complex structure of the implant threads interacting with the bone, with superglue in between for the experimental samples, but this was all reduced into one homogeneous material in the simulation. The implant and abutment were also treated as one structure for each simulation, assuming a perfectly rigid connection between the components.

There were also limitations in the available experimental data. Since the ASIST is currently in development for dental implants, the experimental data is limited to what was available at the time of analysis. The benchtop experiments focused only on bone-level implant types from Straumann as those are the most common type of implant used in the local clinic with which we collaborated. However, similar testing and analysis could be done with many other implant systems.

8.4 Future Considerations

This work should be extended to incorporate more realistic geometries and properties of the implant and surrounding bone. To better represent the clinical data that could be collected, the bone should be changed to a more realistic geometry of a bone with more realistic boundary conditions that represent the human jaw (both in benchtop experiments and model simulations). The properties of the bone should be incorporated into the model. The model should further be used to investigate the relationships between the bone and BII properties and the stability of the implant and interface stiffness. In this work, the properties were selected as a percentage of the Sawbones block used in experiments, but more work could be done to investigate the effects of bone density and elasticity of both the interface and the surrounding block on the ASC.

The ASIST has so far been tested on dental implants only in artificial bone. The next step for the validation of the ASIST with dental implants is ex vivo and in vivo studies using real bone. It should be tested in a clinical setting to measure the in vivo development of the BII, and an experimental setting using bone tissue to examine the more realistic responses that the change in geometry and properties would create. Both of these could then be incorporated in the FE model and compared.

This work described the process of creating the model of one dental crown. Dental crowns vary according to the person, and tooth that is being replaced. The process of cleaning a dental crown model or simplifying a dental crown model could be refined to ease the use of this model in representing clinical data for patients after their healing abutment is replaced. There are also many more implant and abutment geometries that could be modelled to analyze the responses of each implant or abutment in a clinical setting.

References

[1] J. Aida, "Tooth Loss," in *Oral Epidemiology* , Sao Paulo, Springer, 2013, pp. 224-231.

[2] W. Marcenes and U. Ryda, "Socio-Psychological Aspects of Traumatic Dental Injuries," in *Textbook and Color Atlas of Traumatic Injuries to the Teeth*, Copenhagen, Blackwell Munksgaard, 2007, pp. 197-206.

[3] P. Axelsson, "Etiology of Periodontal Diseases," in *Diagnosis and Risk Prediction of Periodontal Diseases, Vol 3*, Karlstad , Quintessence Publishing Co, Inc, 2002, pp. 1-94.

[4] M. Saintrain and E. Souza, "Impact of Tooth Loss on Quality of Life," *Gerodontology,* vol. 29, no. 2, pp. 632-636, 2011.

[5] K. Higuchi, "Ortho-Integration: The Alliance Between Orthodontics and Osseointegration," in *Orthodontic Applications of Osseointegrated Implants*, Hong Kong, Quintessence Publishing Co, Inc, 2000, pp. 1-20.

[6] R. Schenk and D. Buser, "Osseointegration: A Reality," *Periodontology,* vol. 17, no. 1, pp. 22-35, 1998.

[7] H. Gotz and others, "Effect of Surface Finish of the Osseointegration of Laser-Treated Titanium Alloy Implants," *Biomaterials,* vol. 25, pp. 4057-4064, 2004.

[8] Z. Lian and others, "Effect of Bone to Implant Contact Percentage on Bone Remodelling Surrounding A Dental Implant," *International Association of Oral and MAxillofacial Surgeons,* vol. 39, pp. 690-698, 2010.

[9] N. Lioubavina-Hack, N. Lang and T. Karrig, "Significance of Primary Stability for Osseointegration of Dental Implants," *Clinical Oral Implants Research,* vol. 17, no. 3, pp. 244-250, 2006.

[10] Y. Lim and others, "A New Method of Measuring the Volumetric Change of Alveolar Bone Around Dental Implants Using Computed Tomography," *Journal of Clinical Medicine,* vol. 9, no. 4, p. 1238, 2020.

[11] M. Atsumi, S. Park and H. Wang, "Methods Used to Assess Implant Stability: Current Status," *The International Journal of Oral and Maxillofacial Implants,* vol. 22, pp. 743-754, 2007.

[12] M. Herrero-Climent and others, "InVitro Comparative Analysis of Two Resonance Frequency Measurement Devices: Osstell Implant Stability Coefficient and Penquin Resonance Frequency Analysis," *Clinical Implant Dentistry and Related Research,* vol. 21, no. 6, pp. 1124-1131, 2019.

[13] R. Swain, Development and Modeling of an Impact Test to Determine the Bone-Implant Interface Properties of Osseointegrated Implants, Edmonton Alberta Canada: University of Alberta, Department of Mechanical Engineering, 2006.

[14] L. Westover and others, "Advanced System for Implant Stability Testing," *Journal of Biomechanics,* vol. 49, pp. 3651-3659, 2016.

[15] L. Westover and others, "Comparison of Implant Stability Measurement Devices for Bone-Anchored Hearing Aid Systems," *The Journal of Prosthetic Dentistry,* vol. 119, no. 1, pp. 178-184, 2018.

[16] C. Jar and others, "Measuring dental implant stability with the Advanced System for Implant Stability Testing (ASIST)," in *Annual Alberta Biomedical Engineering Conference*, Banff, Alberta, Canada, 2022.

[17] M. Mohamed and others, "Stability Assessment of Osseointegrated Transfemoral Bone-Implant Systems using Finite Element Modal Analysis," in *CSME Congress*, Edmonton, AB, Canada, 2022.

[18] M. Mohamed, H. Pisavadia and L. Westover, "A Finite Element Model for Evaluating the Effectiveness of the Advanced System for Implant Stability Testing," *Journal of Biomechanics,* vol. 124, p. 110570, 2021.

[19] J. Turp and K. Alt, "Anatomy and Morphology of Human Teeth," in *Dental Anthropology*, New York, Springer-Verlag/Wien, 1998, pp. 71-94.

[20] R. Wang and S. Weiner, "Human Root Dentin: Structural Anisotropy and Vickers Micreohardness Isotropy," *Connective Tissue Research,* vol. 39, no. 4, pp. 269-279, 1998.

[21] J. J. Kruzic, R. K. Nalla, J. H. Kinney and R. O. Ritchie, "Mechanistic Aspects of In Vitro Fatigue-Crack Growth in Dentin," *Biomaterials,* vol. 26, pp. 1195-1204, 2005.

[22] P. Robinson, Tooth Extraction A Practical Guide, London: Wright, 2000.

[23] M. Silva-Junior and others, "Oral Health Condition and Reasons for Tooth Extraction Among an Adult Population (20-64 Years Old)," *Ciência & Saúde Coletiva,* vol. 22, no. 8, pp. 2693-2702, 2017.

[24] World Health Organization, "Global Oral Health Status Report," 18 November 2022. [Online]. Available: https://www.who.int/publications/i/item/9789240061484. [Accessed 11 January 2023].

[25] N. Kassebaum and others, "Global Burden of Severe Tooth Loss," *Journal of Dental Research,* vol. 93, no. 7Suppl., pp. 20S-28S, 2014.

[26] A. Simon-Soro and A. Mira, "Solving the Etiology of Dental Caries," *Trends in Microbiology,* vol. 23, no. 2, pp. 76-82, 2015.

[27] J. Murray, J. Nunn and N. Steele, Diet and Dental Caries, New York: Oxford, 2003, pp. 7-.

[28] R. Macey and others, "Tests to detect and inform the diagnosis of caries," Cochrane Library, 10 December 2018. [Online]. Available: https://www.cochranelibrary.com/cdsr/doi/10.1002/14651858.CD013215/full. [Accessed 11 January 2023].

[29] J. Broadbent, W. Thomson and R. Poulton, "Progression of Dental Caries and Tooth Loss Between the Third and Fourth Decades of Life: A Birth Cohort Study," *Caries Research,* vol. 40, pp. 459-465, 2006.

[30] H. Chauncey, R. Glass and J. Alman, "Dental Caries," *Caries Research,* vol. 23, pp. 200-205, 1989.

[31] F. Gottrup, S. Jensen and J. Andreasen, "Wound Healing Subsequent to Injury," in *Textbook and Color Atlas of Traumatic Injuries to the Teeth*, Copenhagen, Blackwell Munkgaard, 2007, p. 1.

[32] F. Peterson, S. Jensen and M. Dahl, "Implant Treatment After Traumatic Tooth Loss: A Systematic Review," *Dental Traumatology,* vol. 38, no. 2, pp. 105-116, 2022.

[33] E. Peterson, L. Anderson and S. Sorenson, "Traumatic oral vs non-oral injusries," *Swedish Dental Journal,* vol. 21, no. 1, pp. 55-68, 1997.

[34] J. Andreasen and F. Andreasen, "Avulsions," in *Textbook and Colour Atlas of Traumatic Injuries to the Teeth*, Copenhagen, Blackwell Munksgaard, 2007, pp. 444-488.

[35] J. Andreasen and F. Andreasen, "Intrusive Luxation," in *Textbook and Color Atlas of Traumatic Injuries to the Teeth*, Copenhagen, Blackwell Munksgaard, 2007, pp. 428-443.

[36] G. Zarb and others, "Introduction: Clinical Considerations for Implant-Supported Prosthesis in Elderly Patients," in *Aging, Osteoporosis, and Dental Implants*, Quintessence Publishing Co, Inc, 2002, pp. 1-15.

[37] A. Hohmann and W. Hielscher, Principles of Design and Fabrication in Prosthedontics, Bielefeld: Quintessence Publishing Co, Inc, 2016.

[38] A. Jokstad, "Implant Dentistry: A Technology Assessment," in *Osseointegration and Dental Implants*, Wiley-Blackwell, 2009, pp. 3-26.

[39] H. Elani and others, "Trends in Dental Implant Use in the U.S., 1999-2016, and Projections to 2026," *Journal of Dental Research,* vol. 97, no. 13, pp. 1424-1430, 2018.

[40] J. McCord and others, "Implant Options," in *Missing Teeth: A guide to Treatment Options*, Churchill Livingstone, 2003, pp. 51-66.

[41] Straumann, *Surgical User Guide,* Basel: Institut Straumann AG, 2017.

[42] C. Misch, "Autogenous Bone Grafting for Dental Implants," in *Oral and Maxillofacial Surgery* , St. Louis, Saunders Elsevier, 2009, pp. 406-427.

[43] A. Carr and others, "Retrospective Cohort Study of the Clinical Performance of 1-Stage Dental Implants," *The International Journal of Oral and Maxillofacial Implants,* vol. 18, no. 3, pp. 399-405, 2003.

[44] L. Clarizio, "Immediate Implant Loading," in *Oral and Maxillofacial Surgery*, St. Louis, Missouri, Saunders Elsevier, 2009, pp. 511-524.

[45] S. Wang, "Can Male Patient's Age Affect the Cortical Bone Thickness of Jawbone for Dental Implant Placement? A Cohort Study," *International Journal of Environmental Research and Public Health,* vol. 18, no. 8, p. 4284, 2021.

[46] J. Hsu and others, "Effects of the 3D Bone-to-Implant Contact and Bone Stiffness on the Initial Stability of a Dental Implant: Micro-CT and Resonance Frequency Analysis," *International Journal or Oral and Maxillofacial Surgery,* vol. 42, pp. 276-280, 2013.

[47] H. Huang, "Initial Stability and Bone Strain Evaluation of the Immediately Loaded Dental Implant: an in vitro Model Study," *Clinical Oral Implant Research ,* vol. 22, no. 7, pp. 691-698, 2010.

[48] Y. Ko and others, "Association Between Age of Menopause and Thickness of Crestal Cortical Bone at Dental Implant Site: A Cross-Sectional Observational Study," *International Journal of Environmental Research and Public Health,* vol. 17, no. 16, p. 5868, 2020.

[49] S. Ott, "Cortical or Trabecular Bone: What's the Difference?," *American Journal of Nephrology,* vol. 47, pp. 373-375, 2018.

[50] A. Al-Ekrish and others, "Revised, Computed Tomography-Based Lekholm and Zarb Jawbone Quality Classification," *The International Journal of Prosthodontics,* vol. 31, no. 4, pp. 342-345, 2018.

[51] D. Stefano and others, "Stability of Dental Implants and Thickness of Cortical Bone: Clinical Research and Future Perspectives. A Systematic Review," *Materials,* vol. 14, no. 23, p. 7183, 2021.

[52] G. Zarb, "Looking Back: The Emergence and the Promise of Osseointegration," in *Osseointegration*, Quintessence Books, 2008, pp. 1-22.

[53] P. Branemark, G. Zarb and T. Albrektsson, Tissue-Integrated Prosthesses: Osseointegration in Clinical Dentistry., Chicago, IL, USA: Quintessence Publishing Company Inc., 1985.

[54] S. Lundgren and L. Sennerby, Bone Reformation: Contemporary Bone Augmentation Procedures in Oral and MAxillofacial Implant Surgerry, Surrey: Quintessence Publishing Co, Inc, 2008.

[55] G. Zarb and T. Albrektsson, "Treatment Outcomes," in *Osseointegration*, Quintessence Publishing Co, Inc, 2008, pp. 23-34.

[56] C. Villar and others, "Wound Healing Around Dental Implants," *Endodontic Topics,* vol. 25, pp. 44-62, 2012.

[57] T. Albrektsson, V. Franke-Stenport and A. Wennerberg, "Healing Response," in *Osseointegration*, Quintessence Publishing Co, Inc, 2008, pp. 47-50.

[58] C. Misch, "Generic Root Form Component Terminology," Pocket Dentisry, 7 January 2015. [Online]. Available: https://pocketdentistry.com/2-generic-root-form-component-terminology-2/. [Accessed 29 March 2023].

[59] A. Jokstad, "Biological Response," in *Osseointegration and Dental Implants* , Wiley-Blackwell, 2008, pp. 205-255.

[60] D. Paquette, N. Brodala and R. Williams, "Risk Factors for Endosseous Dental Implant Failure," *Dental Clinics of North America,* vol. 50, pp. 361-374, 2006.

[61] T. Albrektsson and A. Wennerberg, "Oral Implant Surfaces: Part 1 - Review Focusing on Topographic and Chemical Properties of Different Surfaces and In Vivo Responses to Them," *International Journal of PRosthedontics,* vol. 17, no. 5, pp. 544-564, 2004.

[62] J. Davies, "Understanding Peri-Implant Endosseous Healing," *Journal of Dental Education ,* vol. 67, no. 8, pp. 932-949, 2003.

[63] I.-S. Yeo, S.-K. Mim and Y. An, "Influence of Bioactive Material Coating of Ti Dental Implant Surfaces on Early Healing and Osseointegration of Bone," *Journal of the Korean Physical Society,* vol. 57, no. 6, pp. 1717-1720, 2010.

[64] A. Jokstad, "jokstad.net," 8 February 2008. [Online]. Available: https://www.jokstad.net/2008.02.08%20Lecture%20Implant%20CCP%20In-house%20UofToronto.pdf. [Accessed 19 January 2023].

[65] K. Karthik, S. Sivaraj and V. Thangaswamy, "Evaluation of Implant Success: A Review of Past and Present Concepts," *Journal of Pharmacy and Bioallied Sciences,* vol. 5, pp. S117-S119, 2013.

[66] L. Westover and others, "Application of the Advanced System for Implant Stability Testing (ASIST) to NAtural Teeth for Noninvasive Evaluation of the Tooth Root Interface," *Journal of Biomechanics,* vol. 69, pp. 129-137, 2018.

[67] L. Westover and others, "Longitudinal Evaluation of Bone-Anchored Hearing Aid Implant Stabiity Using the Advanced System for Implant Stability Testing (ASIST)," *Otology and Neurology,* vol. 39, pp. 489-495, 2018.

[68] M. Mohamed and L. Westover, "Evaluating the Dynamic Behavior of Bone Anchored HEaring Aids Using a Finite Element Model and its Applications to Implant Stability Assessment," *Medical and Biological Engineering and Computing,* vol. 60, pp. 2779-2795, 2022.

[69] T. Vandenberg, "Development of a Finite Element Model to Examine the Response if the Advanced System for Implant Stability Testing," in *Annual Alberta Biomedical Engineering Conference*, Banff, Alberta, Canada, 2022.

[70] "Biomechanical Materials for Precise, Repeatable Testing - Materials Guide," Sawbones, 2016. [Online]. Available: https://www.sawbones.com/biomechanical-product-info. [Accessed 13 04 2022].

[71] Medizintechnik Gulden e.K., "med-gulden," 1 10 2015. [Online]. Available: https://www.med-gulden.com/downloads/02_english/02_Operating%20Manual/Periotest_Classic.pdf. [Accessed 1 February 2023].

[72] W. Winter and others, "Parameters of Implent Stability Measurements Based on Resonance Frequency and Damping Capacity: A Comparative Finite Element Analysis," *The International Journal of Oral and Maxillofacial Implants,* vol. 25, no. 3, pp. 532-539, 2010.

[73] Y. Liu and others, "Challenges of Using REsonance Frequency Analysis to Identify Stability of a Dental Implant Placed in the Mandible," *The International Journal of Oral and Maxillofacial Implants,* vol. 36, no. 2, pp. e7-e21, 2021.

[74] J. Yang and H. Xiang, "A three-Dimensional Finite Element Study on the Biomechanical Behavior of an FGBM Dental Implant in Surrounding Bone," *Journal of Biomechanics,* vol. 40, pp. 2377-2385, 2007.

[75] A. Halldin and others, "The Effect of Static Bone Strain on Implant Stability and Bone Remodeling," *Bone,* vol. 49, pp. 783-789, 2011.

[76] A. Natali and others, "Investigation of the Integration Process of Dental Implants by Means of a Numerical Analysis of Dynamic Response," *Journal of Dental Materials,* vol. 13, pp. 325-332, 1997.

[77] "lookpolymers," Songhan Plastic Technology Co.,Ltd, [Online]. Available: http://www.lookpolymers.com/polymer_Sawbones-Solid-Rigid-Polyurethane-Foam-40-pcf-Density.php. [Accessed 31 03 2023].

[78] "Titanium-Commercially Pure (CP)," American Elements, [Online]. Available: https://www.americanelements.com/titanium-commercially-pure-cp-7440-32-6. [Accessed 31 03 2023].

[79] "Titanium, Ti," MatWeb Material Property Data, 1999. [Online]. Available: https://www.matweb.com/search/DataSheet.aspx?MatGUID=66a15d609a3f4c829cb6ad08f0dafc01&ckck=1. [Accessed 13 04 2022].

[80] "316 Stainless Steel," MatWeb Material Property Data, 1990. [Online]. Available: https://www.matweb.com/search/DataSheet.aspx?MatGUID=dfced4f11d63459e8ef8733d1c7c1ad2. [Accessed 13 04 2022].

[81] "Overview of Materials for Cyanoacrylate Adhesive," MatWeb Material Property Data, [Online]. Available: https://www.matweb.com/search/DataSheet.aspx?MatGUID=d0d7dbec7666421caf8aa08724b634c5. [Accessed 31 03 2023].

[82] L. Westover, Evaluation of the Interface Mechanical Properties of Craniofacial Implants and Natural Teeth Through Development of the Advanced System for Implant Stability Testing (ASIST), Edmonton Alberta Canada: University of Alberta, Department of Mechanical Engineering, 2016.

[83] R. Alaqueely, N. Babay and M. AlQutub, "Dental Implant Primary Stability in Different Regions of the Jawbone: CBCT-based 3D Finite Element Analysis," *Saudi Dental Journal,* vol. 32, pp. 101-107, 2019.

[84] H. Guan and others, "Dynamic Modelling and Simulation of the Dental Implant Insertion Process - A Finite Element Study," *Finite Elements In Analysis and Design,* vol. 47, pp. 886-897, 2011.

[85] S. Jones and others, "Simulation of Impact Test for Determining Health of Percutaneous Bone Anchored Implants," *Journal of Biomedical Engineering,* vol. 128, pp. 647-653, 2006.

[86] E. Kitamura and others, "Influence of Marginal Bone Resorption on Stress Around an Implant - A Three-Dimensional Finite Element Analysis," *Journal of Oral Rehabilitation,* vol. 32, pp. 279-286, 2005.

[87] L. Lindquist and others, "Bone Resorption around Fixtures in Edentulous Patients Treated with Mandibular Fixed Tissue-Integrated Prostheses," *The Journal of Prosthetic Dentistry,* vol. 59, no. 1, pp. 59-63, 1988.

[88] M. Cassetta and others, "Early Peri-Implant Bone Loss: A Prospective Cohort Study," *International Journal of Maxillofacial Surgery,* vol. 44, pp. 1138-1145, 2015.

[89] S. Vervaeke and others, "A Multifactorial Analysis to Identify Predictors of Implant Failure and Beri-Implant Bone Loss," *Clinical Implant Dentisrtry and Related REsearch,* vol. 17, pp. e298-e307, 2015.

[90] Straumann, "Basic Information on the Surgical Procudures for the Straumann Bone Level Tapered Implant," [Online]. Available: https://www.straumann.com/content/dam/media-

center/straumann/en-us/documents/brochure/product-information/NAMLIT.1043.BLT.Surgical.Procedures.Brochure.pdf. [Accessed 04 04 2023].

[91] A. O'Mahoney and others, "Anisotropic Elastic Properties of Cancellous Bone from a Human Edentulous Mandible," *Clinical Oral Implants Research ,* vol. 11, no. 5, pp. 415-421, 2001.

[92] C. Schwartz-Dabney and P. Dechow, "Variations in Cortical Material Properties Throughout the Human Dentate Mandible," *American Journal of Physical Anthropology,* vol. 120, no. 3, pp. 252-277, 2003.

[93] P. Ercal and others, "Impact of Peri-Implant Bone Resorption, Prosthetic Materials, and Crown to Implant Ratio on the Stress Distribution of Short Implants: A Finite Element Analysis," *Medical & Biological Engineering & Computing,* vol. 59, pp. 813-824, 2021.

[94] O. Karaer and others, "In Silico Finite Element Analysis of Implant Supported CAD-CAM Resin Composite Crowns," *Journal of Prosthedontics,* pp. 1-8, 2022.

[95] V. Klimecs, "Bone Loss Around Dental Implants 5 Years After Implantation of Biphasic Calcium Phosphate (HAp/BTCP) Granules," *Journal of Healthcare Engineering,* vol. 2018, no. Article ID 4804902, pp. 1-7, 2018.

[96] Sawbones, "Top Biomechanical Products & Materials Provider for Testing & Validation," Sawbones, 2022. [Online]. Available: https://www.sawbones.com/biomechanical-product-info. [Accessed 1 February 2023].

[97] S.-M. Choi and others, "Comparative Finite Element Analysis of Mandibular Posterior Single Zirconia and Titanium Implants: a 3-Dimensional Finite Element Analysis," *Journal of Advanced Prosthodontics,* vol. 13, no. 6, pp. 396-407, 2021.

Appendix A: Equations of Motion of the ASIST analytical Model

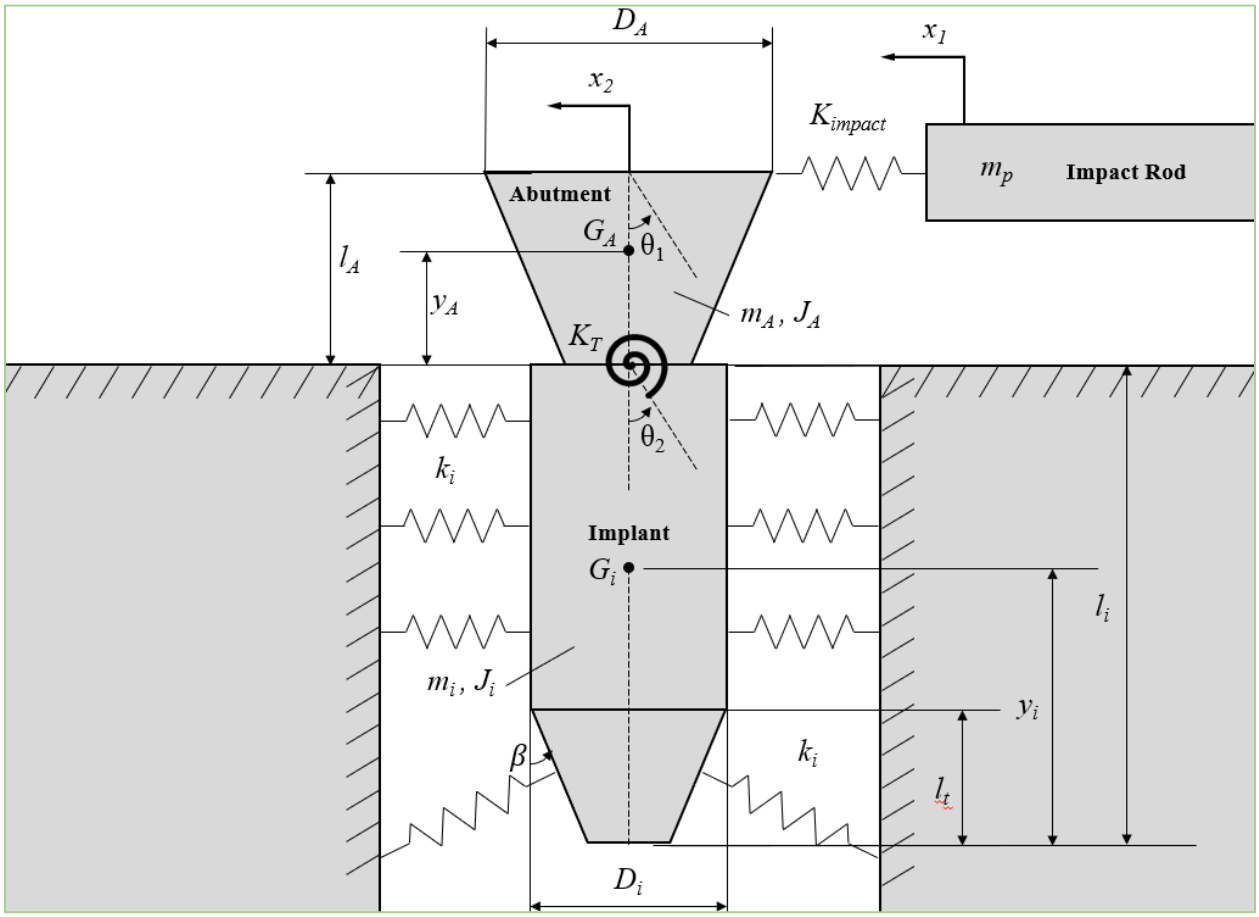

$$[M]\{\ddot{x}\} + [C]\{\dot{x}\} + [K]\{x\} = 0$$

$$[M] = \begin{bmatrix} m_p & 0 & 0 & 0 \\ 0 & m_A + m_i & m_A \times y_A - (m_i + m_A)h & -m_i(l_i - y_i) \\ 0 & m_A \times y_A - (m_i + m_A)h & J_A + m_a(h - y_a)^2 + m_i \times h^2 & m_i \times h(l_i - y_i) \\ 0 & -m_i(l_i - y_i) & m_i \times h(l_i - y_i) & J_i + m_i(l_i - y_i)^2 \end{bmatrix}$$

$$[K] = \begin{bmatrix} K_{11} & K_{12} & 0 & 0 \\ K_{21} & K_{22} & K_{23} & K_{24} \\ 0 & K_{32} & K_{33} & K_{34} \\ 0 & K_{42} & K_{43} & K_{44} \end{bmatrix}$$

$$K_{11} = K_{impact}$$

$$K_{12} = K_{21} = -K_{impact}$$

$$K_{22} = -K_{impact} + 2k_i \times D_i \times (l_i - l_t) + k_i \cos^2(\beta)\left(\frac{[-2l_t \sin(\beta)][2L_i \times l_t - l_t^2]}{l_t} + D_i \times l_t\right)$$

$$K_{23} = K_{32} = -2k_i \times D_i \times (l_i - l_t) - k_i \cos^2(\beta)\left(\frac{[-2l_t \sin(\beta)][2L_i \times l_t - l_t^2]}{l_t} + D_i \times l_t\right)h$$

$$K_{24} = -k_i \times D_i \times (l_i - l_t)^2 - \frac{2}{3}k_i \cos^2(\beta)\left(\frac{[-2l_t \sin(\beta)][3l_i^2 \times l_t - 3l_i \times l_t^2 - l_t^3]}{l_t} + \frac{3}{4}D_i \times l_t\right)$$

$$K_{33} = 2k_i \times D_i \times (l_i - l_t) + k_i \cos^2(\beta)\left(\frac{[-2l_t \sin(\beta)][2L_i \times l_t - l_t^2]}{l_t} + D_i \times l_t\right)h^2 + K_T$$

$$K_{34} = K_{43} = k_i \times D_i \times (l_i - l_t)^2 + \frac{2}{3}k_i \cos^2(\beta)\left(\frac{[-2l_t \sin(\beta)][3l_i^2 \times l_t - 3l_i \times l_t^2 - l_t^3]}{l_t} + \frac{3}{4}D_i \times (2L_i \times l_t - l_t^2)\right)h - K_T$$

$$K_{44} = \frac{2}{3}k_i \times D_i \times (l_i - l_t)^3 + \frac{1}{2}k_i \cos^2(\beta)\left(\frac{[-2l_t \sin(\beta)][-4l_i^3 \times l_t + 6l_i^2 \times l_t^2 - 4l_i \times l_t^3 + l_t^4]}{l_t} + \frac{2}{3}D_i \times (3l_i^2 \times l_t - 3l_i \times l_t^2 - l_t^3)\right) + K_T$$

$$[C] = \begin{bmatrix} 0 & 0 & 0 & 0 \\ 0 & 2c \times D_i \times l_i & -2c \times D_i \times l_i \times h & -2c \times D_i \times l_i^2 \\ 0 & -2c \times D_i \times l_i \times h & 2c \times D_i \times l_i \times h^2 & 2c \times D_i \times l_i^2 \times h \\ 0 & -2c \times D_i \times l_i^2 & 2c \times D_i \times l_i^2 \times h & \frac{2}{3}c \times D_i \times l_i^3 \end{bmatrix}$$

Appendix B: ANOVA Tables

ANOVA Table Evaluating the Effects of Implant Type and Block Type on ASC

ANOVA: Two-Factor with Replication

SUMMARY	40pcf	30pcf	20pcf	10pcf	Total
RC					
Count	2	2	2	2	8
Sum	33.30	18.90	6.86	3.88	62.94
Average	16.65	9.45	3.43	1.94	7.87
Variance	0.60	0.07	0.06	1.77	38.78
NC					
Count	2	2	2	2	8
Sum	26.40	17.68	7.19	2.44	53.71
Average	13.20	8.84	3.60	1.22	6.71
Variance	0.00	2.33	0.05	0.00	25.05
Total					
Count	4	4	4	4	
Sum	59.70	36.58	14.05	6.32	
Average	14.93	9.15	3.51	1.58	
Variance	4.17	0.93	0.04	0.76	

ANOVA

Source of Variation	*SS*	*df*	*MS*	*F*	*P-value*	*F crit*
Sample	5.3	1	5.3	8.72	1.8E-02	5.32
Columns	434.4	3	144.8	237.24	3.7E-08	4.07
Interaction	7.5	3	2.5	4.09	4.9E-02	4.07
Within	4.9	8	0.6			
Total	452.1	15				

ANOVA Table Evaluating the Effects of Implant Type and Block Type on Interface Stiffness

ANOVA: Two-Factor with Replication

SUMMARY	40pcf	30pcf	20pcf	10pcf	Total
RC					
Count	2	2	2	2	8
Sum	1.63E+12	9.22E+11	3.35E+11	1.89E+11	3.07E+12
Average	8.13E+11	4.61E+11	1.68E+11	9.45E+10	3.84E+11
Variance	1.51E+21	1.62E+20	1.45E+20	4.15E+21	9.24E+22
NC					
Count	2	2	2	2	8
Sum	1.60E+12	9.55E+11	4.35E+11	1.48E+11	3.14E+12
Average	8.01E+11	4.78E+11	2.18E+11	7.41E+10	3.92E+11
Variance	5.00E+17	1.13E+20	1.81E+20	5.00E+17	8.74E+22
Total					
Count	4	4	4	4	
Sum	3.23E+12	1.88E+12	7.70E+11	3.37E+11	
Average	8.07E+11	4.69E+11	1.93E+11	8.43E+10	
Variance	5.52E+20	1.82E+20	9.42E+20	1.52E+21	

ANOVA

Source of Variation	*SS*	*df*	*MS*	*F*	*P-value*	*F crit*
Sample	2.92E+20	1	2.92E+20	0.37	5.59E-01	5.32
Columns	1.25E+24	3	4.16E+23	531.77	1.52E-09	4.07
Interaction	3.04E+21	3	1.01E+21	1.29	3.41E-01	4.07
Within	6.26E+21	8	7.83E+20			
Total	1.26E+24	15				